Photocopy and Use Authorization

In presenting this thesis in partial fulfillment of the requirements for an advanced degree at Idaho State University, I agree that the Library shall make it freely available for inspection. I further state that permission for extensive copying of my thesis for scholarly purposes may be granted by the Dean of the Graduate School, Dean of my academic division, or by the University Librarian. It is understood that any copying or publication of this thesis for financial gain shall not be allowed without my written permission.

Signature ___________________________________

Date _______________________________________

Stream drying controls in semi-arid headwater streams: baseflow, topographic metrics, and diel cycles

by

Sara R. Warix

A thesis

Submitted in partial fulfillment of the requirements for the degree of

Master of Science in the Department of Geosciences

Idaho State University

Spring 2020

Committee Approval

To the Graduate Faculty:

The members of the committee appointed to examine the thesis of Sara Renee Warix find it satisfactory and recommend that it be accepted.

Dr. Sarah E. Godsey
Major Advisor

Dr. Kathleen A. Lohse
Committee Member

Dr. Rebecca L. Hale
Graduate Faculty Representative

Acknowledgements

I would like to thank my advisor, Sarah Godsey, for her mentorship and support throughout my time at Idaho State University. I extend thanks to my committee members, Kathleen Lohse and Rebecca Hale for their valuable feedback and time. Thanks to Carrie Bottenberg for her assistance with acquiring satellite images. Thank you to the office staff, Kate Zajanc for help with finances and to Michele Hughes for solving all possible travel problems. I thank the National Science Foundation (Awards: #1653998 & RC CZO Coop Agreement EAR 1331872), as well as the Geological Society of America, Exxon Mobil, and the Idaho State University Geslin Fund for project funding.

My field work would not have been possible without the knowledge and logistic support provided by Zane Cram, Barry Caldwell, and Mark Seyfried at the Agricultural Research Service. I am grateful to the numerous students who helped during my field campaign, including Inbar Milstein, Chris Santore, Madison Skinner, Madison Thibado, Drew Wolford, and Logan Mahoney. Thank you to Jeff Prancevic for assistance with TopoToolbox. The graduate students at Idaho State University greatly improved my experience in Idaho and I thank them all for their emotional support and for being great skiing, climbing, and biking partners. Jenna Dohman provided logistic and emotional support as a member of the Godsey Lab, even after completing her degree. Finally, I would like to thank Tyler Paladino for his coding expertise, but also for his constant support and for always listening.

TABLE OF CONTENTS

List of Figures

List of Tables

Stream drying controls in semi-arid headwater streams: baseflow, topographic metrics, and diel cycling

Thesis Abstract – Idaho State University (2020)

To understand stream drying controls, we observed drying patterns using a dense spatiotemporal network of flow sensors interspersed between baseflow monitoring locations in two headwater streams at the Reynolds Creek Critical Zone Observatory in Idaho. Our findings include very fine-scale variations in drying, discontinuous surface flows, and locally variable baseflow fluxes. These indicate: 1) wet-dry diel cycles in streamflow precede seasonal stream drying, 2) the timing of stream drying varies with controls on evapotranspiration when all other conditions for stream drying are met, and 3) a stable baseflow flux enables surface water to persist even when precipitation is low. Short lags between peak temperature and drying suggests local effects outweigh network effects. Future studies should 1) continuously monitor evapotranspiration in riparian and hillslope locations, and 2) add spatially distributed hydraulic conductivity and geophysical imaging to improve stream drying predictions.

Keywords: stream drying, intermittent, diel cycling, evapotranspiration, baseflow, subsurface characteristics, headwaters, topographic metrics, Reynolds Creek, Critical Zone Observatory, Idaho

1. Chapter 1: What controls stream drying patterns?

1.1. Introduction

Much of the research in hydrology has historically focused on floods. From 1990 to 2000, in the journal *Water Resources Research* only 21 articles were published with the word "drought" in the title and 64 with the word "flood". In contrast, from 2010 to 2020 (as of March 22), 80 drought and 76 flood titles were published; ~400% more drought-related research was conducted while flood work remained stable. This example of shifting research priorities reflects changing societal needs, scientific unknowns, and the effects of climate change affecting both extremes in hydrologic science. As climate change has begun to alter water resources by decreasing precipitation magnitude (Earman and Dettinger, 2011; Klos et al., 2014) and, especially in mountainous regions, accelerating snowmelt (Mote et al., 2018), improving our understanding of low-flow processes has become more important. Low-flow hydrological research in stream networks was largely abandoned in the 1970's due to the finding that drainage density was not a first-order control on hydrologic response (Dingman, 1978). However, in the last twenty years, hydrologists have again begun to study intermittent and ephemeral streams, settings where surface water disappears (Blasch et al., 2002; Gallo et al., 2012; Godsey and Kirchner, 2014; González-Ferreras and Barquín, 2017; Jaeger et al., 2014; Jensen et al., 2019; Valencia-Cardona et al., 2016; Ward et al., 2018; Yu (于松延) et al., 2018). Intermittent streams are channels that do not sustain surface flows year-round. Because surface flows may expand and contract within the channel network, intermittent streams vary both spatially and temporally, and greater than 50% of streams in the United States are intermittent (Costigan et al., 2016; Datry et al., 2011; Levick et al., 2008). Intermittent streams are most common in headwater streams in the uppermost reaches of a watershed.

First- and second-order headwater streams feed downstream surface water resources such as rivers and lakes. Downstream surface water resources are vital to maintain our current agricultural, industrial, and private water demands. Thus, to understand downstream surface waters, we must study headwater systems (Bishop et al., 2008), and in particular their drying patterns (Hale and Godsey, 2019). Although patterns of stream network expansion and contraction have been characterized (Godsey and Kirchner, 2014; Goulsbra et al., 2014; Peirce and Lindsay, 2015; von Schiller et al., 2011; Whiting and Godsey, 2016), gaps in our understanding of headwater drying remain. For example, what are high-frequency patterns of stream drying in headwater streams? What controls variability in spatiotemporal stream drying patterns? Improving our understanding of these gaps will enable hydrologists to establish a hierarchy of the most important stream drying controls, which will in turn enable policy makers to best protect intermittent streams. This thesis is dedicated to quantifying stream drying in potentially vulnerable mountain systems near the rain-snow transition (see section 1.5.2), and to characterizing the mechanisms that control spatiotemporal drying variability.

1.2. Why intermittent streams?

Headwater stream networks source over half the discharge to the global river network (Costigan et al., 2016) and provide essential habitat for migrating riparian species (US EPA, 2015). Headwater streams transport downstream sediment, solutes, nutrients, and contribute to water supplies (Gomi et al., 2002). Half the length of headwater stream networks is comprised of intermittent streams. In arid and semi-arid regions such as the western United States, intermittent streams are particularly critical in supporting the vitality of downstream water resources because of limited precipitation (Levick et al., 2008). Despite the abundance and importance of intermittent streams, hydrologists still struggle to understand when and where they dry.

Intermittent streams have been more often studied to understand the ecological consequences of stream drying than to assess the hydrological controls on drying (Datry et al., 2014, 2011; Perkin and Gido, 2012; Steward et al., 2012). Early stream drying literature focused on the relationship between drainage density and hydrologic response (Anderson and Burt, 1978; Blyth and Rodda, 1973; Carlston, 1963; Day, 1978; Dingman, 1978), but stopped after the conclusion that drainage density was not a primary control on flow presence (Dingman, 1978). During the last six years, however, our understanding of the hydrologic controls that influence stream drying has increased considerably. Dense spatiotemporal observations suggest that stream drying is highly variable and often consists of isolated dry segments between continuous flow (Costigan et al., 2016; Datry et al., 2014; Dohman et al., in prep; Godsey and Kirchner, 2014; González-Ferreras and Barquín, 2017; Jaeger et al., 2019; Jensen et al., 2019; Peirce and Lindsay, 2015; Queener, 2015; Whiting and Godsey, 2016; Yu (于松延) et al., 2018), rather than contraction only from the uppermost reaches.

Furthermore, our understanding of possible controls on stream drying has also developed. The frequency, duration, and intensity of weather events as well as wet and dry oscillations are important to water availability and thus influence stream drying probability (Costigan et al., 2016; Jaeger et al., 2019; Ward et al., 2018). Watershed topography has been identified as a major control on stream expansion and contraction (Prancevic and Kirchner, 2019) and metrics like slope, curvature, and topographic wetness index have been identified as predictors of stream drying (Jaeger et al., 2019; Ward et al., 2018). The ability of water to pass through the subsurface is thought to impact stream drying patterns (Boulton et al., 2017; Dohman et al., in prep; Godsey et al., 2013; Lovill et al., 2018), and grain size, lithology permeability, soil type, hydraulic conductivity, and porosity have been identified as potential stream drying controls (Costigan et al., 2016; Dohman, 2018; Gutiérrez-Jurado et al., 2019; Jaeger et al., 2019; Ward et al., 2018; Zimmer and McGlynn, 2017a). The source of streamflow, sometimes represented as the ratio of runoff to baseflow, where runoff refers to shallow inputs to surface water and baseflow refers to deeper groundwater inputs to surface flows, influences the ability of surface flow to persist between precipitation events (Jaeger et al., 2019; Segura et al., 2019). Despite the identification of many potential stream drying controls, hydrologists still do not understand the relative importance of each of these controls at different spatial and temporal scales.

1.3. Baseflow

The importance of groundwater in sustaining stream flows has long been recognized (section 1.3.1). Our reliance on hydrochemical tracers to better understand flowpaths may need to be modified slightly to understand stream drying, as discussed below. Nonetheless because stream drying occurs during low-flow periods, when groundwater is particularly important, it is valuable to review the baseflow literature in the context of low- to no-flow conditions.

1.3.1 Baseflow calculations and end-member mixing analysis

Baseflow has long been defined as the component of discharge coming from groundwater storage (Hall, 1968); however, even in early baseflow literature, there was confusion around the exact definition of baseflow and the best way to quantify it because it is inherently difficult to measure directly (Costelloe et al., 2015). Early attempts to quantify baseflow utilized stream hydrograph recession (Hall, 1968) and groundwater stage-groundwater discharge rating curves (Sklash and Farvolden, 1979). Discharge chemistry was also used to determine the groundwater component of discharge (Pinder and Jones, 1969). Hydrograph recession methods were improved by a modified digital filter technique (Arnold and Allen, 1999) and a physically based filter derived from a mass balance equation (Furey and Gupta, 2001). Stewart et al. (2007) modified the methods of Pinder and Jones (1969) by using streamflow conductivity to calculate baseflow with a mass-balance approach, and this method was later improved by Miller et al. (2014) who introduced continuous baseflow calculation using stream discharge and specific conductivity. The end-member mixing analysis (EMMA) utilized in Miller et al. (2014) is common across hydrology. EMMA and PCA have been combined to delineate water sources (Christophersen and Hooper, 1992), and quantified uncertainty using these methods (Genereux, 1998; Liu et al., 2004). EMMA is beneficial when a flowpath cannot be directly measured, such as baseflow. Although EMMA tools extend beyond the 2-endmember approach, we employ it here after careful consideration of the underlying assumptions.

The 2-endmember approach for calculating baseflow used in this thesis makes several assumptions. We first establish a run-off endmember and a baseflow endmember using specific conductivity data for each location by identifying the minimum and maximum conductivity at each baseflow monitoring locations. When defining these two endmembers, we assume several things: 1) no other water source is contributing significantly to streamflow generation, 2) the specific conductivities of the two endmembers remain constant over the period of the record, 3) runoff and baseflow endmembers are significantly different from another, and 4) the runoff and baseflow endmembers vary throughout the length of a single headwater stream and thus require unique endmembers for each baseflow monitoring location. Evidence from our field campaign supports these assumptions. Peaks in specific conductivity at a single location approached the same magnitude, suggesting that the local groundwater source contributing to baseflow remained constant throughout the season. We also observed the lowest specific conductivity at all locations at the start of the season. After fall rainstorms, specific conductivity dropped again, but never below the runoff dominated periods observed in early June. Each baseflow monitoring location had a unique maximum and minimum specific conductivity, and specific conductivity increased downstream in both streams. These observations suggest that the stream is either sourced by unique groundwater sources, or that groundwater is also flowing downgradient and accumulating additional solutes along its flowpath, thus requiring unique endmembers for each location.

1.3.2 Baseflow and low flow

Between precipitation events, and especially during low flow periods, surface flow is dependent on groundwater inputs, or baseflow, to persist (Segura et al., 2019; Winter, 2007). The frequency and duration of low-flow periods is expected to increase as climate change continues to alter the magnitude and timing of low-flow periods in the western U.S. and thus it is vital to understand of how baseflow is sourced to streams, and how baseflow might change as climate continues to change.

Despite the importance of baseflow to streamflow generation during low flow periods (Liu et al., 2013), its spatiotemporal heterogeneity makes it difficult to quantify and predict. Baseflow has been observed to be spatiotemporally dynamic (Duvert et al., 2018; Zimmer and McGlynn, 2017a), as it is influenced by many surface attributes such as topography, watershed size, evapotranspiration, and precipitation inputs (Cadol et al., 2012; Partington et al., 2012; Payn et al., 2012; Segura et al., 2019). The transport of groundwater to streams is also complicated by interactions between spatially heterogeneous and dynamic subsurface and surface processes (Fleckenstein et al., 2006; Ghosh et al., 2016; Kirchner, 2009a; McDonnell et al., 2007). To resolve these challenges, we need to quantify baseflow and stream drying at dense spatiotemporal scales in order to establish the baseflow-stream drying relationship.

1.4. Evapotranspiration losses

In addition to understanding baseflow inputs, drying is also influence by ET losses. Two ways such losses may be quantified at the watershed scale include: 1) evaluating diel cycles in streamflow, and 2) remote sensing of vegetation greenness as a proxy for ET losses.

1.4.1 Diel cycling

Diel cycling occurs when stream discharge experiences sinusoidal variations in a 24-hour period (Graham et al., 2013). During periods with limited precipitation, diel cycling is thought to be due to either evapotranspiration demands or snowmelt signals, each with an opposing effect (Bond et al., 2002; Geisler, 2016; Kirchner et al., in review, Wondzell et al., 2010). In springtime in snow-dominated systems, solar radiation peaks, snowmelt increases, and this causes a surge in discharge during the day (Loheide and Lundquist, 2009). In contrast, in systems without melting snow and with vegetation, increasing solar radiation leads to increases in evapotranspiration, thus decreasing stream discharge during the day because of uptake by plants (Graham et al., 2013).

Diel cycling has been observed in discharge (Daiji et al., 1990; Runkel et al., 2016; Sullivan and Drever, 2001), stream chemistry (Fortner et al., 2013), specific conductivity (Chapin et al., 2014), organic matter (Cullis et al., 2014; Worrall et al., 2015), and trace metals (Brick and Moore, 1996). In addition, diel cycling has been observed across a number of climates and watershed scales (Graham et al., 2013). During low-flow periods when snowmelt is not present, diel variability in discharge and water level has been used to estimate evapotranspiration demands (Boronina et al., 2005; Cadol et al., 2012; Fahle and Dietrich, 2014; White, 1932). Diel cycling variability has also been used to estimate the hydrologic connectivity between hillslopes and streams (Barnard et al., 2010), and the contributing area of vegetative water use (Bond et al., 2002).

While the link between vegetation water use and stream water level response is clear, gaps remain in understanding the spatial extent of vegetation that cause an in-stream response. For example, are diel changes in stream water levels due to local riparian evapotranspiration, local hillslope and riparian evapotranspiration, or an integration of hillslope and riparian evapotranspiration throughout the entire upstream portion of the watershed? Barnard et al. (2010) found that transpiration on hillslopes plays an important role in diel discharge patterns. Similarly, Wondzell et al. (2010) suggested that models attempting to explain diel fluctuations need to integrate lateral and hyporheic flows and should consider the local redistribution of water, the transport of evapotranspiration across the entire stream network, and the influence of hillslope transpiration. Building on these findings, a more comprehensive model is needed to explain how hillslope, riparian, and in stream processes impact diel cycling in headwater streams during low-flow, baseflow-dominated periods.

1.4.2 Vegetation greenness as a proxy for ET losses

Remotely sensed vegetation greenness metrics such as normalized difference vegetation index (NDVI) have served as indicators for changes in water availability to vegetation (Aguilar et al., 2012) as surface water and shallow groundwater sustains vegetation greenness (Fu and Burgher, 2015; Werstak et al., 2010). In arid and semi-arid regions throughout the western United States, vegetation is often dominated by drought tolerant plants such as sagebrush and grasses. These plants can thrive without persistent precipitation and are often brown or tan in color, particularly during summer months when precipitation is scarce. Dense, green vegetation is commonly found near stable water sources that allow water-dependent plant species to thrive. In southwestern Idaho, where sagebrush and grasses dominate the landscape, dense green riparian vegetation lines stream corridors where accumulated water enables water-dependent plant species to exist.

1.5. Site selection and the Reynolds Creek Experimental Watershed

1.1.1. Reynolds Creek Critical Zone Observatory

The Reynolds Creek Experimental Watershed (RCEW), also known as the Reynolds Creek Critical Zone Observatory (RC CZO), is a 239-km^2 catchment located in the Owyhee Range in southwestern Idaho. Elevations range from 1100 meters at the outlet to 2245 meters at the highest point (Seyfried et al., 2018). The watershed was instrumented by the Agricultural Research Service (ARS) and has been maintained for research since 1960. Reynolds Creek has variable geology (basalt, granite, andesite, and rhyolite) and vegetation throughout the watershed (Seyfried et al., 2018). Reynolds Creek drains the watershed before eventually flowing into the Snake River. It has long-term discharge (eleven stations) and weather records (32 stations) (Seyfried et al., 2018). In 2013, RCEW was established as a Critical Zone Observatory, prompting detailed studies on the linkages between carbon and water cycling in semi-arid systems (e.g. Chandler et al., 2018; Flerchinger et al., 2019; Kormos et al., 2014; Patton et al., 2019, 2018; Radke et al., 2019; Seyfried et al., 2018).

1.1.2. Site-selection within the rain-snow transition zone

The RC CZO is located at the rain-snow transition zone (Kormos et al., 2015) making it an ideal location to study the impacts of changing precipitation phase and associated shifts in partitioning of storage between the surface and subsurface on stream permanence. The rain-snow transition zone is the transition between wintertime precipitation regimes that are near 100% rain to near 100% snow (Klos et al., 2014). The current rain-snow transition zone has been identified in several locations using long-term climate observations and is recognized to be important to water resources at both regional and continental scales (Marks et al., 2013). However, the extent and elevation of the rain-snow transition zone is expected to react to changing climate (Nayak et al., 2010). Despite this importance, few published watershed-scale climate datasets exist (Godsey et al., 2018). Reynolds Creek is one of the few locations with a detailed long-term climate study at the rain-snow transition zone, making it an ideal location to advance our understanding of stream drying patterns across this transition in a changing climate.

This study focuses on two headwater sub-catchments within RCEW: Murphy Creek and Reynolds Mountain East (RME). Murphy Creek is located below the rain-snow transition zone and RME is located above (Kormos et al., 2016). The two sub-watersheds have different geology, vegetation, drainage areas, elevation, and primary recharge mechanisms (Table 1.1). The variation in these controls among the two sub-watersheds makes them an ideal place to study stream drying and establish which controls are the most important to our understanding of intermittent streams.

Table 1.1 Stream drying controls and the studies that identify the control as well as a brief summary of how the metric varies between RME and Murphy. Stream drying controls differ in RME and Murphy, and stream drying patterns are observed to vary as well.

Stream Drying Control	Citation	Murphy	RME
Upstream watershed area, Slope, TWI	Prancevic and Kirchner, 2019	Larger watershed (43.43 km^2) Steeper slopes Lower TWI	Smaller Watershed (43.43 km^2) Gentle slopes Higher TWI
Climate	Costigan et al., 2016; Jaeger et al., 2019; Jensen et al., 2019	Rain-dominated Less annual precip (464.96 mm/yr) Higher average temperature (7.16˚C)	Snow-dominated More annual precip (911.72 mm/yr) Cooler average temperature (4.73˚C)
Subsurface Properties	Costigan et al., 2016; Jaeger et al., 2019; Jensen et al., 2019; Ward et al., 2018	Salmon Creek volcanics and Reynolds Basin basalt and latite	Fractured basalt, Reynolds Basin basalt and latite
Evapotranspiration	Costigan et al., 2016; Jaeger et al., 2019; Jensen et al., 2019	Riparian bushes and hillslopes with sagebrush and willow	Aspen, conifers, sagebrush, willow, and meadows
Vegetation cover consistency	Warix & Godsey, 2020	Sparse clusters of riparian vegetation	Lower elevations: consistent riparian canopy Upper elevations: sparse riparian bushes/meadow

1.6. Thesis overview

In this thesis, I first explore diel cycles in stream drying and their likely controls and implications (Chapter 2) before detailing subsurface baseflow contributions to intermittent streams (Chapter 3). Finally, I discuss the implications of this work in the context of revisions to the Clean Water Rule and make suggestions for future stream drying studies in Chapter 4.

1.7. References

Aguilar, C., Zinnert, J.C., Polo, M.J., Young, D.R., 2012. NDVI as an indicator for changes in water availability to woody vegetation. Ecol. Indic. 23, 290–300. https://doi.org/10.1016/j.ecolind.2012.04.008

Anderson, M.G., Burt, T.P., 1978. Analysis of spatial water quality and stream networks in the southern Cotswolds during and after the drought of 1976. Earth Surf Process. 3, 59–69. https://doi.org/10.1002/esp.3290030106

Arnold, J.G., Allen, P.M., 1999. Automated methods for estimating baseflow and ground water recharge from streamflow records. J. Am. Water Resour. Assoc. 35, 13353–13366.

Barnard, H.R., Graham, C.B., Van Verseveld, W.J., Brooks, J.R., Bond, B.J., McDonnell, J.J., 2010. Mechanistic assessment of hillslope transpiration controls of diel subsurface flow: a steady-state irrigation approach. Ecohydrology 3, 133–142. https://doi.org/10.1002/eco.114

Bishop, K., Buffam, I., Erlandsson, M., Fölster, J., Laudon, H., Siebeet, J., Temnerud, J., 2008. Aqua Incognita: the unknown headwaters. Hydrol. Process. 22, 2267–2274. https://doi.org/10.1002/hyp.7049

Blasch, K.W., Ferré, T.P.A., Christensen, A.H., Hoffmann, J.P., 2002. New Field Method to Determine Streamflow Timing Using Electrical Resistance Sensors. Vadose Zo. J. 1, 289. https://doi.org/10.2136/vzj2002.2890

Blyth, K., Rodda, J.C., 1973. A stream length study 9, 1454–1461.

Bond, B.J., Jones, J.A., Moore, G., Phillips, N., Post, D., McDonnell, J.J., 2002. The zone of vegetation influence on baseflow revealed by diel patterns of streamflow and vegetation water use in a headwater basin. Hydrol. Process. 16, 1671–1677. https://doi.org/10.1002/hyp.5022

Boronina, A., Golubev, S., Balderer, W., 2005. Estimation of actual evapotranspiration from an alluvial aquifer of the Kouris catchment (Cyprus) using continuous streamflow records. Hydrol. Process. 19, 4055–4068. https://doi.org/10.1002/hyp.5871

Boulton, A.J., Rolls, R.J., Jaeger, K.L., Datry, T., 2017. Hydrological Connectivity in Intermittent Rivers and Ephemeral Streams, Intermittent Rivers and Ephemeral Streams: Ecology and Management. Elsevier Inc. https://doi.org/10.1016/B978-0-12-803835-2.00004-8

Brick, C.M., Moore, J.N., 1996. Diel variation of trace metals in the upper Clark Fork River, Montana. Environ. Sci. Technol. 30, 1953–1960. https://doi.org/10.1021/es9506465

Cadol, D., Kampf, S., Wohl, E., 2012. Effects of evapotranspiration on baseflow in a tropical headwater catchment. J. Hydrol. 462–463, 4–14. https://doi.org/10.1016/j.jhydrol.2012.04.060

Carlston, C.W., 1963. Drainage density and streamflow. U.S. Geol. Surv. Prof. Pap. No. 42 2–C, 8pp.

Chandler, D.G., Cheng, Y., Seyfried, M.S., Madsen, M.D., Johnson, C.E., Williams, C.J., 2018. Seasonal Wetness, Soil Organic Carbon, and Fire Influence Soil Hydrological Properties and Water Repellency in a Sagebrush-Steppe Ecosystem. Water Resour. Res. 54, 8514–8527. https://doi.org/10.1029/2017WR021567

Chapin, T.P., Todd, A.S., Zeigler, M.P., 2014. Robust, low-cost data loggers for stream temperature, flow intermittency, and relative conductivity monitoring. Water Resour. Res. 50, 6542–6548. https://doi.org/10.1002/2013WR015158

Christophersen, N., Hooper, R.P., 1992. Multivariate analysis of stream water chemical data: The use of principal components analysis for the end-member mixing problem. Water Resour. Res. 28, 99–107.

Costelloe, J.F., Peterson, T.J., Halbert, K., Western, A.W., Mcdonnell, J.J., 2015. Groundwater surface mapping informs sources of catchment baseflow. Hydrol. Earth Syst. Sci. 19, 1599–1613. https://doi.org/10.5194/hess-19-1599-2015

Costigan, K.H., Jaeger, K.L., Goss, C.W., Fritz, K.M., Goebel, P.C., 2016. Understanding controls on flow permanence in intermittent rivers to aid ecological research: integrating meteorology, geology and land cover. Ecohydrology 9, 1141–1153. https://doi.org/10.1002/eco.1712

Cullis, J.D.S., Stanish, L.F., McKnight, D.M., 2014. Diel flow pulses drive particulate organic matter transport from microbial mats in a glacial meltwater stream in the McMurdo Dry Valleys. Water Resour. Res. 50, 86–97. https://doi.org/10.1002/2013WR014061

Daiji, K., Suzuki, K., Nomura, M., 1990. Diurnal fluctuation in stream flow and in specific electric conductance during drought periods. J. Hydrol. 115, 105–114. https://doi.org/10.1016/0022-1694(90)90200-H

Datry, T., Arscott, D.B., Sabater, S., 2011. Recent perspectives on temporary river ecology. Aquat. Sci. 73, 453–457. https://doi.org/10.1007/s00027-011-0236-1

Datry, T., Larned, S.T., Tockner, K., 2014. Intermittent rivers: A challenge for freshwater ecology. Bioscience 64, 229–235. https://doi.org/10.1093/biosci/bit027

Day, D.G., 1978. Drainage density changes during rainfall. Earth Surf. Process. 3, 319–326. https://doi.org/10.1002/esp.3290030310

Dingman, S.L., 1978. Drainage Density and Streamflow : A Closer Look. Water Resour. Res. 14, 1183–1187. https://doi.org/0043-1397/78/068W-0818$01.00

Dohman, J., 2018. Three-dimensional subsurface controls on stream intermittency in a semi-arid landscape. Idaho State University.

Duvert, C., Butman, D.E., Ribolzi, O., Marx, A., Hutley, L.B., 2018. CO2 evasion along streams driven by groundwater inputs and geomorphic controls. Nat. Geosci. 11, 813–818. https://doi.org/10.1038/s41561-018-0245-y

Earman, S., Dettinger, M., 2011. Potential impacts of climate change on groundwater resources - A global review. J. Water Clim. Chang. 2, 213–229. https://doi.org/10.2166/wcc.2011.034

Fahle, M., Dietrich, O., 2014. Estimation of evapotranspiration using diurnal groundwater level fluctuations: Comparison of different approaches with groundwater lysimeter data. Water Resour. Res. 50, 273–286. https://doi.org/10.1002/2013WR014472

Fleckenstein, J.H., Niswonger, R.G., Fogg, G.E., 2006. River-aquifer interactions, geologic heterogeneity, and low-flow management. Ground Water 44, 837–852. https://doi.org/10.1111/j.1745-6584.2006.00190.x

Flerchinger, G.N., Fellows, A.W., Seyfried, M.S., Clark, P.E., Lohse, K.A., 2019. Water and Carbon Fluxes Along an Elevational Gradient in a Sagebrush Ecosystem. Ecosystems. https://doi.org/10.1007/s10021-019-00400-x

Fu, B., Burgher, I., 2015. Riparian vegetation NDVI dynamics and its relationship with climate, surface water and groundwater. J. Arid Environ. 113, 59–68. https://doi.org/10.1016/j.jaridenv.2014.09.010

Furey, P.R., Gupta, V.K., 2001. A physically based filter for separating base flow from streamflow time series. Water Resour. Res. 37, 2709–2722. https://doi.org/10.1029/2001WR000243

Gallo, E.L., Lohse, K.A., Brooks, P.D., McIntosh, J.C., Meixner, T., McLain, J.E.T., 2012. Quantifying the effects of stream channels on storm water quality in a semi-arid urban environment. J. Hydrol. 470–471, 98–110. https://doi.org/10.1016/j.jhydrol.2012.08.047

Geisler, E.T., 2016. Riparian zone evapotranspiration using streamflow diel signals. Boise State University. https://doi.org/10.1017/CBO9781107415324.004

Genereux, D., 1998. Quantifying uncertainty in tracer-based hydrograph separations. Water Resour. Res. 34, 915–919. https://doi.org/10.1029/98WR00010

Ghosh, D.K., Wang, D., Zhu, T., 2016. On the transition of base flow recession from early stage to late stage. Adv. Water Resour. 88, 8–13. https://doi.org/10.1016/j.advwatres.2015.11.015

Godsey, S.E., Kirchner, J.W., 2014. Dynamic, discontinuous stream networks: Hydrologically driven variations in active drainage density, flowing channels and stream order. Hydrol. Process. 28, 5791–5803. https://doi.org/10.1002/hyp.10310

Godsey, S.E., Kirchner, J.W., Tague, C.L., 2013. Effects of changes in winter snowpacks on summer low flows: case studies in the Sierra Nevada, California, USA. https://doi.org/10.1002/hyp.9943

Godsey, S.E., Marks, D., Kormos, P.R., Seyfried, M.S., Enslin, C.L., Winstral, A.H., McNamara, J.P., Link, T.E., 2018. Eleven years of mountain weather, snow, soil moisture and streamflow data from the rain-snow transition zone - The Johnston Draw catchment, Reynolds Creek Experimental Watershed and Critical Zone Observatory, USA. Earth Syst. Sci. Data 10, 1207–1216. https://doi.org/10.5194/essd-10-1207-2018

Gomi, T., Sidle, R.C., Richardson, J.S., 2002. Understanding processes and downstream linkages of headwater systems. Bioscience 52, 905–916. https://doi.org/10.1641/0006-3568(2002)052[0905:UPADLO]2.0.CO;2

González-Ferreras, A.M., Barquín, J., 2017. Mapping the temporary and perennial character of whole river networks. Water Resour. Res. 53, 6709–6724. https://doi.org/10.1002/2017WR020390

Goulsbra, C., Evans, M., Lindsay, J., 2014. Temporary streams in a peatland catchment: Pattern, timing, and controls on stream network expansion and contraction. Earth Surf. Process. Landforms 39, 790–803. https://doi.org/10.1002/esp.3533

Graham, C.B., Barnard, H.R., Kavanagh, K.L., McNamara, J.P., 2013. Catchment scale controls the temporal connection of transpiration and diel fluctuations in streamflow. Hydrol. Process. 27, 2541–2556. https://doi.org/10.1002/hyp

Gutiérrez-Jurado, K.Y., Partington, D., Batelaan, O., Cook, P., Shanafield, M., 2019. What triggers streamflow for intermittent rivers and ephemeral streams in low-gradient catchments in mediterranean climates. Water Resour. Res. 55, 9926–9946. https://doi.org/10.1029/2019WR025041

Hale, R.L., Godsey, S.E., 2019. Dynamic stream network intermittence explains emergent dissolved organic carbon chemostasis in headwaters. Hydrol. Process. 33, 1926–1936. https://doi.org/10.1002/hyp.13455

Hall, F.R., 1968. Base-Flow Recessions—A Review. Water Resour. Res. 4, 973–983. https://doi.org/10.1029/WR004i005p00973

Jaeger, K.L., Olden, J.D., Pelland, N.A., 2014. Climate change poised to threaten hydrologic connectivity and endemic fishes in dryland streams. Proc. Natl. Acad. Sci. U. S. A. 111, 13894–13899. https://doi.org/10.1073/pnas.1320890111

Jaeger, K.L., Sando, R., McShane, R.R., Dunham, J.B., Hockman-Wert, D.P., Kaiser, K.E., Hafen, K., Risley, J.C., Blasch, K.W., 2019. Probability of Streamflow Permanence Model (PROSPER): A spatially continuous model of annual streamflow permanence throughout the Pacific Northwest. J. Hydrol. X 2, 100005. https://doi.org/10.1016/J.HYDROA.2018.100005

Jensen, C.K., McGuire, K.J., McLaughlin, D.L., Scott, D.T., 2019. Quantifying spatiotemporal variation in headwater stream length using flow intermittency sensors. Environ. Monit. Assess. 191. https://doi.org/10.1007/s10661-019-7373-8

Kirchner, J.W., 2009. Catchments as simple dynamical systems: Catchment characterization, rainfall-runoff modeling, and doing hydrology backward. Water Resour. Res. 45, 1–34. https://doi.org/10.1029/2008WR006912

Klos, Z.P., Link, T.E., Abatzoglou, J.T., 2014. Extent of the rain-snow transition zone in the western U.S. under historic and projected climate. Geophys. Prospect. 6413–6419. https://doi.org/10.1002/2014GL061184.Received

Kormos, P.R., Marks, D., Seyfried, M., Havens, S., Hendrick, A., Lohse, K.A., Masarik, M., Flores, A.N., 2016. 31 years of spatially distributed air temperature, humidity, precipitation amount and precipitation phase from a mountain catchment in the rain-snow transition zone. https://doi.org/10.18122/B2B59V

Kormos, P.R., Marks, D., Williams, C.J., Marshall, H.P., Aishlin, P., Chandler, D.G., McNamara, J.P., 2014. Soil, snow, weather, and sub-surface storage data from a mountain catchment in the rain-snow transition zone. Earth Syst. Sci. Data 6, 165–173. https://doi.org/10.5194/essd-6-165-2014

Kormos, P.R., McNamara, J.P., Seyfried, M.S., Marshall, H.P., Marks, D., Flores, A.N., 2015. Bedrock infiltration estimates from a catchment water storage-based modeling approach in the rain snow transition zone. J. Hydrol. 525, 231–248. https://doi.org/10.1016/j.jhydrol.2015.03.032

Levick, L.R., Goodrich, D.C., Hernandez, M., Fonseca, J., Semmens, D.J., Stromberg, J., Tluczek, M., Leidy, R.A., Scianni, M., Guertin, D.P., 2008. The ecological and hydrological significance of ephemeral and intermittent Streams in the arid and semi-arid American Southwest.

Liu, F., Hunsaker, C., Bales, R.C., 2013. Controls of streamflow generation in small catchments across the snow-rain transition in the Southern Sierra Nevada, California. Hydrol. Process. 27, 1959–1972. https://doi.org/10.1002/hyp.9304

Liu, F., Williams, M.W., Caine, N., 2004. Source waters and flow paths in an alpine catchment, Colorado Front Range, United States. Water Resour. Res. 40, 1–16. https://doi.org/10.1029/2004WR003076

Loheide, S.P., Lundquist, J.D., 2009. Snowmelt-induced diel fluxes through the hyporheic zone. Water Resour. Res. 45, 1–9. https://doi.org/10.1029/2008WR007329

Lovill, S.M., Hahm, W.J., Dietrich, W.E., 2018. Drainage from the Critical Zone: Lithologic Controls on the Persistence and Spatial Extent of Wetted Channels during the Summer Dry Season. Water Resour. Res. 54, 5702–5726. https://doi.org/10.1029/2017WR021903

Marks, D., Winstral, A., Reba, M., Pomeroy, J., Kumar, M., 2013. An evaluation of methods for determining during-storm precipitation phase and the rain/snow transition elevation at the surface in a mountain basin. Adv. Water Resour. 55, 98–110. https://doi.org/10.1016/j.advwatres.2012.11.012

McDonnell, J.J., Sivapalan, M., Vaché, K., Dunn, S., Grant, G., Haggerty, R., Hinz, C., Hooper, R., Kirchner, J., Roderick, M.L., Selker, J., Weiler, M., 2007. Moving beyond heterogeneity and process complexity: A new vision for watershed hydrology. Water Resour. Res. https://doi.org/10.1029/2006WR005467

Miller, M.P., Susong, D.D., Shope, C.L., Heilweil, V.M., Stolp, B.J., 2014. Continuous estimation of baseflow in snowmelt-dominated streams and rivers in the Upper Colorado River Basin: A chemical hydrograph separation approach. Water Resour. Res. 50, 6986–6999. https://doi.org/10.1002/2013WR014939

Mote, P.W., Li, S., Lettenmaier, D.P., Xiao, M., Engel, R., 2018. Dramatic declines in snowpack in the western US. npj Clim. Atmos. Sci. 1. https://doi.org/10.1038/s41612-018-0012-1

Nayak, A., Marks, D., Chandler, D.G., Seyfried, M., 2010. Long-term snow, climate, and streamflow trends at the reynolds creek experimental watershed, Owyhee Mountains, Idaho, United States. Water Resour. Res. 46, 1–15. https://doi.org/10.1029/2008WR007525

Partington, D., Brunner, P., Simmons, C.T., Werner, A.D., Therrien, R., Maier, H.R., Dandy, G.C., 2012. Evaluation of outputs from automated baseflow separation methods against simulated baseflow from a physically based, surface water-groundwater flow model. J. Hydrol. 458–459, 28–39. https://doi.org/10.1016/j.jhydrol.2012.06.029

Patton, N.R., Lohse, K.A., Godsey, S.E., Crosby, B.T., Seyfried, M.S., 2018. Predicting soil thickness on soil mantled hillslopes. Nat. Commun. 9. https://doi.org/10.1038/s41467-018-05743-y

Patton, N.R., Lohse, K.A., Seyfried, M., Will, R., Benner, S.G., 2019. Lithology and coarse fraction adjusted bulk density estimates for determining total organic carbon stocks in dryland soils. Geoderma 337, 844–852. https://doi.org/10.1016/j.geoderma.2018.10.036

Payn, R.A., Gooseff, M.N., McGlynn, B.L., Bencala, K.E., Wondzell, S.M., 2012. Exploring changes in the spatial distribution of stream baseflow generation during a seasonal recession. Water Resour. Res. 48, 1–15. https://doi.org/10.1029/2011WR011552

Peirce, S.E., Lindsay, J.B., 2015. Characterizing ephemeral streams in a southern Ontario watershed using electrical resistance sensors. Hydrol. Process. 29, 103–111. https://doi.org/10.1002/hyp.10136

Perkin, J.S., Gido, K.B., 2012. Fragmentation alters stream fish community structure in dendritic ecological networks. Ecol. Appl. 22, 2176–2187. https://doi.org/10.1890/12-0318.1

Pinder, G.F., Jones, J.F., 1969. Determination of the ground-water component of peak discharge from the chemistry of total runoff. Water Resour. Res. 5, 438–445.

Prancevic, J.P., Kirchner, J.W., 2019. Topographic Controls on the Extension and Retraction of Flowing Streams. Geophys. Res. Lett. 46, 2084–2092. https://doi.org/10.1029/2018GL081799

Queener, N., 2015. Spatial and temporal variability in baseflow and stream drying in the Mattole River Headwaters. Humboldt State University. https://doi.org/10.1007/springerreference_226434

Radke, A.G., Godsey, S.E., Lohse, K.A., McCorkle, E.P., Perdrial, J., Seyfried, M.S., Holbrook, W.S., 2019. Spatiotemporal heterogeneity of water flowpaths controls dissolved organic carbon sourcing in a snow-dominated, headwater catchment. Front. Ecol. Evol. 7. https://doi.org/10.3389/fevo.2019.00046

Runkel, R.L., McKnight, D.M., Andrews, E.D., 2016. Analysis of Transient Storage Subject to Unsteady Flow : Diel Flow Variation in an Antarctic Stream. J. North Am. Benthol. Soc. 17, 143–154.

Segura, C., Noone, D., Warren, D., Jones, J.A., Tenny, J., Ganio, L.M., 2019. Climate, Landforms, and Geology Affect Baseflow Sources in a Mountain Catchment. Water Resour. Res. 55, 5238–5254. https://doi.org/10.1029/2018WR023551

Seyfried, M., Lohse, K., Marks, D., Flerchinger, G., Pierson, F., Holbrook, W.S., 2018. Reynolds Creek Experimental Watershed and Critical Zone Observatory. Vadose Zo. J. 17, 1–20. https://doi.org/10.2136/vzj2018.07.0129

Sklash, M.G., Farvolden, R.N., 1979. The role of groundwater in storm runoff. J. Hydrol. 43, 45–65. https://doi.org/10.1016/0022-1694(79)90164-1

Steward, A.L., Von Schiller, D., Tockner, K., Marshall, J.C., Bunn, S.E., 2012. When the river runs dry: Human and ecological values of dry riverbeds. Front. Ecol. Environ. 10, 202–209. https://doi.org/10.1890/110136

Stewart, M., Cimino, J., Ross, M., 2007. Calibration of base flow separation methods with streamflow conductivity. Ground Water 45, 17–27. https://doi.org/10.1111/j.1745-6584.2006.00263.x

Sullivan, A.B., Drever, J.I., 2001. Spatiotemporal variability in stream chemistry in a high-elevation catchment affected by mine drainage. J. Hydrol. 252, 237–250. https://doi.org/10.1016/S0022-1694(01)00458-9

U.S. Environmental Protection Agency and U.S. Army Corps of Engineers, 2015. Technical Support Document for the Clean Water Rule: Definition of Waters of the United States. U.S. Environ. Prot. Agency.

Valencia-Cardona, J.J., Shukla, G., Wu, Z., Houser, C., Yuen, D.A., Wentzcovitch, R.M., 2016. Influence of the iron spin crossover in ferropericlase on the lower mantle geotherm.

von Schiller, D., Acuña, V., Graeber, D., Martí, E., Ribot, M., Sabater, S., Timoner, X., Tockner, K., 2011. Contraction, fragmentation and expansion dynamics determine nutrient availability in a Mediterranean forest stream. Aquat. Sci. 73, 485–497. https://doi.org/10.1007/s00027-011-0195-6

Ward, A.S., Schmadel, N.M., Wondzell, S.M., 2018. Simulation of dynamic expansion, contraction, and connectivity in a mountain stream network. Adv. Water Resour. 114, 64–82. https://doi.org/10.1016/j.advwatres.2018.01.018

Werstak, C.E.J., Housman, I., Maus, P., Fisk, H., Gurrieri, J., Carlson, C.P., Johnston, B.C.; Stratton, B.; Hurja, J.C., 2010. Groundwater-Dependent Ecosystem Inventory Using Remote Sensing, RSAC-10011-RPT1, U.S. Department of Agriculture, Forest Service, Remote Sensing Applications Center.

White, W.N., 1932. A method of estimating ground-water supplies based on discharge by plants and evaporation from soil. USGS Water-Supply Pap. no. 659-A.

Whiting, J.A., Godsey, S.E., 2016. Discontinuous headwater stream networks with stable flowheads, Salmon River basin, Idaho. Hydrol. Process. 30, 2305–2316. https://doi.org/10.1002/hyp.10790

Winter, T.C., 2007. The role of ground water in generating streamflow in headwater areas and in maintaining base flow. J. Am. Water Resour. Assoc. 43, 15–25. https://doi.org/10.1111/j.1752-1688.2007.00003.x

Wondzell, S.M., Gooseff, M.N., McGlynn, B.L., 2010. An analysis of alternative conceptual models relating hyporheic exchange flow to diel fluctuations in discharge during baseflow recession. Hydrol. Process. 24, 686–694. https://doi.org/10.1002/hyp.7507

Worrall, F., Howden, N.J.K., Burt, T.P., 2015. Understanding the diurnal cycle in fluvial dissolved organic carbon - The interplay of in-stream residence time, day length and organic matter turnover. J. Hydrol. 523, 830–838. https://doi.org/10.1016/j.jhydrol.2015.01.075

Yu (于松延), S., Bond, N.R., Bunn, S.E., Xu, Z., Kennard, M.J., 2018. Quantifying spatial and temporal patterns of flow intermittency using spatially contiguous runoff data. J. Hydrol. 559, 861–872. https://doi.org/10.1016/j.jhydrol.2018.03.009

Zimmer, M.A., McGlynn, B.L., 2017. Bidirectional stream–groundwater flow in response to ephemeral and intermittent streamflow and groundwater seasonality. Hydrol. Process. 31, 3871–3880. https://doi.org/10.1002/hyp.11301

2. Chapter 2: Diel cycling and stream drying: How do changes in temperature and solar radiation impact the timing of drying?

2.1. Abstract

Headwater stream networks source over half the discharge to the global river network, and over half the length of headwater streams have been observed to be intermittent. Though intermittent streams are common, many aspects of spatiotemporal stream drying behavior have not been captured and thus the drivers behind drying are poorly understood. We use a dense spatiotemporal stream drying dataset coupled with solar radiation and temperature measurements to quantify stream drying patterns and their controls in two headwater streams in the Reynolds Creek Critical Zone Observatory in southwestern Idaho. We are among the first to observe and characterize daily wet-dry cycles before the stream dries seasonally at multiple locations throughout the stream network. During a diel cycle, the stream begins drying within one hour of peak solar radiation independent of location in the stream and time of year. Additionally, the time that a stream spends dry during each wet-dry diel cycling pulse increases with each subsequent day. However, large increases or decreases ($\pm$100 W/m^2/day or more) in solar radiation prolong or shorten, respectively, the time that a location spends dry during a diel cycling period. Finally, we synthesize work on the relative importance of different controls on stream drying and highlight remaining research gaps.

2.2. Introduction

Hillslopes, headwater streams, and downstream waters are all components of an integrated hydrological system (Nadeau and Rains, 2007). Headwater streams are first and second order streams that originate at the uppermost elevations of a watershed and are sourced by hillslopes where flow accumulates and contributes to downstream tributaries. Headwater streams source over half the discharge to the global river network (Costigan et al., 2016), provide essential habitat for migrating riparian species (US EPA, 2015), and transport sediment, solutes, and nutrients downstream water supplies (Gomi et al., 2002). Headwater streams are commonly intermittent or ephemeral (Datry et al., 2014; Nadeau and Rains, 2007) and often contract from their uppermost reaches, as modeled in Ward et al. (2018). Stream drying is spatiotemporally heterogeneous even within a single headwater stream (González-Ferreras and Barquín, 2017; Jensen et al., 2019; Queener, 2015; Yu (于松延) et al., 2018). Short dry segments (<50 m) have been observed between flowing segments (Hale and Godsey, 2019; MacNeille et al., in prep), indicating that stream drying controls vary significantly throughout the length of a single stream. Heterogeneity complicates the ability of hydrologists to predict spatiotemporal stream drying patterns accurately (González-Ferreras and Barquín, 2017; Jaeger et al., 2019; Ward et al., 2018), and it remains difficult to model the flowing extent of a stream at any given time. In order to model or even classify streams, we need a more developed understanding of the range of spatiotemporal stream drying behavior at a fine scale and the mechanisms controlling its behavior.

One of the most common temporal patterns in streamflow is the diel – or ~24-hour – cycle. Diel cycles have been observed in stream discharge (Daiji et al., 1990; Runkel et al., 2016; Sullivan and Drever, 2001), chemistry (Brick and Moore, 1996; Fortner et al., 2013), and organic matter (Cullis et al., 2014; Worrall et al., 2015). Evapotranspiration (ET) and snowmelt are the primary drivers of diel fluctuations (Bond et al., 2002; Geisler, 2016; Kirchner et al., in review, Wondzell et al., 2010). Daily variation in flows and stream chemistry can be attributed to the complex hydrologic network connecting plants and soil to the stream (Wondzell et al., 2010). When ET (as opposed to snowmelt) is driving diel cycling, streamflow and groundwater levels are lowest in the late afternoon to evening (Kirchner et al., in review). Both hillslope and riparian vegetation influence diel cycling, but their relative importance is still in debate (Graham et al., 2013). In addition, diel changes in water level have been used to estimate evapotranspiration losses (Boronina et al., 2005; Cadol et al., 2012; Fahle and Dietrich, 2014; White, 1932), especially during low flow and baseflow-dominated periods (Bond et al., 2002; Cadol et al., 2012; Wondzell et al., 2010), but no studies have yet explored diel cycles of daytime drying and nighttime wetting. Diel cycles of stream drying may be an effective tool to link diel groundwater level and evapotranspiration patterns to understand stream drying.

The objective of this study is both to characterize and interpret the primary mechanisms controlling spatiotemporal variation in stream drying patterns. We seek to answer the following questions: 1) what are fine-scale patterns of stream drying throughout a network over a seasonal recession and 2) do large changes in daily peak solar radiation and temperature influence the timing of stream drying patterns? To address these questions, we measured the presence or absence of surface water throughout two headwater streams at 15-minute intervals during the seasonal recession from June to October and compared their drying patterns to daily peak temperature and solar radiation.

2.3. Site Description

Two headwater streams in the Reynolds Creek Experimental Watershed and Critical Zone Observatory (RC CZO) were selected to study stream drying patterns, Murphy Creek and

Reynolds Mountain East Creek (RME) (Figure 2.1A). The RC CZO is well instrumented and provides long-term data with respect to stream flow and precipitation. However, stream drying patterns have not been characterized. We chose Murphy Creek and RME to study stream drying patterns because they both have long-term discharge and climate records, exhibit different spatial and temporal stream drying patterns, are located above and below the rain-snow transition zone, and have different vegetation and geology as detailed below. Comparison of drying patterns and landscape features at these two watersheds will enable identification of how relative importance of stream drying controls may vary over different land types.

The Murphy Creek watershed (1598 m mean elevation) spans the local rain-snow transition and is drained by a 2.5 km channel (Figure 2.1B). RME drains the highest elevations of RC CZO (2075 m mean elevation) via two branches that converge, totaling 1.1 km of channel (Figure 2.1C). Murphy and RME drain 1.29 km^2 and 0.43 km^2, respectively. The primary source of recharge (mean annual precipitation = 912 mm/year) in RME is snowmelt as the watershed receives >50% of its mean annual precipitation as snow (Kormos et al., 2016); Murphy Creek is located below the rain-snow transition and receives >50% of its mean annual precipitation as rain (mean annual precipitation = 639 mm/year) (Kormos et al., 2016). The mean annual streamflow at the outlets of Murphy Creek and RME are 0.00752 and 0.00671 m^3s^{-1}, respectively (Pierson et al., 2000).

The lower portion of Murphy Creek is composed of andesite with olivine basalt, a thin tuff unit, and latite in the upper portions of the watershed; in RME, latite, olivine basalt, and andesite are present. Murphy's hillslopes are covered by sagebrush and grasses such as big sagebrush (*Artemisia tridentata*), bitter brush (*Purshia tridentata*), low sagebrush (*Artemisia arbuscula*), snowberry (*Symphoricarpos*), rabbit brush (*Ericameria nauseosa*), Sandberg bluegrass (*Poa secunda*), and Idaho Fescue (*Festuca idahoensis*) (Stephenson, 1970). The Murphy Creek channel is lined with riparian vegetation consisting of small bushes and willow, such as peach leaf willow (*Salix amygdaloides*), coyote willow (*Salix exigua*), red osier dogwood (*Cornus sericea*), woods rose (*Rosa woodsii*), chokecherry (*Prunus virginiana*), wax currant (*Ribes cereum*), and shrubby cinquefoil (*Dasiphora fruticose*) (personal communication with Mark Seyfried & Pat Clark). RME is primarily covered by sagebrush (*Artemesia spp.*) and grasses, but also contains patchy conifer (principally Douglas fir, *Pseudotsuga menzeii (Mirb*.)) and quaking aspen groves (*Populus tremuloides Michx.*) that vary with elevation, aspect, and wind distribution of snow. Riparian channels primarily contain willow (*Salix spp.*) (Radke, 2018). In 2015, the Soda Fire burned the Murphy watershed, and basin characteristics such as foliar cover, discharge, and sediment fluxes largely recovered from the fire within two years (Glossner et al., in prep; Lohse et al., in prep; Vega et al., 2020).

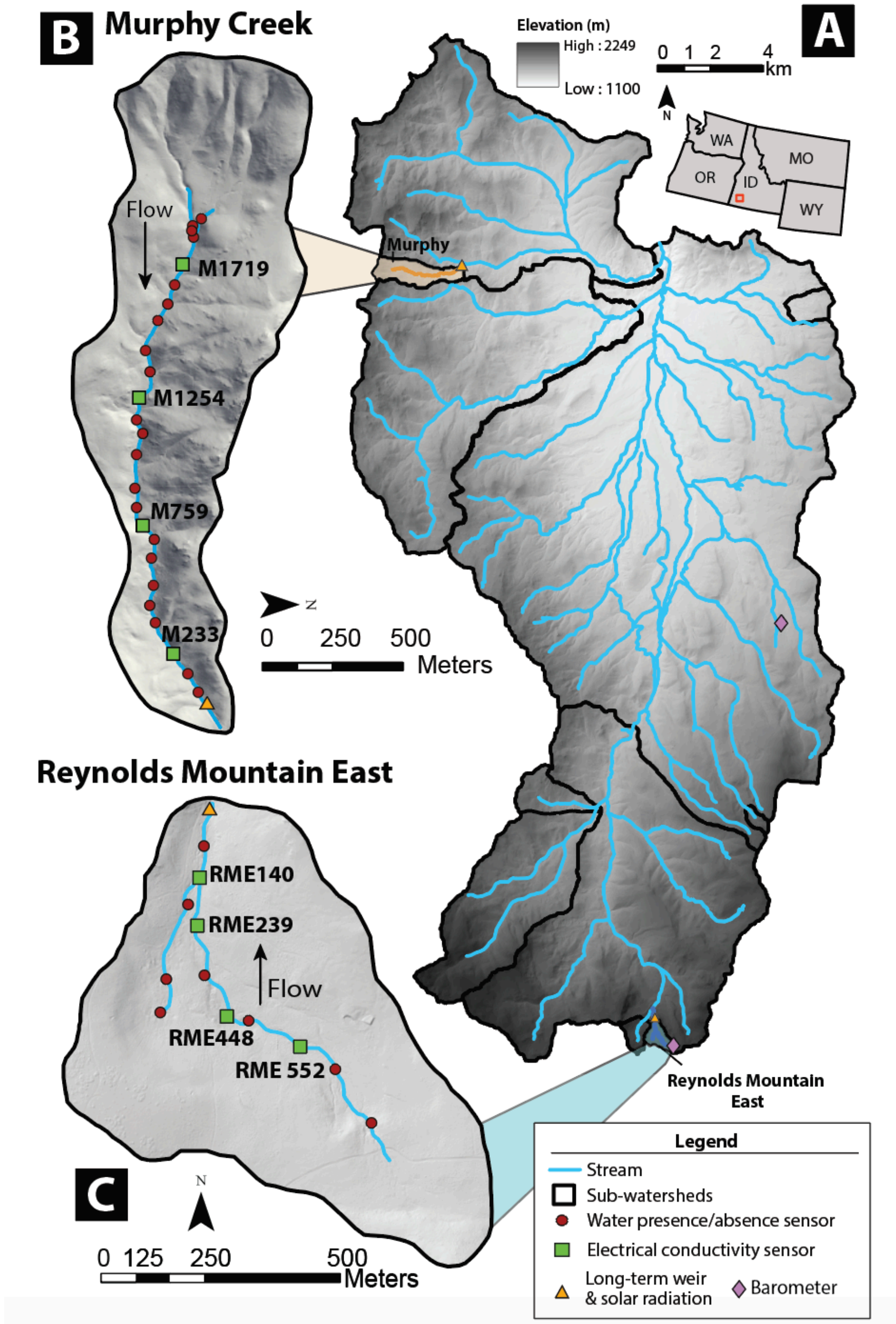

Figure 2.1 **(A)** Reynolds Creek Critical Zone Observatory with sub-watersheds Murphy Creek and Reynolds Mountain East (RME) highlighted in orange and blue, respectively. Instrumentation at **B.** Murphy Creek and **C.** RME, is described in section 2.4.1.

2.4. Methods

2.4.1. Field data collection

Water presence or absence was observed with both freshwater HOBO electrical conductivity (EC) dataloggers (Onset Hobologger, U-24) and HOBO Pendant Loggers (Onset HOBO Pendant/Light 64K Datalogger UA-002-64) to record relative conductivity and temperature. The Pendant/Light 64K Dataloggers were modified following methods from Chapin et al. (2014). Pendants were housed in Polyvinyl chloride (PVC) and installed so that the two pole electrodes at the bottom of the plastic housing were in constant contact with the stream bed and thus were able to detect the lowest of flows. Pendants were located at the deepest part of the channel, typically in pools below steps. EC sensors were housed in PVC tubing that was drilled with holes facing the stream bed and placed in pools.

Twenty-one Pendant loggers were installed throughout Murphy Creek, and four EC loggers were interspersed between every five Pendant sensors (Figure 2.1B). In RME, four EC loggers were interspersed between eight Pendant sensors (Figure 2.1C). Each Pendant sensor is hereby referred to as MX or RMEX, where X is the distance in meters from the downstream outlet weir at each respective watershed and M and RME refer to the Murphy and Reynolds Mountain East sub-watersheds, respectively. All sensors were recording at 15-minute intervals from June 3, 2019 to October 1, 2019. Seven of the Pendant sensors in Murphy Creek were added on July 10, 2019 (M454, M716, M823, M1121, M1377, and M1653). For each of these seven additional sensors, continuous flow was assumed from June 3 to 12, 2019; this assumption was validated by field observations. If no gaps in flow were observed between July 10 to 17, 2019, continuous flow was assumed from June 3, 2019 to July 10, 2019 (M454, M716, M1377, and M1653). If any gaps in flow were observed between July 10 and July 17, 2019, we made no assumptions about whether the stream was flowing or dry between June 12, 2019 to July 10, 2019 (M823, M1121, M1951). Any other gaps in flow presence records are due to logger failure (M1166, M1653, M1799).

RME and Murphy Creeks were mapped in-person six times during summer 2019 (Table 2.1) by noting where flow started and stopped using the Avenza Maps phone application. Flow maps were generated in ArcGIS Pro (ESRI, California).

Table 2.1. Dates when the entirety of Murphy and RME creeks were mapped in-person.

Murphy Creek	RME
06/04/2019	06/05/2019
06/12/2019	06/11/2019
07/09/2019	07/08/2019
08/08/2019	08/07/2019
09/09/2019	09/10/2019
10/01/2019	10/01/2019

Solar radiation was measured in the Murphy Creek sub-watershed using an Epply sensor at 15-minute intervals throughout the duration of the field season in W/m^2. In this thesis, solar radiation data was not used to assess drying patterns at RME. Solar radiation measurements are collected and maintained by the USDA Agricultural Research Service.

2.4.2 Flow presence data processing

Modified relative conductivity Pendant sensors can distinguish between flowing and dry conditions (Chapin et al., 2014; Jensen et al., 2019). Relative conductivity differed by orders of magnitude between adjacent Pendants because they were not calibrated for electrical conductivity but rather measured an arbitrary relative conductivity. As a result, thresholds for flowing and dry were determined for each unique sensor and varied with each sensor relaunch. When the stream was visibly flowing when the Pendant was launched, we assumed that drying occurred when the relative conductivity dropped below 45% of its first stable reading after relaunch. Similarly, if the

Pendant was launched in a dry streambed, we assumed that flow resumed when the relative conductivity value jumped above a value greater than or equal to 45% of the first stable, non-zero relative conductivity reading. If the relative conductivity changed by more than 1000 μS/cm upon relaunching the sensor, a new threshold of 45% of its first stable reading after relaunch was used. All threshold decisions were validated by in-stream observations for that relaunch period. The 45% relative conductivity threshold was first selected by observing the threshold at which sand drying out was distinguishable from water-saturated sand in experiments by Chapin et al. (2014), and was validated by comparing our dry stream bed observations to relative conductivity readings. The 45% relative conductivity threshold and above quality control methods always yielded a flow/no flow status that reflected our field observations.

2.4.3 Data analysis

We used the entire season's flow presence data collected from 25 sensors in Murphy Creek to create hierarchical clusters. Clusters were determined using Ward's method (Milligan, 1980). Missing values were imputed by singular value decomposition using the program JMP Pro 14.

The change in peak solar radiation from day to day was calculated using equation 2.1, where R is the solar radiation in W/m^2/day and t is the time of the peak in solar radiation. Here, i refers to the day of interest and $i-1$ refers to the previous day. The change in daily peak temperature was calculated in the same way (Equation 2.2).

$$Change\ of\ peak\ solar\ radiation = R_{solar\ peak_i} - R_{solar\ peak_{i-1}} \qquad \text{Equation (2.1)}$$

$$Change\ of\ peak\ temperature = T_{peak_i} - T_{peak_{i-1}} \qquad \text{Equation (2.2)}$$

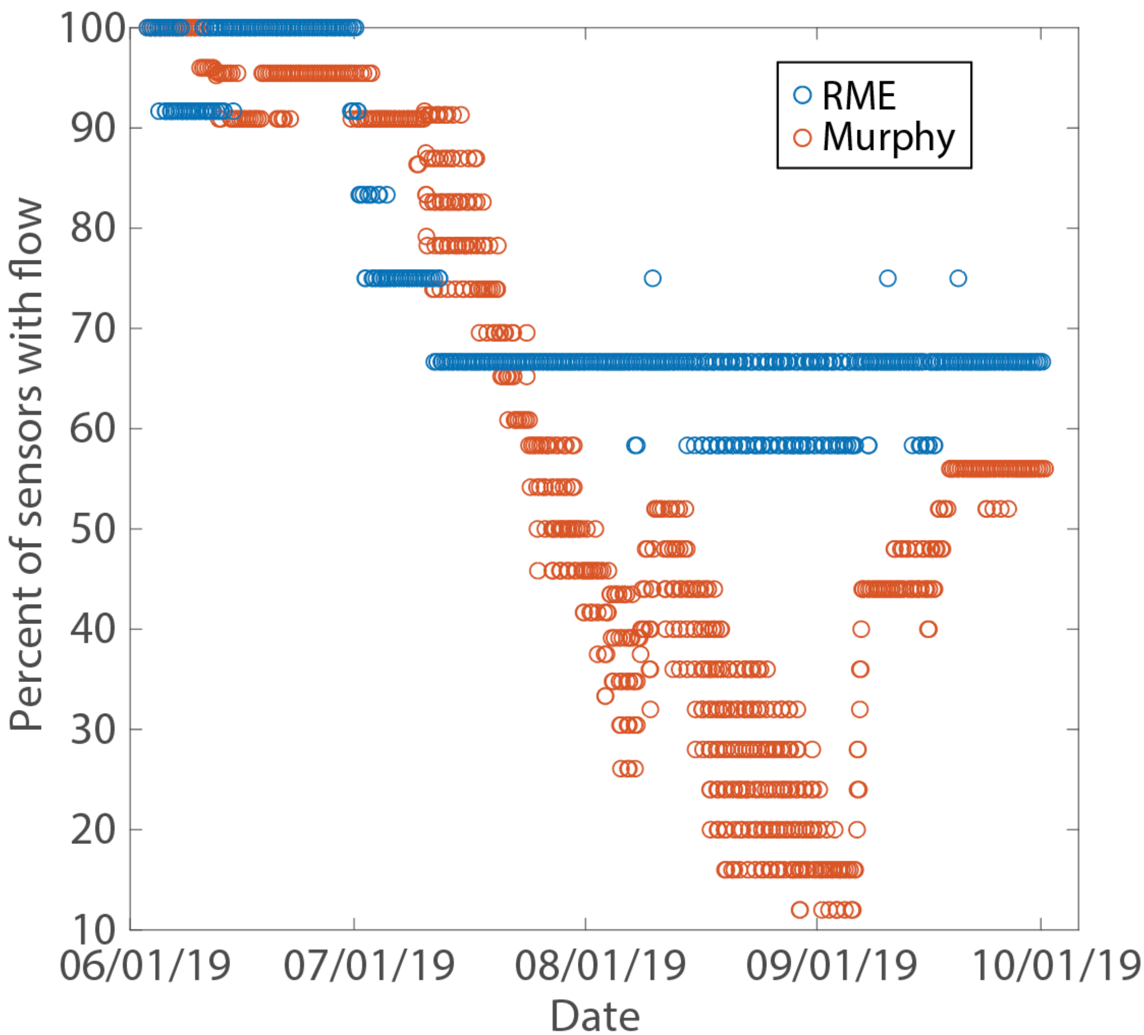

Figure 2.2. Seasonal stream drying patterns at RME (blue) and Murphy (orange). Each point represents the instantaneous network extent, or the percent of sensors (Murphy, max n = 25; RME, max n = 12) with surface flow at a given moment. In Murphy Creek, drying increased until the first week of August when a brief rewetting event occurred, after which drying resumed and persisted until September 6th when a large hailstorm caused several sensors to rapidly rewet. In RME, several upstream sensors dried in early July and most remained dry throughout the rest of the season.

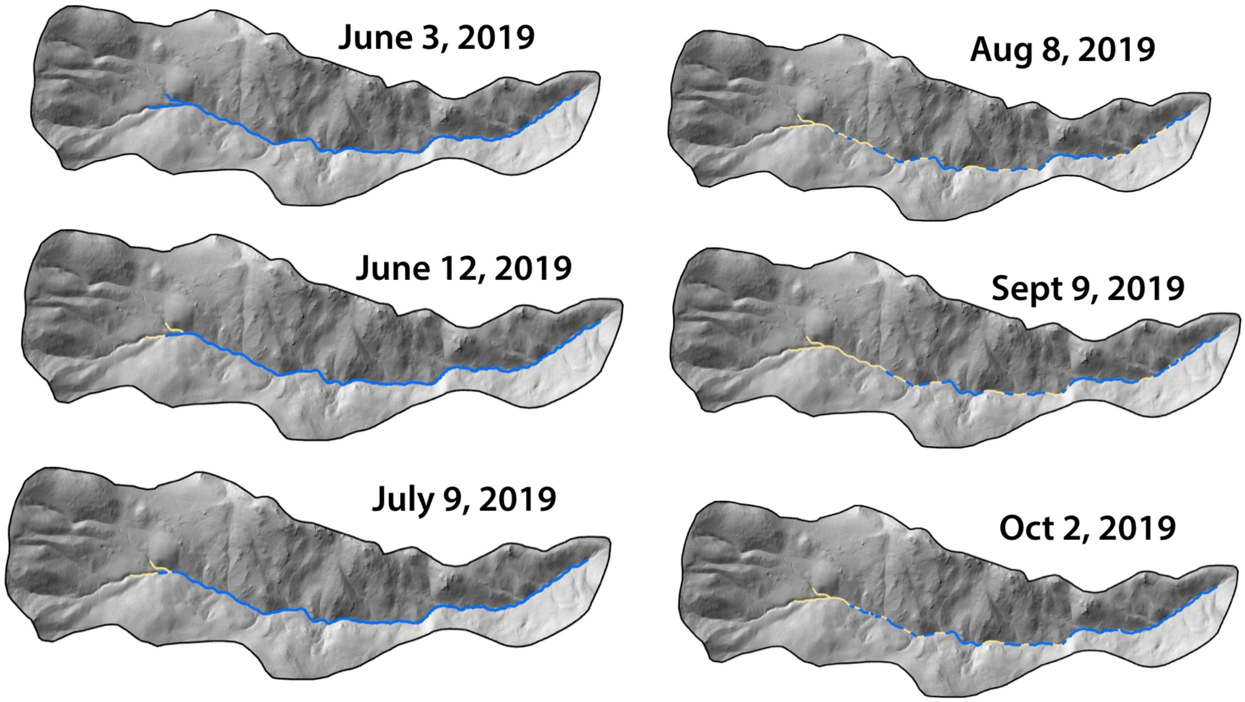

Figure 2.3. Drying maps for Murphy. Blue indicates flow, yellow indicates no flow. Drying commonly occurs in spatially disconnected segments; flowing segments separated by dry reaches were common in August through October. Despite deploying a dense sensor network, some short dry or flowing reaches were not captured except during in-person mapping at a very fine spatial scale.

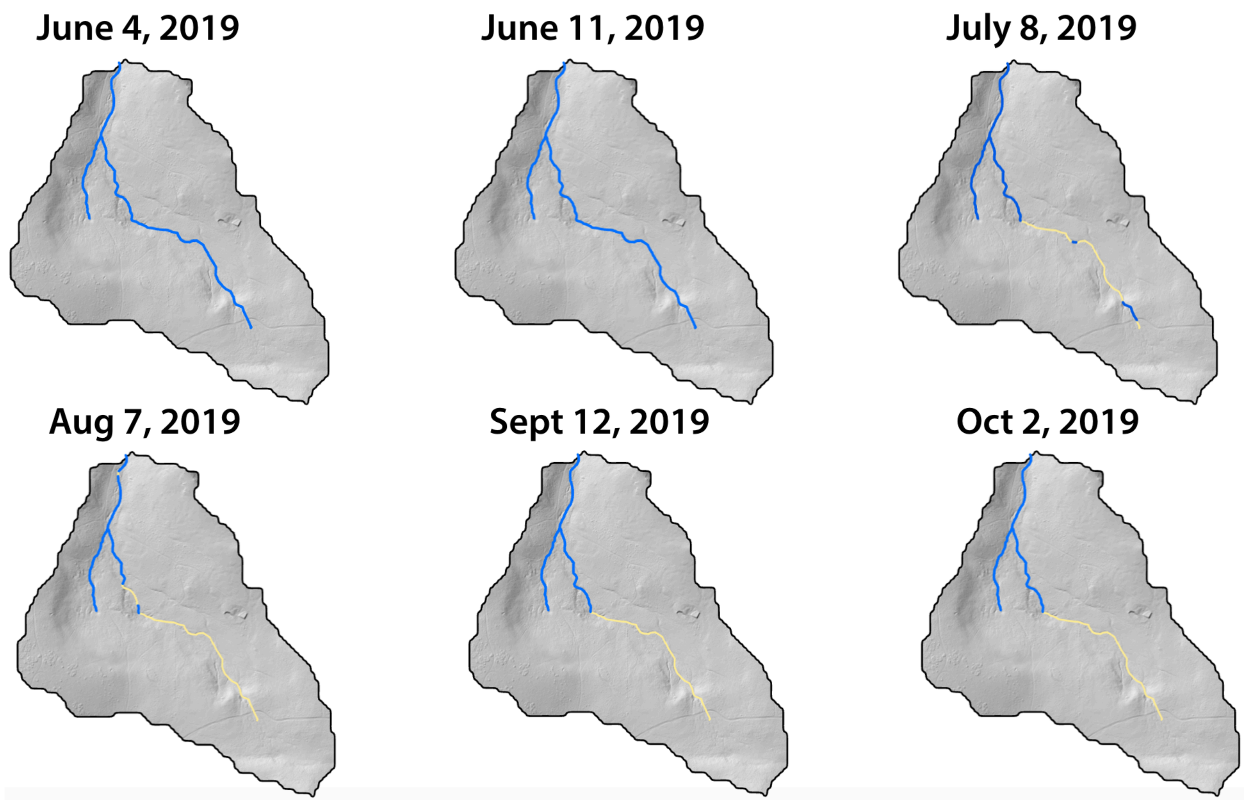

Figure 2.4. Drying maps for RME. Blue indicates flow, yellow indicates no flow. The uppermost portions of RME dried in early July after a snowdrift melted.

2.5. Results

2.5.1. Spatiotemporal Drying Patterns

At the beginning of the observation season during the first week of June 2019, Murphy and RME were flowing continuously between the outlet weirs and headwaters that were 2000 m and 880 m upstream of those weirs, respectively (Figure 2.2). As the summer progressed, Murphy Creek and RME exhibited very different drying patterns (Figures 2.3 & 2.4). Murphy Creek was characterized by spatially discontinuous and temporally variable flow while in RME the uppermost reaches dried early and stayed dry throughout the summer.

The 25 sensors in Murphy Creek and 12 sensors in RME did not capture all drying heterogeneity: in-person mapping (Figures 2.3 & 2.4) shows that short (as small as 15-m) drying segments were commonly observed between sensors that were spaced ~80 m apart, on average. Thus, in order to fully capture drying heterogeneity in Murphy Creek, flow sensors would need to be placed at 15-m intervals. Fine-scale observations are important during the initial characterization of stream drying so that hydrologists can detect the smallest scale at which stream drying varies, which enables accurate identification of the controls on drying heterogeneity.

2.5.2. Murphy Creek

At the beginning of the season in Murphy Creek, all 25 sensors exhibited flow (Figure 2.5). As the summer progressed, drying was patchy throughout the stream: we observed just three perennial locations and 22 intermittent or ephemeral locations. Disconnected flowing and dry segments were common throughout the network; at any given time, surface flow was interrupted by dry reaches at multiple points in the stream.

Downstream locations (sensors < 950 meters above the weir) were flowing for at least 50% of the season (that is, the entire period from Jun through Oct). From 950 m to 1800 m, conditions were highly variable, and sensors detected flow between 32 and 100% of the season. The uppermost sensor locations (>1800 meters above the weir) were flowing between 5 and 40% of the season. Drying from 950 to 1800 meters above the weir was the most spatially variable: for example, sensor M1377 dried for 32% of the season and was located immediately upstream of persistently flowing reaches like M1030. Drying in Murphy accelerated in early to mid-July and continued through August. A large hailstorm on September 6 caused seven locations to rewet rapidly within a 17-hour period (10:15 9/6/2019 to 03:15 9/7/2019 MDT). Following the storm, three additional sensors rewetted before the end of the field season. At the end of the field season on October 1, 2019, 11 of 25 sensors (44%) were still dry (Figure 2.5).

Our cluster analysis highlighted five primary patterns of drying: constant flow through the season, rewetting in September, first drying in mid-July, first drying in early-July, and first drying in June (Figure 2.6A). These five clusters were not grouped spatially along the stream network. Instead a sensor from any given cluster was often adjacent to sensors from a different cluster that exhibited different drying patterns (Figure 2.6B). Despite the spatial variability in clusters, there was a negative relationship between the upstream distance and the first day that drying occurred (Figure 2.6C). Typically, the higher the elevation in the watershed, the earlier the location dried.

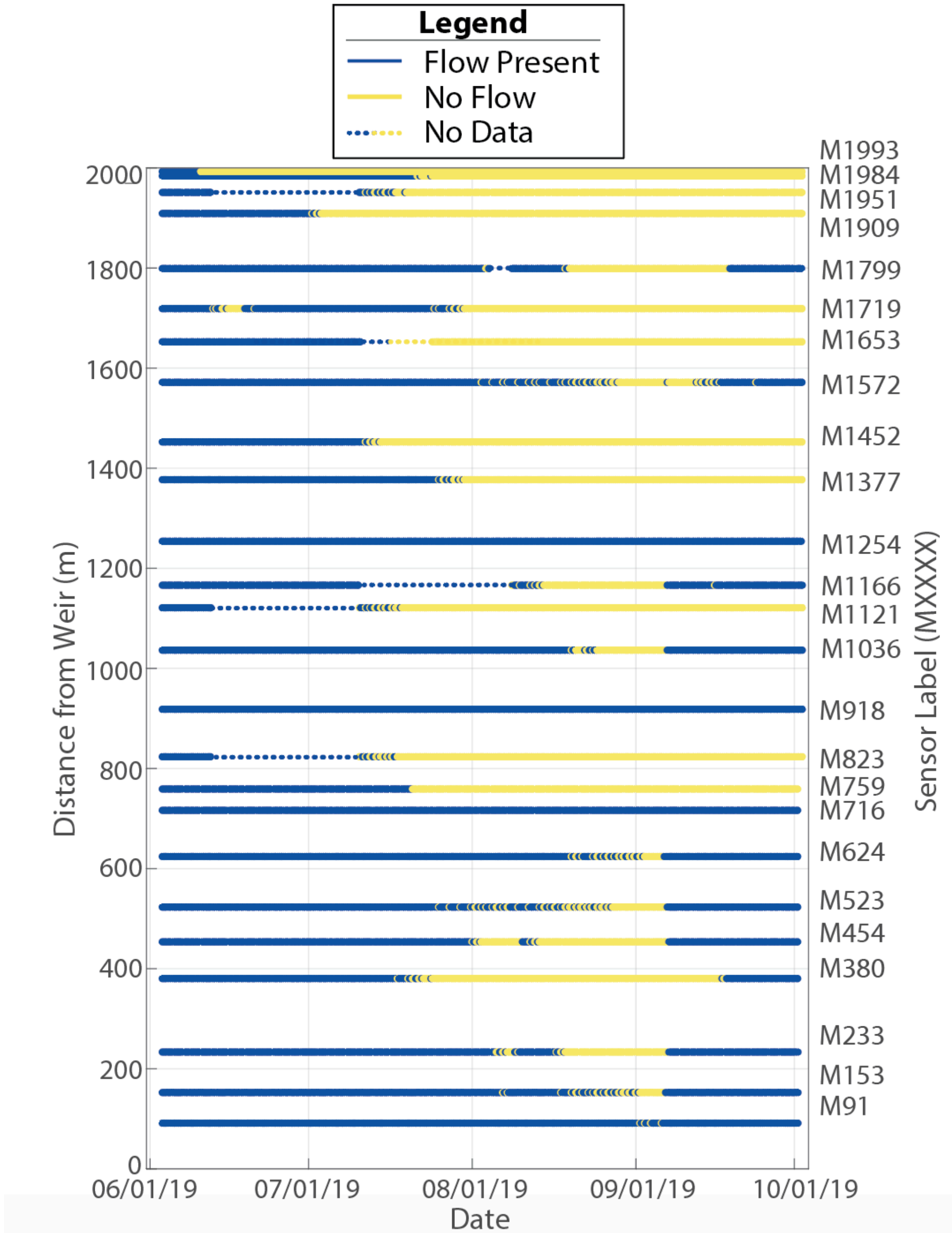

Figure 2.5. Drying patterns for Murphy Creek. Each horizontal line shows all data for a single sensor throughout the observation period. Sensors are plotted by distance from the outlet weir from bottom to top. Blue indicates flow, yellow indicates no flow, and a blue dashed line means that there is no data for the time period. The right y-axis shows the sensor label coded in meters above the weir. All sensors were flowing at the beginning of the season. Several locations dried between June and mid-August, and of those, eleven rewetted before the end of the season. Diel cycling occurs where yellow and blue points alternate in quick succession.

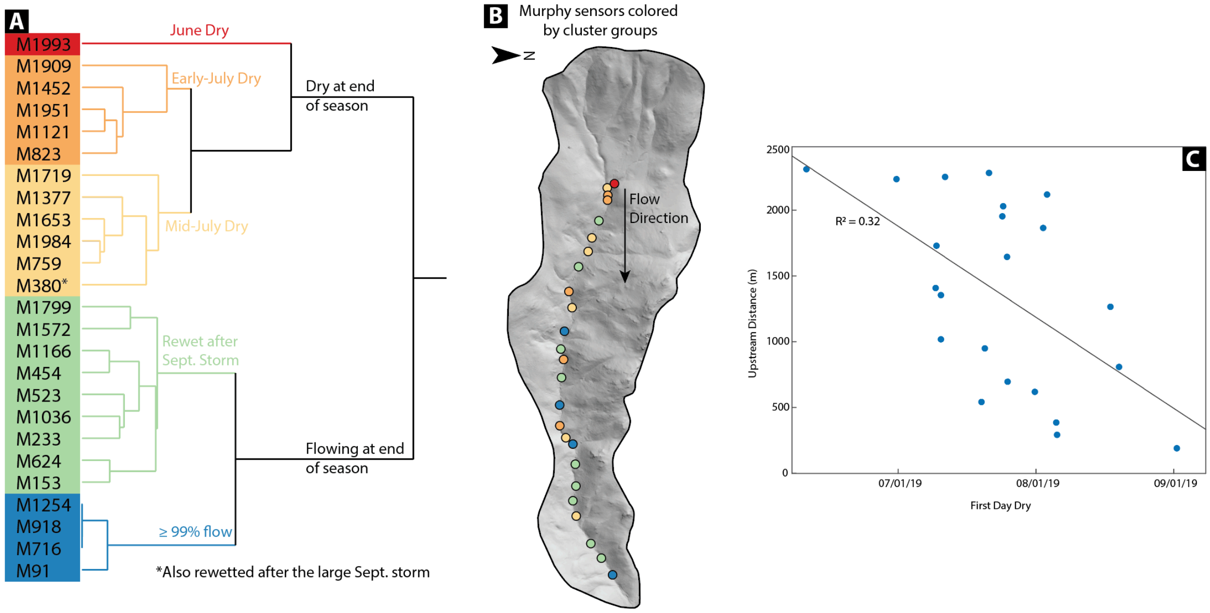

Figure 2.6. (A) Hierarchical cluster with five clusters colored. Clusters relate to the timing and duration of drying patterns. From top to bottom in cluster order: the red group is M1984, the only sensor to dry in June; the orange group includes sensors that dried in early July and stayed dry through the season; the yellow group shows sensors that dried in mid-July and stayed dry through the season; the green group includes sensors that rewetted during an early September storm; and the blue group includes sensors that were flowing ≥99% of the season. **(B)** Map of Murphy Creek with the twenty-five sensors plotted on a hillshade. Sensors are colored by their cluster groups as displayed in panel A. **(C)** The first day dry at each sensor that dried plotted against the distance upstream from the outlet weir (n=22). Upper watershed locations dried first, but the variability displayed in the watershed map (B) is also visible in the relatively weak correlation; sensors are colored by the cluster analysis in (A).

2.5.3. RME

In RME, drying patterns were less dynamic and more spatially clustered than in Murphy Creek (Fig 2.7). At the beginning of the observation season, RME was flowing continuously between the outlet weir and RME headwaters located 880 m upstream of the weir (Figures 2.4). The four uppermost sites all experienced seasonal drying within 11 days of each other in early July after brief drying and rewetting in June. Seasonal drying occurred just above RME448 first (after short periods of drying at RME552, RME676, and RME838, followed by resumed continuous flow), which was then followed by progressive upstream drying during the next twelve days until the uppermost location dried (Figure 2.7). A snow drift at the crest of the watershed sustained flow in the upper reaches while further downstream locations dried. When the snowdrift completely melted, the uppermost locations finally dried. Three of these locations (RME552, RME 676, RME 838) exhibited short dry periods in June or July before drying seasonally. All downstream locations exhibited flow throughout the field season, with the exception of RME76, which exhibited diel cycling starting in August, but never dried for longer than fifteen consecutive hours.

RME sites exhibit three clusters of drying behavior: 1) most stream segments down-gradient of 2057 m flowed throughout the year, 2) the exceptional downstream site RME 76 showed late-summer diel cycling, and 3) up-gradient locations above 2057m dried after the snowdrift melted. All locations upstream of RME448 dried during early to mid-July and stayed dry throughout the season. RME413 and RME448 marked the uppermost flowheads observed (at elevations of 2055 and 2053m, respectively) after locations above RME448 dried in July. RME448 was located below a break in slope where flow started, and RME413 was located at a perennial spring.

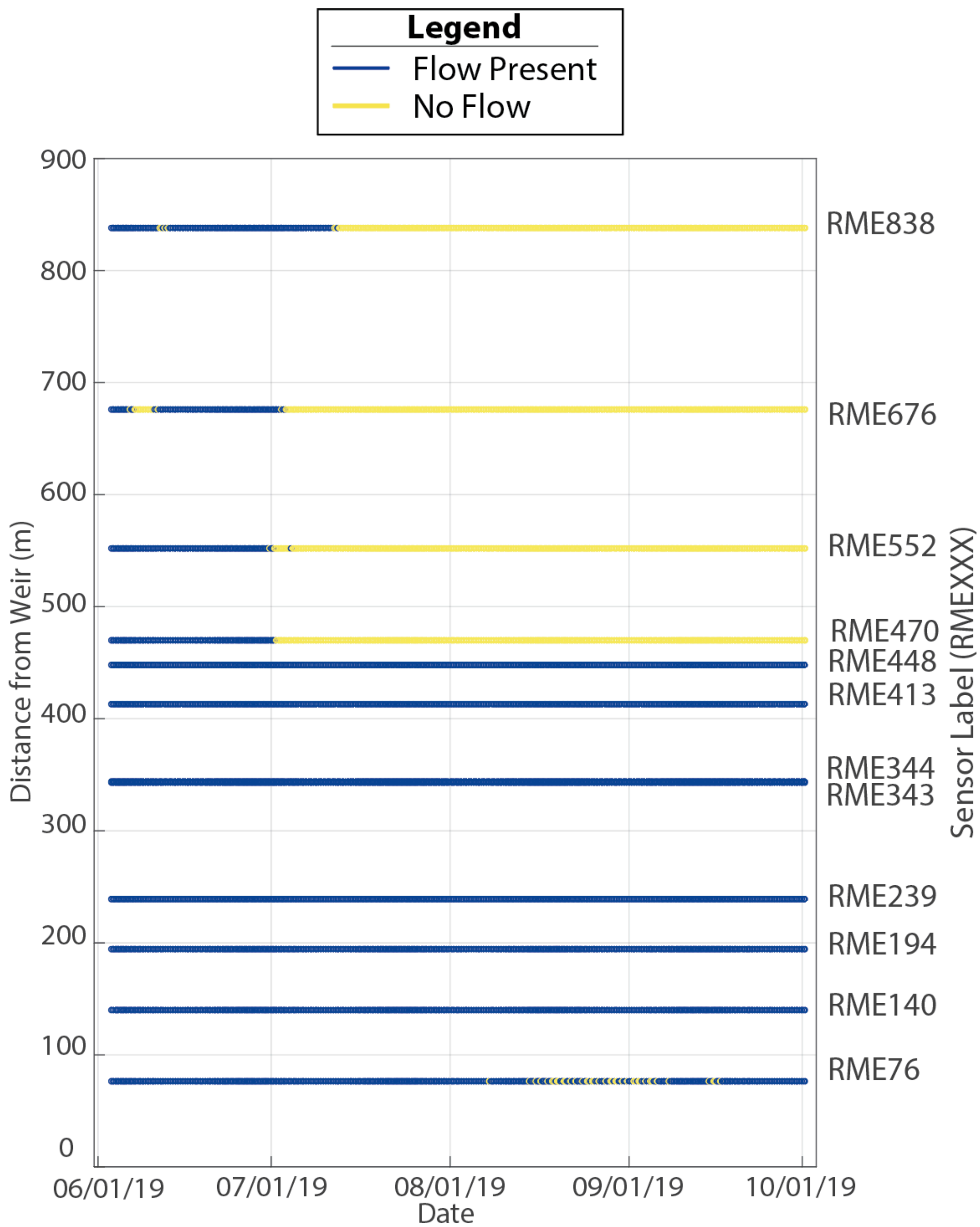

Figure 2.7. Drying patterns for RME. Each horizontal line shows all data for a single sensor throughout the observation period. Sensors are plotted by distance from the outlet weir from bottom to top Blue indicates flow and yellow indicates no flow. The upper locations in RME dried in Jun to early July and remained dry after early to mid-July. Flow persisted throughout the drying period at sensors below 450m, except at the most downstream sensor.

2.5.4. Diel cycling

A diel cycle of drying is defined as any sub-24-hour cycling between the presence and absence of surface flow. Building from this, a diel cycle period is a string of days with diel cycling, and a diel cycle period can be interrupted by complete rewetting or drying. We found that diel cycling periods commonly preceded persistent drying in Murphy Creek while only about 1/3 of sensors exhibited diel cycling in RME (RME76, RME552, RME676, and RME838) (Figures 2.5, 2.7). Because of the small numbers at RME, we focus our remaining analysis on Murphy Creek. In Murphy Creek, the start of drying was captured at 21 sensors (Figure 2.5). Of those sensors, 19 exhibited diel cycling prior to seasonal drying. Uninterrupted diel cycles lasted anywhere from two to twenty-three days and averaged eight days.

When diel cycling periods began, they often occurred at multiple sensors on the same day. These temporal clusters were not grouped in space: locations undergoing diel cycling were separated by sensors that remained flowing. For example, M823, M1121, M1452, and M1951 all started diel cycles on June 10. Similarly, M1377 and M1799 started a diel cycling period on July 15. M153, M233, M624, M1036, and M1719 all began diel cycling between August 15 and 19. Eight locations started a period of diel cycling, then rewetted for a day or more before starting a second period of diel cycling.

Drying consistently started between 07:00 and 18:00 and flow typically resumed between 19:00 and 07:00 the following day (Figure 2.8). Typically, on the first day of drying during a diel cycling period, the stream was dry for the shortest duration of time during the period and each sequential day was dry for a longer duration of time as summarized by the histogram of slopes in Figure 2.9. The start time and duration of drying was not predictable by location in the network or time of year. If a sensor dried, it almost always (19/21 sensors where the start of drying was captured) exhibited diel cycling as it dried but rarely prior to rewetting (1/11 sensors that rewetted, M1572). Nine of the other sensors that rewetted exhibited rapid rewetting after an intense hailstorm on September 6th, and the final sensor that rewetted (M91) stopped undergoing diel cycling on September 5th.

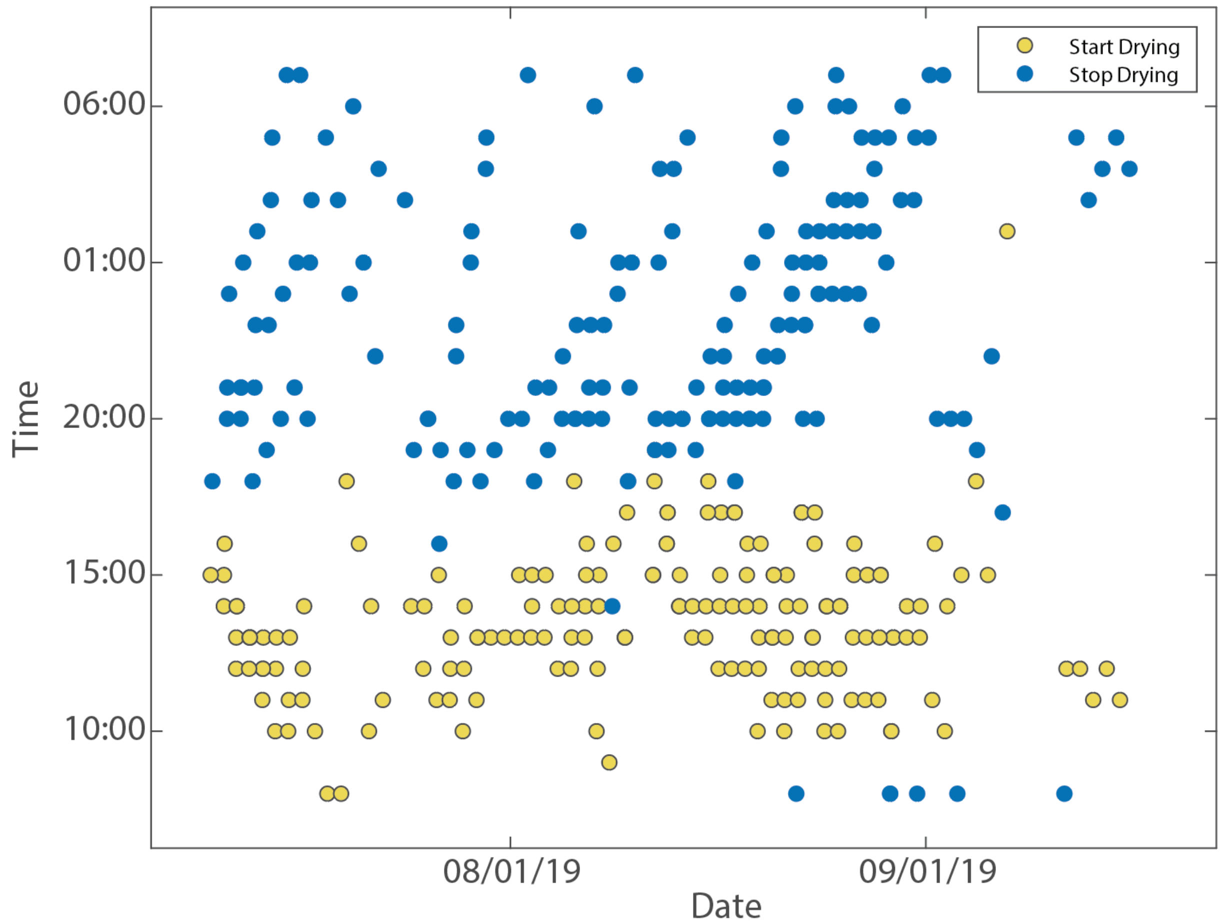

Figure 2.8. Start and stop time for each diel cycle observed in Murphy Creek. Typically, the timing of the start of drying and stop of drying did not overlap significantly, drying started between 07:00 and 18:00 independent of location in the stream and time of year.

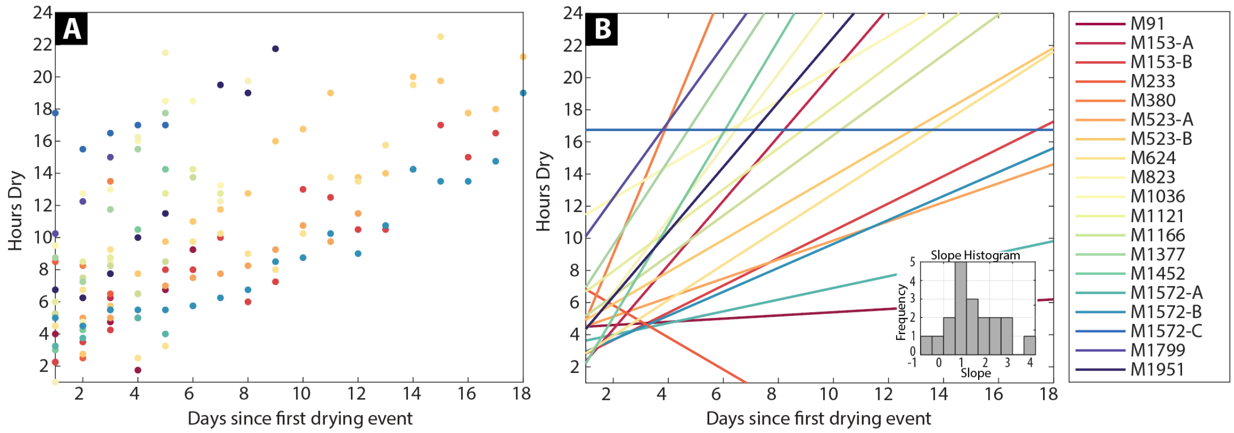

Figure 2.9. (A) Diel cycling patterns were extracted from each of the sensors that exhibited diel drying. We plot the number of days that a single location has undergone continuous diel cycling against the duration of drying [hours] during that day of the diel cycling period. If the stream was entirely dry or wet for at least 24 hours, and later resumed a diel cycling of wetting and drying, a new data series was plotted for the same location. All data is from Murphy Creek. **(B)** Best-fit line for each set of data points in Figure 2.9A is plotted using the same color. A histogram illustrating slope frequency of each best-fit line (n = 19) is plotted in the lower right-hand corner. All but two slopes are positive, and the median slope is 1.10. We plotted the slopes against the TWI ($r^2 = 0.07$), topographic slope ($r^2 = 0.07$), upstream distance ($r^2 = 0.04$), upstream area ($r^2 = 0.06$), first day dry ($r^2 = 0.12$), and the percent of the season with flow ($r^2 = 0.15$) at each location and found no strong correlations (plots not shown).

2.5.5. Diel cycling and daily changes in solar radiation and temperature

During a diel cycling period, the time spent dry was greater with each subsequent day (Figure 2.9). However, there were several exceptions where the stream stayed dry for the same amount of time for two days in a row or remained dry for a shorter period of time than it was the previous day. We also observed rewetting for longer than 24 hours during diel cycling periods at multiple locations in Murphy Creek (M233, M454, M523, and M1166): all of these rewetting periods are consistent with decreases in daily peak solar radiation and temperature.

During the observation season, daily peak radiation decreased by -4.7 $W/m^2/day$ on average. The maximum increase in daily peak solar radiation over from one day to the next was 1347 $W/m^2/day$ and the largest decrease was -817 $W/m^2/day$. We compared the change in solar flux from day to day against the change in time dry over the same time period (Figure 2.10B). We observed that when the change in solar peak radiation from day to day was high (>100 $W/m^2/day$), typically the stream was dry for a longer period than it was the previous day. Conversely, when the change in daily peak solar radiation decreased by more than 100 $W/m^2/day$, the stream exhibited flow longer than the day before or even rewetted for longer than 24 hours. For example, at M532, rewetting occurred after twelve days of consecutive wet-dry periods, and on the first day of continuous 24-hour flow, the change in peak solar radiation from the previous day was -230.28 $W/m^2/day$ (Figure 2.9C).

We plotted a histogram of the start time of drying during for every day of a diel cycling period and overlaid it against the daily solar radiation for every day of the experiment period to show the consistency between the timing of the start of drying and the timing of daily peak solar radiation (Figure 2.11A). We subtracted the time that drying started for every point in the histogram and from the timing that solar radiation peaked the same day and plotted the results in a second histogram (Figure 2.11B). Here, we show that drying consistently begins within $\pm$ 6 hours of peak solar radiation with mean of 0.39 $\pm$ 0.18 (SE) hours.

2.5.6. Vegetation cover and daily changes in temperature

The presence of riparian and hillslope vegetation also affects surface flow in Murphy Creek and RME. Riparian vegetation varies throughout the length of Murphy Creek, particularly after the 2015 Soda Fire. Adjacent hillslopes are covered in grasses and sagebrush and the riparian channel is covered by patchy willows and small bushes. We observed these riparian plants to be grouped in clusters so that some stream segments were completely shaded by willows whereas other stream segments only supported seasonal grasses and the stream was fully exposed to the sun. We noted distinct vegetation cover at two sensors, M233 and M759. M233 was completely covered by dense willows and M759 lacked willows and was exposed to the sun. We plotted daily temperature throughout the day from August 1 to September 4, 2019 and compared the daily range of temperature and the daily peaks in temperature. We observe that where the stream was exposed, daily peak temperature was up to 25˚C greater than in a nearby location that was shaded.

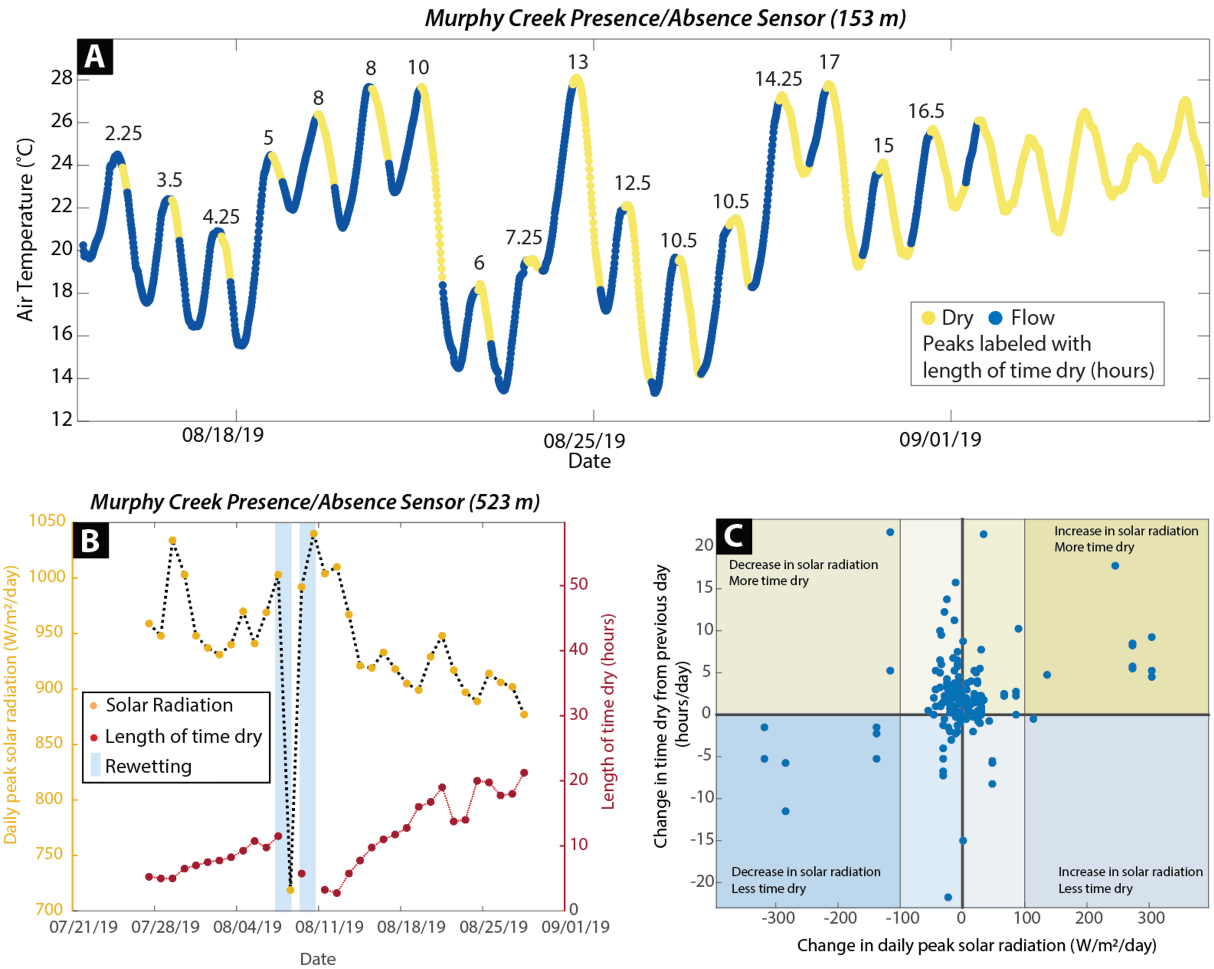

Figure 2.10. (A) Example of diel cycling preceding long-term stream drying at a single sensor in Murphy Creek. 12-hour moving air temperature average is plotted against time and colored by the presence or absence of water. During diel cycle periods, the stream is dry when temperature is at its peak. Each peak is labeled with the length of time dry that day in hours. After large drops in daily peak temperature, the duration of drying decreases, despite the overall trend of increasing duration with each subsequent day. **(B)** Length of time dry (red) for each day during a diel cycling period and the peak daily solar radiation [W/m^2]. When the stream was continuously flowing for more than 24 hours, a blue band is displayed. The daily peak solar radiation is plotted in orange. When the solar radiation decreased on August 8th 2019, the stream rewetted. **(C)** Change in daily peak solar radiation [W/m^2/day] from one day to the next plotted against the change in the amount of time a sensor detected no flow [hours] during the same two days. All wet/dry pulses for all 25 sensors were extracted and plotted. When the largest changes in peak daily solar radiation occurred (>100 W/m^2/day), locations undergoing diel cycling were typically dry longer than the previous day. Similarly, decreases in solar radiation were correlated with a shorter duration of stream drying.

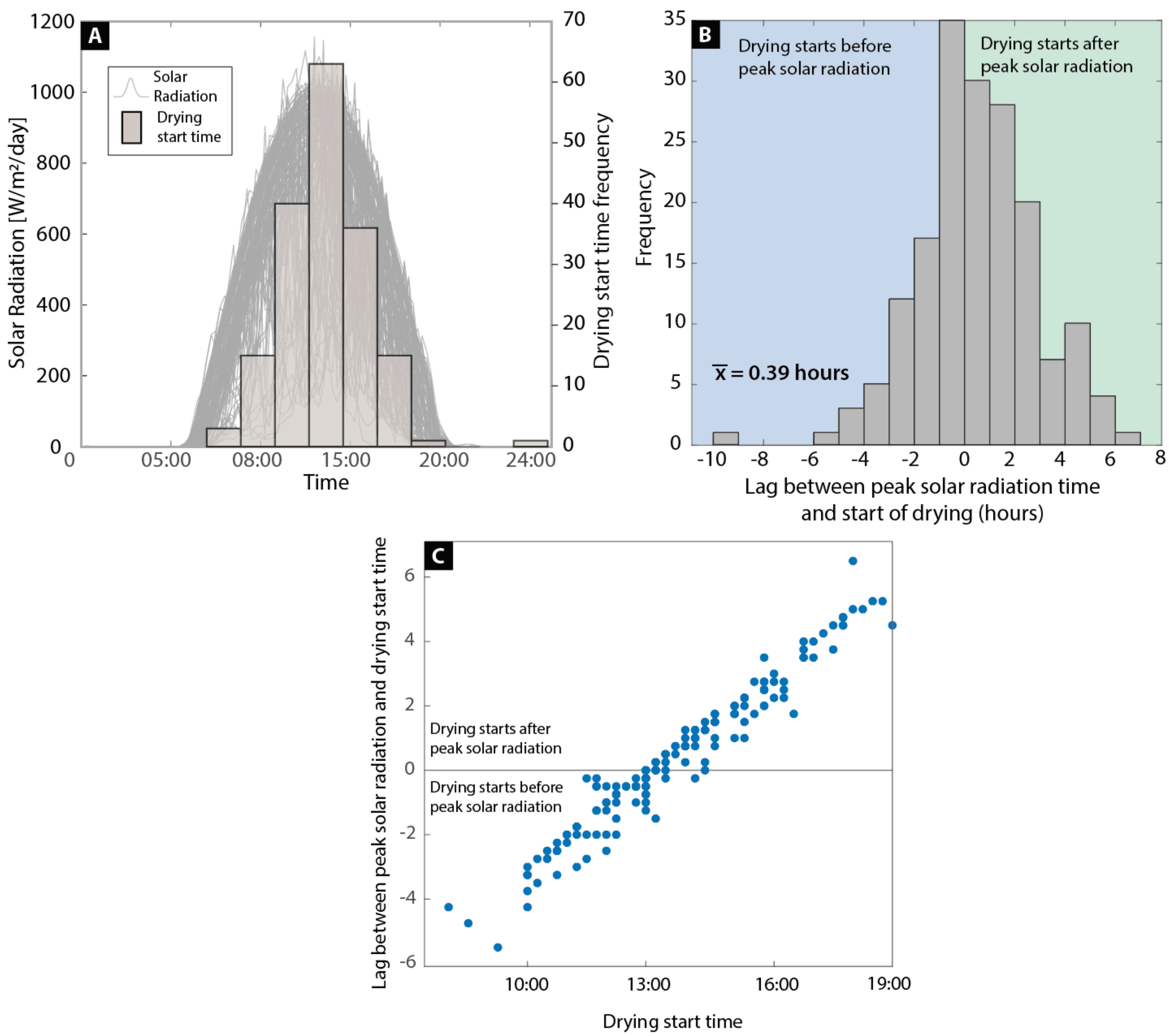

Figure 2.11. (A) Histogram of the start of drying time for every day during a diel cycling period. In the background, the solar radiation for each day of the observation season is plotted at 15-minute timesteps. The timing of the start of drying correlates well with solar radiation. **(B)** Histogram of the difference between the time that daily drying starts and the time that solar radiation peaks on the same day for every day of diel cycling. On average, drying starts 0.39 ± 0.25 hours after solar radiation peaks. Solar radiation and stream flow presence/absence were recorded at 15-minute intervals. **(C)** Zoomed in view of drying start time plotted against the lag between peak solar radiation and drying start time. An outlier started drying at 02:00 and is not visible in this view.

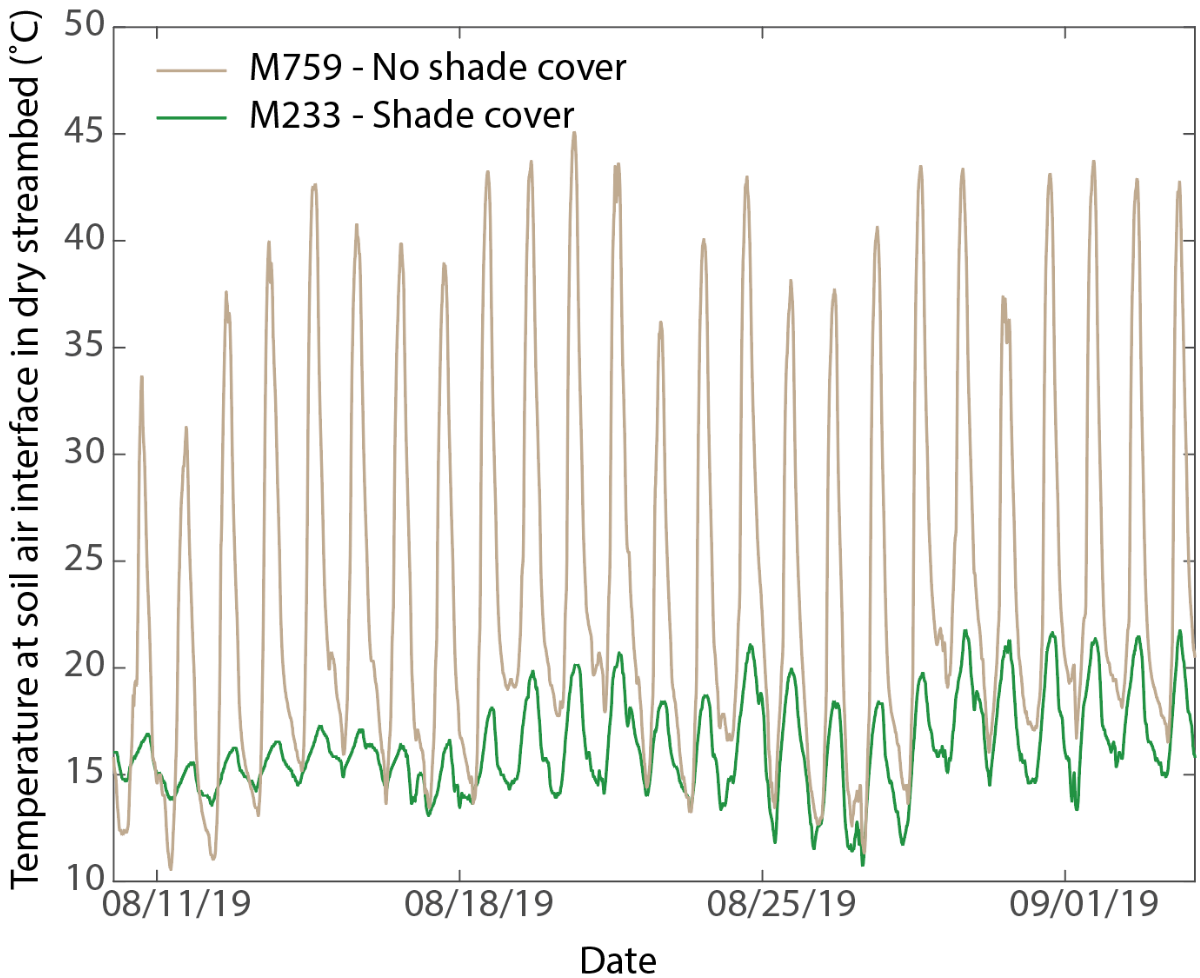

Figure 2.12. Temperature recorded with a HOBO Water Level sensor in a dry stream bed at M233 and M759. M233 had no shade over the stream while M759 was shaded under a willow tree. Shaded temperatures (M759) were significantly lower and varied less throughout the day than unshaded ones (M233). Note that water level sensors were housed in black PVC which caused temperatures to spike above ambient air temperatures.

2.6. Discussion

2.6.1. Previously identified stream drying controls and heterogeneity in stream drying

Although drying is more likely when discharge is low (Stanley et al., 1997), stream drying is not a simple process because it is influenced by factors that range from topography to geology to climate and these factors operate and vary at different spatial and temporal scales (Table 2.2) (Costigan et al., 2016; Jaeger et al., 2019; Jensen et al., 2019; Ward et al., 2018). Each of the factors identified in Table 2.2 influences spatiotemporal stream drying patterns, but the list may not be complete, and the hierarchy of these controls is not yet established.

During expansion and contraction in RME and Murphy Creeks, we observed highly variable stream drying patterns, both within a single headwater stream and between the two locations. Murphy Creek exhibited a weak top-down drying trend (Figure 2.6C), but with lots of exceptions to this trend (Figure 2.6A-B). Both the timing and spacing of stream drying patterns varied, and we hypothesize that this heterogeneity is due to variability in local controls such as hydraulic conductivity and evapotranspiration losses.

Table 2.2. Classification of drivers of stream drying that have been proposed, including both common and unique drivers.

<table>
<tr><th rowspan="2">Authors</th><th colspan="2">Factors important to predicting stream flow</th></tr>
<tr><th>Unique to study</th><th>Common Themes</th></tr>
<tr><td>Costigan et al., 2016</td><td>- Stream morphology (pools/riffles and slope)
- Aggrading or incising reach</td><td rowspan="6">- Frequency, duration, and intensity of weather events
- Subsurface properties (grain size, permeability, soil type, depth to water table, porosity)
- Topographic indices (slope, upstream area, topographic wetness index, topographic position index, valley morphology)
- Land cover
- Evapotranspiration losses</td></tr>
<tr><td>Jaeger et al., 2019</td><td>- Percent of streamflow sourced by baseflow
- Annual daily temperature minimum/maximum</td></tr>
<tr><td>Ward et al., 2016</td><td>- Manning's roughness coefficient
- Downstream discharge
- Stream sinuosity</td></tr>
<tr><td>Jensen et al., 2019</td><td>- Transient infiltration rates</td></tr>
<tr><td>Eng et al., 2016; Jaeger et al., 2014; Jaeger and Olden, 2012</td><td>- No unique controls</td></tr>
<tr><td>this study</td><td>- Daily changes in peak solar flux/temperature
- Presence or absence of riparian vegetation cover</td></tr>
</table>

2.6.2. Solar radiation and stream drying

Daily peaks and troughs in streamflow discharge magnitude have typically been attributed to losses from evapotranspiration and gains from snowmelt in systems with seasonal snowpacks (Worrall et al., 2015, Kirchner et al., in review). Our findings are consistent with this conclusion as the timing of daily diel cycle drying begins when solar flux and temperature is highest during the day and rewets at night when temperatures, solar radiation, and evapotranspiration losses are lower (Figure 2.8). However, because we did not measure evapotranspiration in the field, we rely instead on proxies for evapotranspiration including daily peak solar radiation and temperature. Because of the strong relationship and short lag between the timing of the start of drying and these evapotranspiration proxies, we propose that atmospheric losses driven by high temperatures and radiative fluxes are key controls on the exact timing of drying, particularly during wet-dry diel cycling periods.

The duration of drying during diel cycling periods correlates well with peak solar radiation (Figures 2.9). During diel cycling periods, the number of hours spent dry each day increases with time as illustrated by the positive slopes in Figure 2.9B. Despite the overall positive trend, we observe several exceptions where the stream flows for slightly less time with each subsequent day or even rewets after a number of days with wet-dry periods. Such responses indicate some interruption that alters the otherwise consistent pattern. When the daily peak solar radiation drops by more than -100 W/m^2/day, the stream is dry for a shorter period of time. We observe that when the change in daily peak solar radiation is within +/- 100 W/m^2/day, the change in the time in diel cycling duration is highly variable and does not correlate well with solar radiation. Therefore, we conclude that large changes in solar radiation control both 1) the time of day that a stream dries during a diel cycling period, and 2) the change in time dry from day to day during a diel cycling period. This conclusion is supported by large decreases in daily peak solar radiation coinciding with rewetting periods (Figure 2.9) and decreases in the daily time spent dry, and large increases in solar radiation coinciding with increases in the time spent dry (Figure 2.9).

On average, diel stream drying begins 0.39 ± 0.25 hours after peak solar radiation (Figure 2.11). The very short lag between peak solar radiation and the start of stream drying is consistent with local evapotranspiration losses that could immediately drop water levels, but those losses were not directly quantified here. Despite nearly coincident peak solar radiation and peak solar radiation, we find that diel cycling periods do not occur at the same moment throughout the length of the stream, or even in adjacent portions of the stream (Figures 2.2 and 2.4). Instead we find that diel cycling begins at the same time in the season at multiple spatially disconnected locations, and we argue that this pattern demands an explanation that we propose below.

2.6.3. Potential implications of riparian vegetation cover heterogeneity

We observed riparian vegetation cover to vary significantly throughout the length of Murphy Creek, some stream segments were heavily shaded by willows while other segments lacked riparian shade and the stream was directly exposed to the sun. This spatial heterogeneity in riparian shade cover could create localized variation in solar radiation and temperature at the stream-air interface. We observed that flowing segments separated by upstream and downstream dry segments were often shaded by riparian vegetation which lead to cooler temperatures than in the dry reaches with direct sunlight. For example, when willows covered the entire width of the stream at M1254, temperatures were significantly cooler due to shade locally decreasing incoming solar radiation as compared to M759 which had no riparian shade cover (Figure 2.12). We propose that shading effects by local riparian vegetation significantly impact losses due to solar radiation and temperature and cause different drying rates at shaded vs. unshaded locations where all other conditions are the same. However, the relationship between evapotranspiration and stream flows is notoriously complex (Barnard et al., 2010; Bond et al., 2002; Čermák et al., 2007; Graham et al., 2013). ET losses are not immediately represented in stream flows as transit time causes lags between peaks and troughs in sap flow, stream flows, and groundwater levels (Kirchner et al., in review). As a consequence, the drivers behind a change in stream flows during the course of a diel cycling period may not be clear without spatiotemporally distributed evapotranspiration measurements, which was beyond the scope of this thesis project.

2.6.4. Surface losses control drying timing once all other drying conditions are met

We observed that large changes in daily peak temperature and daily peak solar radiation correlate well with changes in time dry during diel cycling periods. Here, we discuss a scenario where large changes in daily peak solar radiation and daily peak temperature are strongly correlated with evapotranspiration losses. Although radiation and temperature both affect ET, wind and vapor pressure/relative humidity also affect ET, and we did not collect spatially distributed weather information or ET. If we assume that radiation and temperature are good proxies of ET, we can explore the spatially variable evapotranspiration, and explore the impacts of local heterogeneity in riparian vegetation on the timing of stream drying.

Though drying may be locally driven by tradeoffs between surface and subsurface flows (Godsey and Kirchner, 2014), the timing of that local drying also depends on local recharge rates, groundwater discharge to streams, and surface losses to transpiration and evaporation. Controls on stream drying are not uniform throughout the length of a headwater stream and several local conditions must be satisfied for drying to occur. We propose that spatiotemporal diel cycling patterns and the timing of seasonal drying are primed by the spatial drivers (primarily geologic, geomorphic, and climatic factors) listed in Table 2.2. For example, the correlation between large changes in solar flux and temperature and the onset or delay of stream drying is stronger in late summer. Earlier in the season, the stream has sufficient inputs through precipitation or groundwater, and does not dry, even when solar radiation increases significantly from day to day. We find that when hydrologic inputs decrease and surface losses increase throughout the summer, stream drying becomes more probable. The spatial and temporal scales of variability in surface losses are also important as local drying patterns may reflect heterogeneity over small scales over which surface losses such as evapotranspiration would typically be either temporally and or spatially averaged. Surface drying occurs at a given location when 1) the correct geologic, geomorphic, and climatic attributes are met; 2) the location is no longer recharged either from precipitation and/or from deeper groundwater flow at a sufficient rate; and 3) local surface losses cause total discharge to decrease so that it can be entirely accommodated in the subsurface.

2.6.5. Conceptual Model

Assuming that solar radiation and temperature are reasonable proxies for evapotranspiration and acknowledging that we are dismissing possible impacts on ET from changes in vapor pressure, relative humidity and wind, we explore how stream drying controls vary in relative importance, particularly when ET losses are constant.

The central ideas behind this hierarchy of controls is a local mass balance that is controlled at each point by both heterogeneity in local conditions and watershed-scale characteristics. We observe that during low-flow conditions, surface flow is more sensitive to changes in storage, inputs, and outputs. Thus, local heterogeneity in each aspect of the mass balance needs to be considered for accurate local flow predictions. In particular, evapotranspiration losses are often generalized over an entire watershed, but we propose that they should be considered separately at both local and hillslope locations, as explained in the conceptual model below (Figure 2.13).

We assume that both stream geomorphology (including stream slope (S), upstream watershed area (A), topographic wetness index (TWI)) and geology (including the depth to bedrock (z_b), grain size (d), hydraulic conductivity (K)) remain constant within a seasonal recession timescale. This implies that under specified stream inputs (precipitation (P) and groundwater (GW)), the magnitude of surface flow at any given location will be dictated by changes in riparian and hillslope transpiration $(T_{rip}$ & $T_{hs})$ and in-stream/riparian evaporation (E) as well as changes in storage (Equation 2.3) where hillslope evaporation is assumed to be negligibly small. In equation 2.3, the probability of surface flow is a function of changes in evaporation (E), riparian transpiration (T_{rip}), hillslope transpiration (T_{hs}) between times t_1 and t_2 if all geologic, geomorphic, and climatic conditions remain constant between the two timesteps refers to the moment. Here time 1 and time 2 are arbitrary timesteps over which a net change in evaporation, riparian transpiration, and or hillslope transpiration occurs.

$$Prob\left(Q_{sfc_{t2}}\right) = f\left(\Delta S, \Delta E, \Delta T_{rip}, \Delta T_{hs}\right)_{t1 \overset{\Delta}{\rightarrow} t2} \qquad \text{(Equation 2.3)}$$

After geologic, geomorphic, and climatic conditions promote low-flow conditions, the exact timing of drying is dictated by the combination of evapotranspiration losses at a given location and upstream evapotranspiration losses. In order to fully understand the network's spatiotemporal stream drying patterns, we must also look at spatial drivers controlling drying patterns and integrate evapotranspiration losses throughout the entire watershed.

Stream drying patterns are influenced by a number of controls; however, the relative importance of the controls has not yet been established. In order to fully understand stream drying patterns, we need to consistently measure an array of factors at fine resolutions that have been shown to affect drying in some places. These include subsurface properties, topographic indices, land cover, evapotranspiration, and the frequency, duration, and intensity of weather events (detailed in Table 2.2 & 2.3). The following metrics have been useful in at least one study, and therefore should also be evaluated in a more systematic way: stream morphology (aggrading or incising), contribution of baseflow throughout the stream, Manning's roughness coefficient, downstream discharge, stream sinuosity, infiltration rates, daily changes in peak solar flux and temperature, and the presence or absence of riparian vegetation cover. These metrics are numerous, and many are difficult or costly to measure. In addition, many of these controls vary throughout headwater networks, such as subsurface properties, discharge, vegetation cover, evapotranspiration, and topographic metrics.

However, the complexity of stream drying has not yet been fully explained even though various subsets of these metrics have been incorporated into existing models. No model is yet able to accurately predict stream drying on small spatiotemporal scales. Here, we investigate stream drying patterns on a small scale, perhaps smaller than necessary for making accurate stream drying management decisions. However, such fine-scale spatiotemporal measurements will highlight which controls are essential to accurately predict drying and manage intermittent streams.

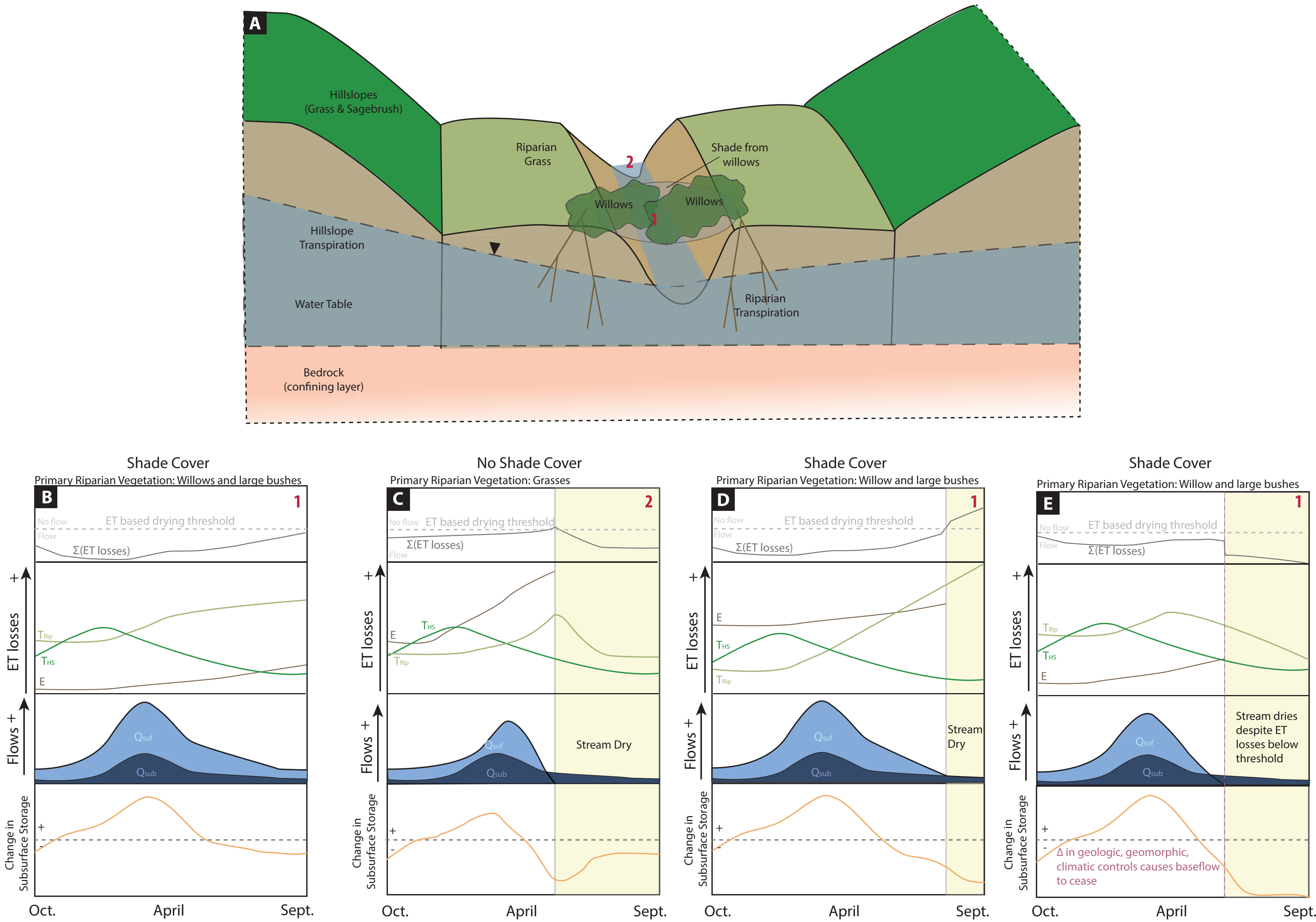
A
Hillslopes
(Grass & Sagebrush)
Riparian
Grass
Shade from
willows
Willows
Willows
2
1
Hillslope
Transpiration
Water Table
Riparian
Transpiration
Bedrock
(confining layer)
Shade Cover
Primary Riparian Vegetation: Willows and large bushes
B
1
No flow
Flow
ET based drying threshold
Σ(ET losses)
ET losses
Flows
Change in
Subsurface Storage
Oct.
April
Sept.
No Shade Cover
Primary Riparian Vegetation: Grasses
C
2
Stream Dry
Shade Cover
Primary Riparian Vegetation: Willow and large bushes
D
1
Stream
Dry
Shade Cover
Primary Riparian Vegetation: Willow and large bushes
E
1
Stream dries
despite ET
losses below
threshold
Δ in geologic, geomorphic,
climatic controls causes baseflow
to cease

Figure 2.13. Conceptual mass-balance diagram showing evapotranspiration losses, surface flow, subsurface flow, and the change in storage over time. **(A)** Conceptual cross section of a stream with the potential to dry. As drawn, the stream is flowing. At point 1, willows shade the stream bed, potentially reducing local evapotranspiration losses. At point 2, grasses are the only riparian vegetation present and evaporation losses may be greater than at point 1. **(B)** Mass balance at point 1. Total evapotranspiration is the sum of continuous riparian and hillslope transpiration and evaporation. Surface flow and subsurface flow peak in the spring and decrease in the summer when riparian transpiration and evaporation increase due to warmer temperatures. Hillslope transpiration decreases in the summer due to grasses drying out. **(C)** Mass balance at point 2, where no riparian shade cover exists. Here, evaporation is large causing a large decrease in subsurface storage, which leads to stream drying (represented by yellow block). Riparian transpiration decreases with the decrease in subsurface storage and grasses dry out in the late summer. Evaporation losses cease when surface flow is no longer present. **(D)** Alternative mass balance at location 1 where riparian transpiration decreases subsurface storage which leads to drying later in the season than in box C. **(E)** Alternative mass balance at location 1 where ET remains below the threshold that would lead to ET-driven stream drying, but drying still occurs because of a change in geologic, geomorphic, and or climatic controls that causes surface flows to cease, and thus evaporation to also cease.

2.7. Conclusion

Diel cycling causes wet-dry cycles to precede stream drying in headwater streams due to evapotranspiration losses. The start of drying during a diel cycling period is consistent among location and time of year. We find that during diel cycling wet-dry periods, large changes in solar radiation and temperature ($\pm$ 100 W/m^2/day) are correlated with the change in time dry during diel cycling periods. We also find that heterogeneity in the riparian vegetation cover (i.e. open canopy versus closed canopy) can cause streambed temperature to vary significantly. Under the assumption that temperature is a good proxy for evaporation losses, we propose that heterogeneity in riparian cover can determine the timing of drying during low flow periods once other geologic, geomorphic, and climatic stream drying controls are met. Finally, we review all hypothesized stream drying controls and propose a conceptual model which highlights the importance of changes in evaporation and transpiration as local controls on the timing of the start of drying. Future stream drying studies will benefit from spatially and temporally distributed evaporation and transpiration measurements coupled with lag analyses to assess network versus local effects. We observed relatively short lags between peak solar radiation and in-stream drying response, suggesting local effects may dominate. However, we only explored the lags between peak solar radiation and the start of drying during diel cycling periods. A more in-depth analysis of lags and water level may reveal an integrated hillslope signal.

2.8. References

Barnard, H.R., Graham, C.B., Van Verseveld, W.J., Brooks, J.R., Bond, B.J., McDonnell, J.J., 2010. Mechanistic assessment of hillslope transpiration controls of diel subsurface flow: a steady-state irrigation approach. Ecohydrology 3, 133–142. https://doi.org/10.1002/eco.114

Bond, B.J., Jones, J.A., Moore, G., Phillips, N., Post, D., McDonnell, J.J., 2002. The zone of vegetation influence on baseflow revealed by diel patterns of streamflow and vegetation water use in a headwater basin. Hydrol. Process. 16, 1671–1677. https://doi.org/10.1002/hyp.5022

Boronina, A., Golubev, S., Balderer, W., 2005. Estimation of actual evapotranspiration from an alluvial aquifer of the Kouris catchment (Cyprus) using continuous streamflow records. Hydrol. Process. 19, 4055–4068. https://doi.org/10.1002/hyp.5871

Brick, C.M., Moore, J.N., 1996. Diel variation of trace metals in the upper Clark Fork River, Montana. Environ. Sci. Technol. 30, 1953–1960. https://doi.org/10.1021/es9506465

Cadol, D., Kampf, S., Wohl, E., 2012. Effects of evapotranspiration on baseflow in a tropical headwater catchment. J. Hydrol. 462–463, 4–14. https://doi.org/10.1016/j.jhydrol.2012.04.060

Čermák, J., Kučera, J., Bauerle, W.L., Phillips, N., Hinckley, T.M., 2007. Tree water storage and its diurnal dynamics related to sap flow and changes in stem volume in old-growth Douglas-fir trees. Tree Physiol. 27, 181–198. https://doi.org/10.1093/treephys/27.2.181

Chapin, T.P., Todd, A.S., Zeigler, M.P., 2014. Robust, low-cost data loggers for stream temperature, flow intermittency, and relative conductivity monitoring. Water Resour. Res. 50, 6542–6548. https://doi.org/10.1002/2013WR015158

Costigan, K.H., Jaeger, K.L., Goss, C.W., Fritz, K.M., Goebel, P.C., 2016. Understanding controls on flow permanence in intermittent rivers to aid ecological research: integrating meteorology, geology and land cover. Ecohydrology 9, 1141–1153. https://doi.org/10.1002/eco.1712

Cullis, J.D.S., Stanish, L.F., McKnight, D.M., 2014. Diel flow pulses drive particulate organic matter transport from microbial mats in a glacial meltwater stream in the McMurdo Dry Valleys. Water Resour. Res. 50, 86–97. https://doi.org/10.1002/2013WR014061

Daiji, K., Suzuki, K., Nomura, M., 1990. Diurnal fluctuation in stream flow and in specific electric conductance during drought periods. J. Hydrol. 115, 105–114. https://doi.org/10.1016/0022-1694(90)90200-H

Datry, T., Larned, S.T., Tockner, K., 2014. Intermittent rivers: A challenge for freshwater ecology. Bioscience 64, 229–235. https://doi.org/10.1093/biosci/bit027

Eng, K., Wolock, D.M., Dettinger, M.D., 2016. Sensitivity of intermittent streams to climate variations in the USA. River Res. Appl. 32, 885–895. https://doi.org/10.1002/rra

Fahle, M., Dietrich, O., 2014. Estimation of evapotranspiration using diurnal groundwater level fluctuations: Comparison of different approaches with groundwater lysimeter data. Water Resour. Res. 50, 273–286. https://doi.org/10.1002/2013WR014472

Fortner, S.K., Lyons, W.B., Munk, L., 2013. Diel stream geochemistry, Taylor Valley, Antarctica. Hydrol. Process. 27, 394–404. https://doi.org/10.1002/hyp.9255

Geisler, E.T., 2016. Riparian zone evapotranspiration using streamflow diel signals. Boise State University. https://doi.org/10.1017/CBO9781107415324.004

Godsey, S.E., Kirchner, J.W., 2014. Dynamic, discontinuous stream networks: Hydrologically driven variations in active drainage density, flowing channels and stream order. Hydrol. Process. 28, 5791–5803. https://doi.org/10.1002/hyp.10310

Gomi, T., Sidle, R.C., Richardson, J.S., 2002. Understanding processes and downstream linkages of headwater systems. Bioscience 52, 905–916. https://doi.org/10.1641/0006-3568(2002)052[0905:UPADLO]2.0.CO;2

González-Ferreras, A.M., Barquín, J., 2017. Mapping the temporary and perennial character of whole river networks. Water Resour. Res. 53, 6709–6724. https://doi.org/10.1002/2017WR020390

Graham, C.B., Barnard, H.R., Kavanagh, K.L., McNamara, J.P., 2013. Catchment scale controls the temporal connection of transpiration and diel fluctuations in streamflow. Hydrol. Process. 27, 2541–2556. https://doi.org/10.1002/hyp

Hale, R.L., Godsey, S.E., 2019. Dynamic stream network intermittence explains emergent dissolved organic carbon chemostasis in headwaters. Hydrol. Process. 33, 1926–1936. https://doi.org/10.1002/hyp.13455

Jaeger, K.L., Olden, J.D., 2012. Eletrical resistance sensor arrays as a means to quantify longitudinal connectivity of rivers. River Res. Appl. 28, 1843–1852. https://doi.org/10.1002/rra.1554

Jaeger, K.L., Olden, J.D., Pelland, N.A., 2014. Climate change poised to threaten hydrologic connectivity and endemic fishes in dryland streams. Proc. Natl. Acad. Sci. U. S. A. 111, 13894–13899. https://doi.org/10.1073/pnas.1320890111

Jaeger, K.L., Sando, R., McShane, R.R., Dunham, J.B., Hockman-Wert, D.P., Kaiser, K.E., Hafen, K., Risley, J.C., Blasch, K.W., 2019. Probability of Streamflow Permanence Model (PROSPER): A spatially continuous model of annual streamflow permanence throughout the Pacific Northwest. J. Hydrol. X 2, 100005. https://doi.org/10.1016/J.HYDROA.2018.100005

Jensen, C.K., McGuire, K.J., McLaughlin, D.L., Scott, D.T., 2019. Quantifying spatiotemporal variation in headwater stream length using flow intermittency sensors. Environ. Monit. Assess. 191. https://doi.org/10.1007/s10661-019-7373-8

Kormos, P.R., Marks, D., Seyfried, M., Havens, S., Hendrick, A., Lohse, K.A., Masarik, M., Flores, A.N., 2016. 31 years of spatially distributed air temperature, humidity, precipitation amount and precipitation phase from a mountain catchment in the rain-snow transition zone. https://doi.org/10.18122/B2B59V

Milligan, G.W., 1980. An examination of the effect of six types of error perturbation on fifteen clustering algorithms. Psychometrika 45, 325–342. https://doi.org/10.1007/BF02293907

Nadeau, T.L., Rains, M.C., 2007. Hydrological connectivity between headwater streams and downstream waters: How science can inform policy. J. Am. Water Resour. Assoc. 43, 118–133. https://doi.org/10.1111/j.1752-1688.2007.00010.x

Pierson, F.B., Slaughter, C.W., Cram, Z.K., 2000. Monitoring discharge and suspended sediment, Reynolds Creek Experimental Watershed, Idaho, USA. ARS Tech. Bull. NWRC.

Queener, N., 2015. Spatial and temporal variability in baseflow and stream drying in the Mattole River Headwaters. Humboldt State University. https://doi.org/10.1007/springerreference_226434

Radke, A.G., 2018. Spatiotemporal heterogeneity of water and dissolved organic carbon sourcing in a snow-dominated, headwater catchment. Idaho State University.

Runkel, R.L., McKnight, D.M., Andrews, E.D., 2016. Analysis of Transient Storage Subject to Unsteady Flow : Diel Flow Variation in an Antarctic Stream. J. North Am. Benthol. Soc. 17, 143–154.

Stanley, E.H., Fisher, S.G., Grimm, N.B., 1997. Ecosystem Expansion and Contraction in Streams. Bioscience 47, 427–435. https://doi.org/10.2307/1313058

Sullivan, A.B., Drever, J.I., 2001. Spatiotemporal variability in stream chemistry in a high-elevation catchment affected by mine drainage. J. Hydrol. 252, 237–250. https://doi.org/10.1016/S0022-1694(01)00458-9

U.S. Environmental Protection Agency and U.S. Army Corps of Engineers, 2015. Technical Support Document for the Clean Water Rule: Definition of Waters of the United States. U.S. Environ. Prot. Agency.

Vega, S.P., Williams, C.J., Brooks, E.S., Pierson, F.B., Strand, E.K., Robichaud, P.R., Brown, R.E., Seyfried, M.S., Lohse, K.A., Glossner, K., Pierce, J.L., Roehner, C., 2020. Interaction of wind and cold-season hydrologic processes on erosion from complex topography following wildfire in sagebrush steppe. Earth Surf. Process. Landforms 45, 841–861. https://doi.org/10.1002/esp.4778

Ward, A.S., Schmadel, N.M., Wondzell, S.M., 2018. Simulation of dynamic expansion, contraction, and connectivity in a mountain stream network. Adv. Water Resour. 114, 64–82. https://doi.org/10.1016/j.advwatres.2018.01.018

White, W.N., 1932. A method of estimating ground-water supplies based on discharge by plants and evaporation from soil. USGS Water-Supply Pap. no. 659-A.

Wondzell, S.M., Gooseff, M.N., McGlynn, B.L., 2010. An analysis of alternative conceptual models relating hyporheic exchange flow to diel fluctuations in discharge during baseflow recession. Hydrol. Process. 24, 686–694. https://doi.org/10.1002/hyp.7507

Worrall, F., Howden, N.J.K., Burt, T.P., 2015. Understanding the diurnal cycle in fluvial dissolved organic carbon - The interplay of in-stream residence time, day length and organic matter turnover. J. Hydrol. 523, 830–838. https://doi.org/10.1016/j.jhydrol.2015.01.075

Yu (于松延), S., Bond, N.R., Bunn, S.E., Xu, Z., Kennard, M.J., 2018. Quantifying spatial and temporal patterns of flow intermittency using spatially contiguous runoff data. J. Hydrol. 559, 861–872. https://doi.org/10.1016/j.jhydrol.2018.03.009

3. Chapter 3: Influence of baseflow on stream drying

3.1. Abstract

Intermittent streams currently make up more than 50% of the global river network and are found across many climates and landscapes. Intermittent streams source downstream water supplies and impact water quality. Hydrologists have begun to understand the controls that influence spatiotemporal stream drying patterns, but there is still no consensus on the dominant controls. We use a network of stream drying sensors interspersed between baseflow monitoring locations in two headwater streams within the Reynolds Creek Critical Zone Observatory to investigate the role that baseflow plays in controlling stream drying patterns. In addition, we use 1-m LiDAR to calculate watershed topographic metrics such as slope, upstream watershed area, curvature, topographic wetness index (TWI), and the down-valley sub-surface storage capacity and compare these metrics to seasonal flow permanence. We find that when baseflow inputs are steady, surface flow is more likely to persist, even during times of limited precipitation. We also find that stream drying is more probable in areas with low upstream watershed area, high slope, and low TWI. Finally, we find that the down-valley subsurface storage capacity and stream curvature correlate poorly with seasonal flow permanence. We suggest that subsurface properties that impact the ability of water to pass through the subsurface, such as hydraulic conductivity are important controls on stream permanence and that spatially distributed subsurface property measurements should be implemented in future stream drying studies.

3.2. Introduction

Ephemeral and intermittent streams networks expand and contract as surface flows vary both spatially and temporally. Over 50% of the streams in the United States are ephemeral or intermittent, and such streams are commonly the headwaters of larger streams and rivers (Gutiérrez-Jurado et al., 2019; Levick et al., 2008). During the last two decades, our understanding of stream drying patterns and the controls that spatiotemporal drying patterns has improved (Blasch et al., 2002; Costigan et al., 2016; Dohman, 2018; Godsey and Kirchner, 2014; Goulsbra et al., 2014; Gutiérrez-Jurado et al., 2019; Jaeger et al., 2014; Jaeger and Olden, 2012; Jensen et al., 2019; Peirce and Lindsay, 2015; Prancevic and Kirchner, 2019; Ward et al., 2018; Yu (于松延) et al., 2018; Zimmer and McGlynn, 2017b). Stream drying is governed by processes at multiple scales, including watershed topography (Prancevic and Kirchner, 2019); shallow subsurface characteristics (Dohman, 2018) including soil and stratigraphy (Gutiérrez-Jurado et al., 2019; Zimmer and McGlynn, 2017b); and meteorology, geology, and land cover (Costigan et al., 2016). Despite our understanding of this range of stream drying controls, the spacing and timing of stream drying cannot yet be reliably predicted, in part because of our poor characterization and understanding of baseflow at different spatial and temporal scales and the processes governing it.

During low-flows, streams depend on stored subsurface water, or baseflow (Freeze, 1974; Godsey et al., 2013; Segura et al., 2019). Baseflow can either be sourced to streams through shallow flowpaths or via deeper flowpaths through bedrock (Frisbee et al., 2011), but partitioning these sources is complicated by interactions between spatially heterogeneous and dynamic subsurface and surface processes (Fleckenstein et al., 2006; Ghosh et al., 2016; Kirchner, 2009b; McDonnell et al., 2007). Like stream drying, baseflow is influenced by watershed size, topography, vegetation, subsurface characteristics, and precipitation inputs (Partington et al., 2012; Payn et al., 2012; Segura et al., 2019). Controls on baseflow are not static, but instead change in response to different forcing functions such as rainfall, evapotranspiration, and groundwater pumping (Partington et al., 2012). Dynamic controls can cause baseflow fluxes to vary both temporally and spatially on the watershed scale (Duvert et al., 2018; Zimmer and McGlynn, 2017a).

Groundwater inputs have been observed to vary in both magnitude and chemistry throughout the length of a single stream (Carey et al., 2013; Frisbee et al., 2011; Liu et al., 2013; Zimmer and McGlynn, 2017b). Despite this, spatiotemporal heterogeneity in baseflow at the stream scale is commonly poorly characterized because it requires a dense spatiotemporal dataset. Collecting data to characterize this heterogeneity not only has the potential to improve our understanding of stream drying, but also variability in runoff processes (Furey and Gupta, 2001) and streamflow magnitude and timing (Wittenberg and Sivapalan, 1999). Indeed, spatiotemporal baseflow dynamics will likely become more important and complex as climate changes, especially in the western U.S. where snowpack is expected to predicted to decline (Earman and Dettinger, 2011; Klos et al., 2014; Lundquist et al., 2009; Mote et al., 2018; Nolin and Daly, 2006; Segura et al., 2019), potentially changing the role of subsurface storage in sustaining surface flows.

Stream drying primarily occurs when baseflow is the primary flow source (Ghosh et al., 2016). However, it is currently unclear the degree of spatiotemporal heterogeneity in baseflow contributions that must be captured in order to accurately model variability in stream expansion and contraction. Furthermore, it is unknown whether stream drying is driven more by changes in subsurface geometry or heterogeneity in hydraulic conductivity at any given location. For example, do stable baseflow inputs suggest that surface flow is more reliable? Are the primary controls on baseflow also the primary controls on stream drying? Can surface flow persist where baseflow is not a strong influence?

To answer these questions, we use multiple baseflow measurements and a dense spatiotemporal network of stream drying observations to relate stream drying and baseflow in two headwater streams. We then deepen this assessment in one of these streams and quantify the spatiotemporal heterogeneity of drying patterns. We explore the connection between baseflow and stream drying patterns to determine whether geomorphic controls such as slope, topographic wetness index, and subsurface capacity can be used to predict both baseflow and stream drying. We use the data detailed above to ask the following questions: 1) How are baseflow and stream drying related on both spatial and temporal scales? 2) Can watershed topography be used to predict stream drying variability?

3.3. Site Description

The Reynolds Creek Critical Zone Observatory (RC CZO) is a 239 km^2 semi-arid watershed located in southwestern Idaho (Seyfried et al., 2018). It consists of thirteen instrumented sub-watersheds that contribute to the larger Reynolds Creek which eventually feeds into the Snake River (Pierson et al., 2000). Two sub-watersheds, Murphy Creek and Reynolds Mountain East (RME) were selected to study the influence of baseflow on stream drying patterns because they span the rain-snow transition, vary in geology and vegetation, and have very different watershed areas (Figure 3.1A), and therefore provide an opportunity to compare how stream setting impacts seasonal drying patterns.

Of the two study watersheds, Murphy Creek (1.29 km^2) is the lower elevation of the two (1598 m mean elevation) and is drained by a 2.5-km channel (Figure 3.1B). Murphy Creek is located below the rain-snow transition and receives >50% of its mean annual precipitation as rain (mean annual precipitation = 639 mm/yr) (Kormos et al., 2016). The Murphy Creek basin is underlain by Salmon Creek volcanics (56%) and Reynolds Basin basalt and latite (44%). Its hillslopes are covered largely with mountain big sagebrush (*Artemisia tridentata*), bitterbrush (*Purshia tridentata*), Idaho fescue (*Festuca idahoensis*), Sandberg bluegrass (*Poa secunda*), bluebunch wheatgrass (*Pseudoroegneria spicata*), squirreltail grass (*Elymus elymoides*), and snowberry (*Symphoricarpos*) (Pierson et al., 2000). Riparian channels are lined with willow and other small bushes (Pierson et al., 2000). In 2015, the Soda Fire burned the Murphy watershed, and the basin functions such as vegetation cover largely recovered from the fire within two years (Glossner et al., in prep; Lohse et al., in prep).

RME (0.43 km^2) drains the highest elevations in the RC CZO (2075 m mean elevation) via two branches that converge totaling 1.1 km of channel (Figure 3.1C). RME is located above the rain-snow transition and receives >50% of its mean annual precipitation as snow (mean annual precipitation = 912 mm/yr) (Kormos et al., 2015). The geology in RME is Reynolds Basin basalt and latite (Pierson et al., 2000). RME is primarily covered by mountain big sagebrush (*Artemisia tridentata*), with natural mountain meadows, but also contains aspen (*Populus tremuloides*), willow (*Salix*), and Douglas fir (*Pseudotsuga menzeii*) that vary strongly with elevation, aspect and wind distribution of snow (Pierson et al., 2000).

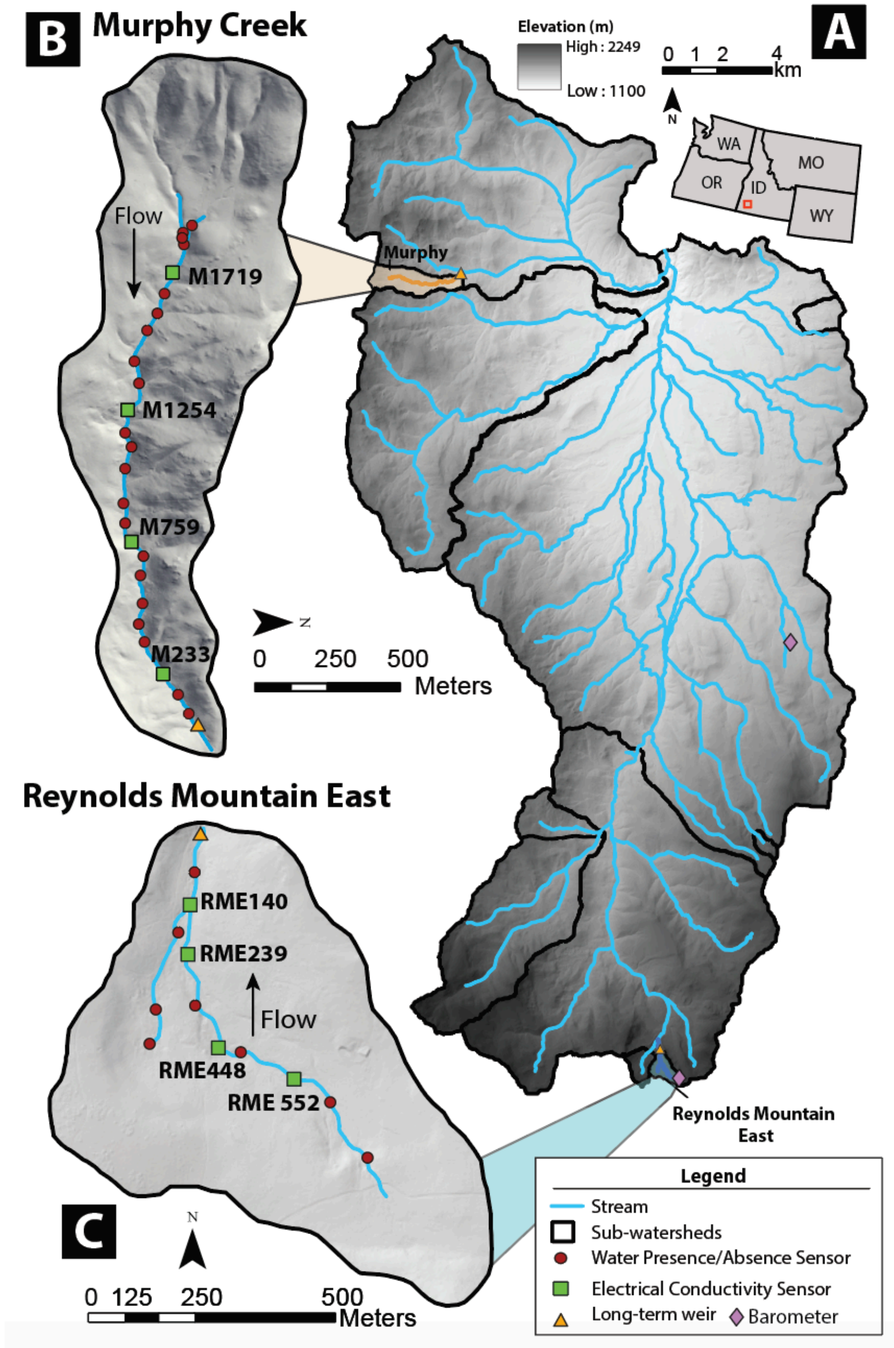

Figure 3.1 (A) Reynolds Creek Critical Zone Observatory with sub-watersheds Murphy Creek and Reynolds Mountain East (RME) highlighted in orange and blue, respectively. Instrumentation at **(B)** Murphy Creek and **(C)** RME, described in section 3.4.1.

3.4. Methods

In order to evaluate the relationships between spatiotemporal stream drying patterns, baseflow inputs, and watershed topography, we collected four different types of data. At Murphy Creek, we collected temporally continuous flow presence and baseflow data and used LiDAR to extract topographic metrics and to estimate the down-valley subsurface storage capacity. At RME, only continuous flow presence and baseflow data were collected; we did not assess the role of topography on stream drying heterogeneity because stream drying patterns varied much less than in Murphy, as discussed in the results.

3.4.1. Field Data Collection

We determined stream specific conductivity and water level at four locations in both RME and Murphy in order to calculate baseflow. We observed specific conductivity (SC) with freshwater HOBO electrical conductivity (EC) dataloggers (Onset Hobologger, U-24) and measured water level with HOBO water level (WL) dataloggers (Onset Hobologger, U-20). We detected water presence and absence with modified HOBO Pendant Loggers (Onset HOBO Pendant/Light 64K Datalogger UA-002-64); experiment set-up and calibration regarding HOBO Pendant loggers are detailed in Chapter 2. A Vaisala HMP155 humidity and temperature probe collected air temperature and a LI-7500RS Open Path CO_2/H_2O Analyzer collected barometric pressure every 30 minutes. Temperature and barometric pressure were measured in the RME sub-watershed and in Nancy's Gulch, a sub-watershed approximately 13 km southeast of Murphy Creek at a similar elevation (Nancy's Gulch Meteorological Station: 1426 m, Murphy Creek Weir: 1392 m) (Figure 3.1).

Water level and electrical conductivity sensors were housed in black 2" PVC that was slightly longer than the length of the sensor. The bottom of the PVC pipe was drilled with holes so that water could freely enter and exit the pipe at the stream bed interface. Pendants were housed in gray PVC so that the two pole electrodes at the bottom of the plastic housing were in constant contact with the stream bed and thus were able to detect the lowest of flows.

The sensor set-up for each watershed is displayed in Figure 3.1A. We installed twenty-one Pendant loggers throughout Murphy Creek and four paired electrical conductivity (EC) and water level (WL) loggers were interspersed between every five Pendant sensors (Figure 3.1B) with approximately 80 m between each sensor. In RME, four EC/WL loggers were interspersed between eight Pendant sensors (Figure 3.1C). Each sensor is hereby referred to as MX or RMEX, where X is the distance in meters from the downstream outlet weir at each respective watershed and M and RME refer to the Murphy and Reynolds Mountain East sub-watersheds, respectively.

All sensors recorded at 15-minute intervals from June 3 to October 1, 2019. Seven of the Pendant sensors in Murphy Creek were added on July 10, 2019 (M454, M716, M823, M1121, M1377, and M1653). For each of these seven additional sensors, continuous flow was assumed from June 3 to 12, 2019; this assumption is validated by in-field observations. If no gaps in flow were observed between July 10 to 17, 2019 continuous flow was assumed from June 3, 2019 to July 10, 2019 (M454, M716, M1377, and M1653). If any gaps in flow were observed between July 10 and July 17, 2019, we made no assumptions about whether the stream was flowing or dry between June 12, 2019 to July 10, 2019 (M823, M1121, M1951). Any other gaps in flow presence records were due to logger failure (M1166, M1653, M1799).

3.4.2. Data Calculations

3.4.2.1 Specific Conductivity Calculation

Specific conductivity was calculated from electrical conductivity using Equation 3.1, where SC is the specific conductivity in µS/cm, EC is the electrical conductivity in µS/cm, α is the temperature-compensation factor 0.02 in˚C^{-1}, and T is the measured temperature in ˚C (USGS, 2019). Quality assurance and control corrections done to maintain high-quality specific conductivity measurements are detailed in Appendix A.

$$SC = \frac{EC}{1+\alpha(T-25^{\circ}C)} \qquad (3.1)$$

3.4.2.2 Water Level Calculation

We determined stream water levels using barometric pressure and in-stream HOBO water level loggers. Barometric pressure and air temperature were collected every 30 minutes and in-stream water level pressure was collected every 15 minutes. A simple linear interpolation was used to estimate air temperature and pressure at the 15- and 45-minute marks every hour. Barometric pressure readings collected at RME (2112 m) and Nancy's Gulch (1426 m) were corrected to the elevation of each in-stream water-level logger using Equation 2, where P is the elevation-corrected pressure in kPa, P_o is the pressure measured at the weather station in kPa, M is the molar mass of dry air in kg/mol, g is gravitational acceleration in m/s^2, z is the elevation difference between the weather station and the in-stream water level logger in meters, R is the universal gas constant for the typical atmospheric composition of mixed gases in J/mol*K, and T is the air temperature at the weather station in Kelvin. Other corrections done to maintain quality water-level measurements are detailed in Appendix A.

$$P = P_o e^{\frac{-Mgz}{RT}} \qquad (3.2)$$

HOBO water-level loggers were calibrated using an in-lab test where the logger was placed at the bottom of a container with vertical walls. Water was gradually added to the container in 2-cm increments from 4- to 12-cm depth, and an out-of-water barometer was used to correct for barometric pressure and convert pressure to water level. After each 2-cm water addition, the container was left to stabilize before the next increment was added. Average water level was logged at each increment and compared to the actual water level corrected for the height of the logger in the container. The instrument-specific linear relationship between the actual and observed water level was used to estimate in-stream water level readings.

3.4.2.3 Stage-Discharge Relationship

We assumed a power-law stage-discharge relationship ($Q = aZ^b$), where a and b are constants and Z is the corrected stage height or water level (cm) determined by the HOBO water level loggers to calculate discharge at 15-minute intervals throughout the observation period. Discharge was measured in the field between two to six times at each baseflow monitoring location. If the stream was dry, discharge was not measured. In both RME and Murphy Creek, discharge measurements were typically collected using the salt dilution method (Moore, 2003) except when flows were high in early June at RME and a FlowTracker was used. All discharge measurements are reported in Appendix A. At locations M759, RME140, RME448, and RME552, flows could not be measured during at least one visit during the field season because the stream was dry, or flows were so low that even salt dilution was not sufficient. In order to maintain reasonable power-law stage-discharge relationships, a small positive water level of ≤ 0.1 cm and a discharge of ≤ 0.01 L/s was assumed for these locations by visually inspecting the stage-discharge curve after each small value adjustment until calculated low discharges reflected our in-field observations.

3.4.2.4 Baseflow Calculation

Discharge and specific conductivity measurements were combined to calculate the baseflow component of the hydrograph at each 15-minute timestep using Equation 3.3 (Miller et al., 2014):

$$Q_{BF} = Q \frac{[SC - SC_{RO}]}{[SC_{BF} - SC_{RO}]} \qquad (3.3)$$

where Q_{BF} is the baseflow (L/s) at time t, Q is the total discharge (L/s) at time t, SC is the specific conductivity (µS/cm) at time t, SC_{RO} is the specific conductivity of the runoff endmember, and SC_{BF} is the specific conductivity of the baseflow end-member. The runoff endmember and baseflow endmembers were the minimum and maximum values of specific conductivity measured during the field season, respectively. If data for a given timestep was missing, baseflow was not calculated for the timestep. Percent baseflow was determined by dividing the baseflow by the total discharge at the same timestep. If no flow was observed, percent baseflow was assigned 100% under the assumption that groundwater is present in the subsurface.

3.4.3. Topographic Metrics

We calculated watershed topographic metrics to determine whether topography can be used to predict stream drying variability, as informed by the flow presence and baseflow sensors. Only Murphy Creek is included in the topographic analysis. We did not assess topographic metrics and their relationship with flow permanence at RME because spatial flow permanence patterns varied much less than in Murphy Creek.

The watershed area, stream network extent, curvature and local slope were computed for the Murphy watershed using TopoToolbox 2, a MATLAB-based software for topographic analysis (Schwanghart and Scherler, 2014), and topographic attributes were extracted at all sensor locations by snapping all sensor locations determined in the field from GPS to the delineated stream. The topographic wetness index (TWI) was also calculated at each sensor location using Equation 3.4 (Beven and Kirkby, 1979):

$$TWI = ln\left(\frac{tan\beta}{a}\right) \qquad (3.4)$$

where $tan\beta$ is the slope in radians and a is the upslope contributing area. TWI is a topographic metric commonly used to quantify topographic controls on hydrologic process (Sørensen et al., 2006). All metrics were then correlated with seasonal flow permanence at each sensor location to assess geomorphic controls on drying patterns. We performed a multiple linear regression with the topographic metrics described above, but found that a single variable was the best predictor of flow permanence.

We estimated the down-valley subsurface capacity at each sensor location in Murphy Creek using an 1-m DEM derived from LiDAR (Ilangakoon et al., 2016) and assumed that the subsurface profile was V-shaped topped with variable amounts of valley fill. To estimate the amount of fill, we extracted topographic profiles $\left(Z(x)\right)$ perpendicular to stream flow at each of the sensor locations and found the minimum elevation in the profile at the thalweg of the stream (point T in Figure 3.2). Next, we visually assessed an approximate valley width (w) at each point based on field observations and the extracted profile. We then used this width to define points A and D, at locations $T - w$ and $T + w$, respectively (Figure 3.2), and searched between points A and D to identify the points on each hillslope with the largest change in slope on each side of point T, indicating the transition from hillslope to valley fill (points B and C in Figure 3.2). We then fit a line to all points above each break in slope (red dashed lines between points A and B or between points C and D in Figure 3.2), and we next projected these hillslope profiles below the observed topographic profile until they intersected to generate the assumed V-shaped valley cross-sectional profile. The difference between this assumed V-shaped valley profile and the actual topographic profile is assumed to represent the down-valley subsurface capacity (hatched area in Figure 3.2). If the projected lines plotted above the topographic profile, the subsurface storage at that point was zero (see red dashed line above the topographic profile for a portion of the projection between points B and T). The calculation is detailed in Appendix C.

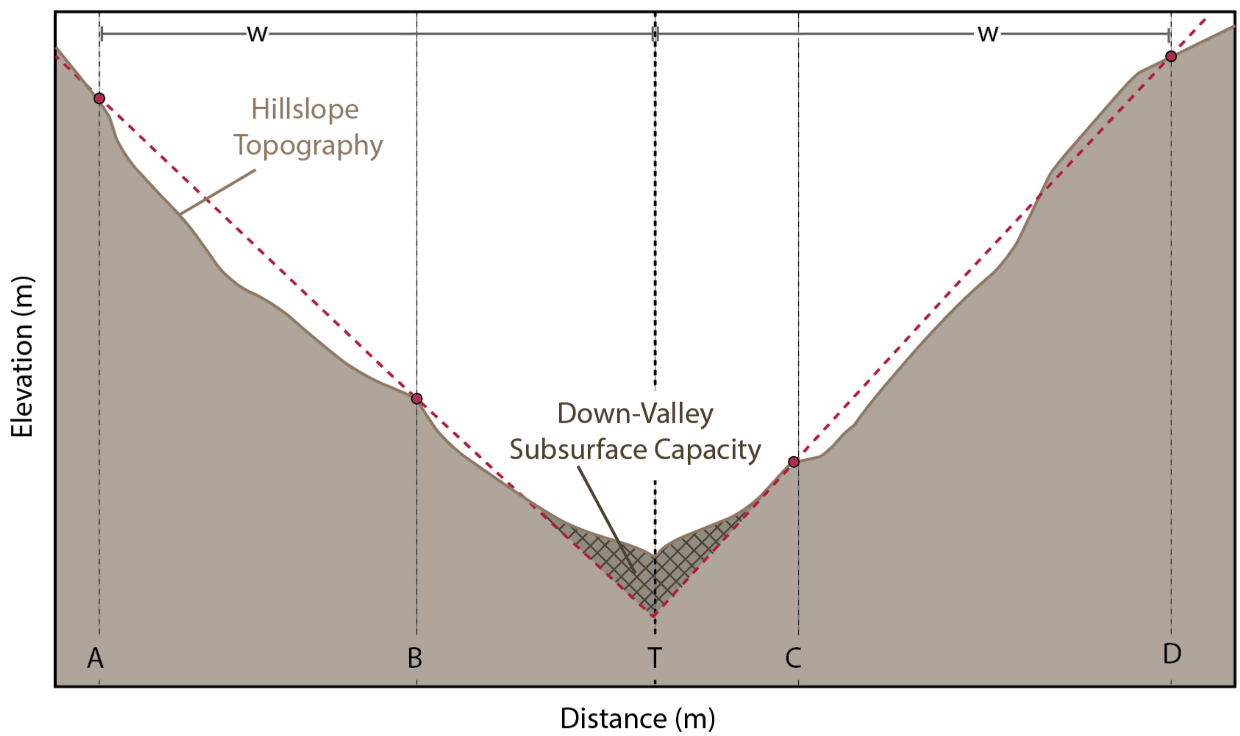

Figure 3.2. Conceptual diagram showing down-valley subsurface capacity calculation. Points A and D are located the estimated valley width, w, from the location of minimum elevation at the thalweg, point T. Points B and C are the locations of the largest change in slope between points A and T and D and T, respectively. The down-valley subsurface capacity (hatched area) is the difference between the observed valley topographic profile and the inferred V-shaped valley as fit by lines from A to B and C to D, shown in dashed red lines.

3.4.4. Stream drying terminology

We quantified spatiotemporal metrics of stream drying, analyzing data both at specific locations in space and throughout the network as well as at a single moment and integrated over the entire observation season. Table 3.1 summarizes the terminology we adopt to distinguish stream drying across time and space, and the metrics that we calculated from the data that we collected. *Flow permanence* refers to the fraction of the season with surface flow at a given location whereas the *flowing network extent* refers to the percent of sensors that are flowing either at a given moment (*instantaneous*) or integrated over the season (*seasonal*). Observations of the *presence or absence* of flow at a given sensor location at a given moment in time form the basis of all of the other integrated metrics.

Table 3.1. Terminology and metrics used to discuss spatial, temporal, and spatiotemporal patterns of stream drying at a point and throughout the network, both at any given moment in time and throughout the season. At RME, eight Pendants and four baseflow monitoring locations were used, leading to a maximum total of twelve sensors for any given metric. At Murphy, twenty-one Pendants and four baseflow monitoring locations were used, leading to a maximum total of twenty-five sensors for any given metric. In each quadrant of the table, a term is listed with a definition of the term directly below in brackets. Below the dashed line, the number of sensors (n) used in the metric and the number of timesteps (t) included (one 15-minute timestep or an average of all timesteps throughout the entire season from June 3 to October 1, 2019).

Spatiotemporal Metrics

	Moment	*Season*
Point	Presence/absence of flow [flow/no flow] RME: n = 1, t = 1 Murphy: n = 1, t = 1	Seasonal flow permanence [% of season with flow at a given location] RME: n = 1, t = season Murphy: n = 1, t = season
Network	Instantaneous flowing network extent [% of sensors flowing at a given moment] RME: n = 12, t = 1 Murphy: n = 25, t = 1	Seasonal flowing network extent [% of sensors flowing integrated across season] RME: n = 12, t = season Murphy: n = 25, t = season

3.5. Results

3.5.1. Overview

We discuss spatiotemporal variability in stream drying patterns, both within RME and Murphy Creek, and between watersheds, before reporting observations from hypothesized drivers of spatiotemporal heterogeneity. Because we expect that variability in baseflow inputs and topographic metrics will inform drying patterns, we detail discharge and specific conductivity measurements used to calculate baseflow, heterogeneity in baseflow inputs, and percent baseflow. Finally, we explain variation in topographic metrics and the down-valley subsurface storage capacity.

3.5.2. Stream Drying Patterns

In both RME and Murphy, both streams had spatially continuous flow in June at the beginning of the study, and gradually dried as the summer progressed. It is likely that the streams had already expanded and contracted prior to the study period in both watersheds because seasonal snowpacks had mostly melted by June after extensive spring rainstorms. Compared to our mapped network, MacNeille et al. (in prep) observed a longer flowing length in Murphy Creek by 800 m in April 2016, one year after the Soda Fire. In RME, the geomorphic channel network extended above our uppermost sensors and was observed to be dry upstream through an upper meadow in June 2019. Of the four baseflow monitoring stations in RME, only the uppermost location dried, and it never rewetted during the observation period. In Murphy, drying was much more dynamic: the uppermost regions dried first and stayed dry through the experiment period. However, unlike RME, mid- and low-elevation locations in Murphy also dried at irregular intervals, and some locations rewetted after a September storm (see Chapter 2 for drying details).

3.5.1.1 Discharge

In both RME and Murphy Creek, seasonal discharge patterns were similar. During the observation period, all baseflow monitoring locations in Murphy and RME exhibited peak flows within the first two weeks of June (Figures 3.3 and 3.4). The maximum flows in Murphy Creek from lowest elevation to highest elevation were 16.2, 11.0, 7.8, and 3.5 L/s, respectively. The maximum flows in RME from lowest elevation to highest elevation were 22.8, 18.0, 15.6, and 12.1 L/s, respectively. The lowest flows were measured in late August to early September. M1254 was the only baseflow monitoring location that did not dry and it had a minimum discharge of <0.1 L/s. In RME, only RME542 dried, but the three lower baseflow monitoring locations had minimum discharges of <0.1 L/s. In both RME and Murphy, discharge was greatest at the outlet and usually decreased with increasing elevation. In Murphy, discharge increased after a large storm in early September and many dry sites rewetted at that time. Both Murphy and RME Creeks exhibited variation in flow along their networks at multiple timescales. For example, in both RME and Murphy Creeks, the magnitude of both daily and seasonal fluctuations in discharge varied throughout the network.

3.5.1.2 Specific Conductivity

In both RME and Murphy, specific conductivity (SC) decreased with elevation in the four baseflow monitoring locations. At all baseflow monitoring locations, SC was lowest at the beginning of the experiment period and increased as the summer progressed. Finally, in all locations with flow at the end of the season (both those locations that sustained flow throughout the season and those locations that rewetted by season's end), SC began to drop in early September and continued to decrease through the end of the experimental period. Despite the consistency in seasonal patterns between watersheds, SC at individual baseflow monitoring locations exhibited short-term trends that were unique to each individual baseflow monitoring location (Figures 3.3 and 3.4). In addition, diel cycles in SC varied throughout both headwater streams.

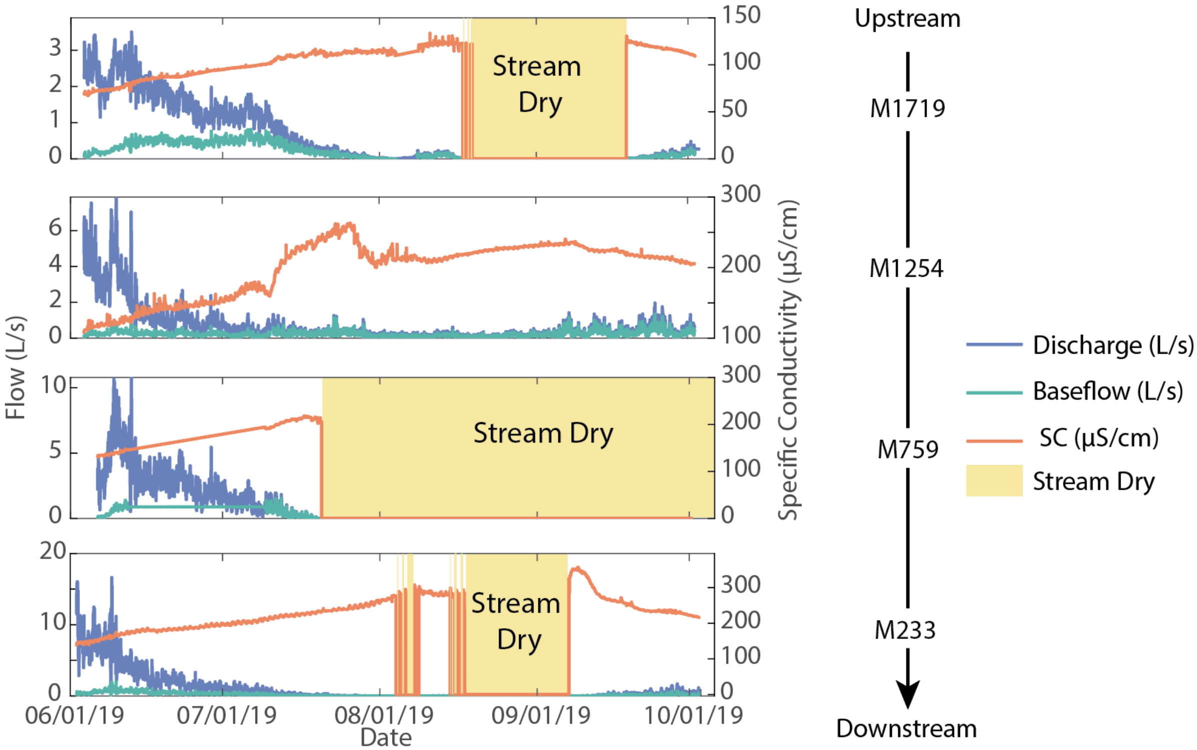

Figure 3.3. Discharge (L/s), baseflow (L/s), and SC (µS/cm) throughout the observation period at each of the four baseflow monitoring stations in Murphy Creek. Discharge and baseflow are plotted on the left-hand-side y-axis while SC is plotted on the right-hand-side y-axis. Plots are ordered from downstream (bottom) to upstream (top); the distance from the outlet weir is coded in the sensor name to the right of the plots using the notation MX where X refers to meters from the outlet weir.

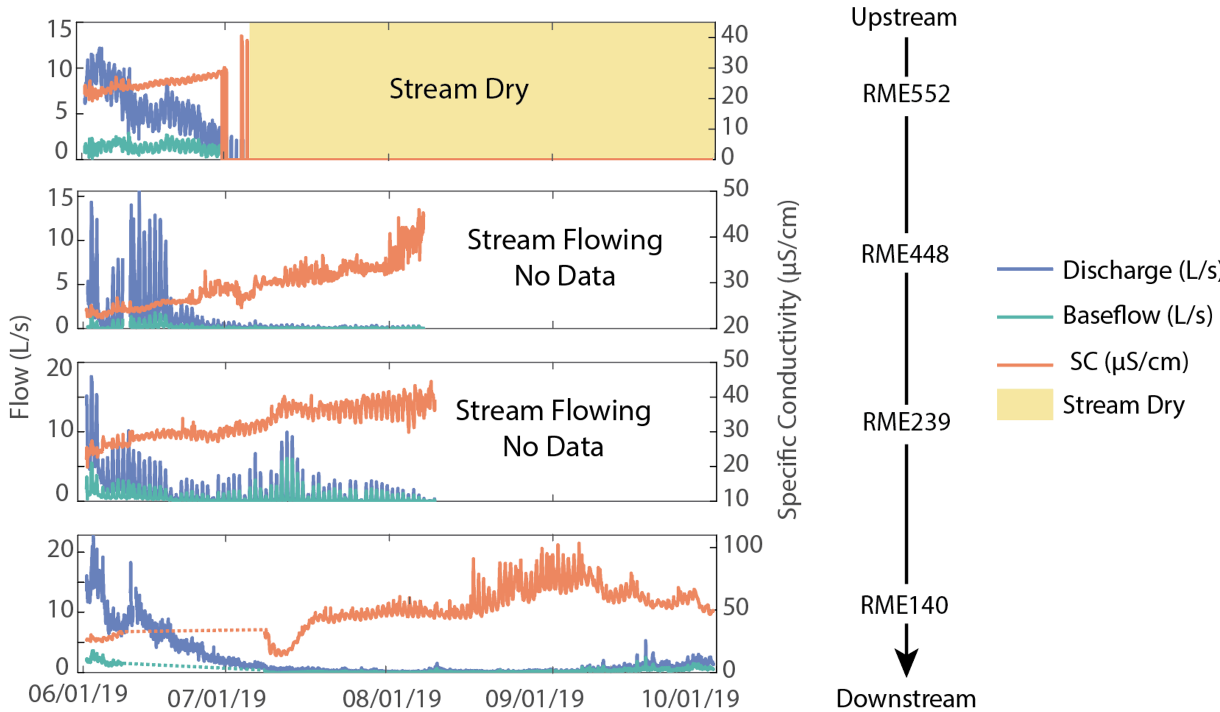

Figure 3.4. Discharge (L/s), baseflow (L/s), and SC (µS/cm) throughout the observation period at each of the four baseflow monitoring stations in RME Creek. Discharge and baseflow are plotted on the left-hand-side y-axis while SC is plotted on the right-hand-side y-axis. Plots are ordered from downstream (bottom) to upstream (top); the distance from the outlet weir is coded in the sensor name to the right of the plots using the notation RMEX where X refers to meters from the outlet weir. At RME 448 and 239, although the stream was flowing, it was heavily disturbed by animals from mid-August through October, and measurements of SC and discharge were unusable.

3.5.3. Baseflow

At all baseflow monitoring locations, the magnitude of baseflow peaked early in the season, declined during the summer, and increased in early September after the onset of fall storms (Figures 3.5 & 3.6). Although discharge predictably decreased with increasing elevation, baseflow did not; the magnitude of baseflow was more consistent than discharge throughout space in both streams. The two-week moving average of baseflow magnitude was consistently less than 1 L/s at all locations in Murphy Creek, and less than 2 L/s at all locations in RME (Figure 3.6).

In Murphy Creek, the only location that did not dry (M1254) had the lowest baseflow contribution at the beginning of the season (<0.4 L/s) and the lowest baseflow standard deviation for the entire season (0.16 L/s). Baseflow magnitude at the three other sites peaked in June to early July, then decreased dramatically in mid-July before drying initiated. In RME, baseflow magnitude was greatest at the start of the season at the most downstream site (RME140); baseflow magnitude then decreased significantly at the start of July when the snowdrift melted (Figure 3.6A), but as a percentage of total flows, RME140 had the most stable seasonal baseflow input. RME552 had the second greatest baseflow magnitude at the start of the season; however, after the snow drift melted completely, it quickly dried. The other two lower baseflow monitoring locations (RME448 and RME239) had lower baseflow magnitudes, but these magnitudes also remained relatively stable once the snow drift ceased. Due to animal interference at RME239 and RME 448, baseflow was not determined during most of August and all of September and October. At RME140, the only location with both continuous flow and baseflow measurements, percent baseflow increased through the summer until fall storms started and increased the contribution of runoff to streams.

3.5.4. Percent Baseflow

The baseflow contribution to discharge, or percent baseflow, was consistently lowest at the beginning of the season in both Murphy and RME (Figure 3.5B and 3.6B). As flows decreased, the percent baseflow rose and typically peaked in late August to early September. In both watersheds, percent baseflow varied more among sites from mid-July to September than during other times (Figures 3.5B and 3.6B). Furthermore, the weekly rates of change in percent baseflow were less consistent among sites during this peak drying period as well. At the beginning and end of the observation period, when streamflow was high, percent baseflow increased at roughly similar rates across all sites (Figures 5B & 6B). Baseflow patterns were most similar with each stream in July and August when baseflow was relatively low.

In Murphy Creek, percent baseflow was most similar at M233, M759, and M1719, the three baseflow monitoring locations that dried (Figure 3.5B). The standard deviation of percent baseflow at the four locations in Murphy Creek was negatively correlated ($R^2 = 0.53$) with the seasonal flow permanence (Figure 3.5D) so that when percent baseflow was more stable, the stream was more likely to remain flowing. In RME, percent baseflow peaked in early July at RME552 and in early September at RME140. Incomplete baseflow records at RME239 and RME448 prevent us from reporting the timing of the percent baseflow peak.

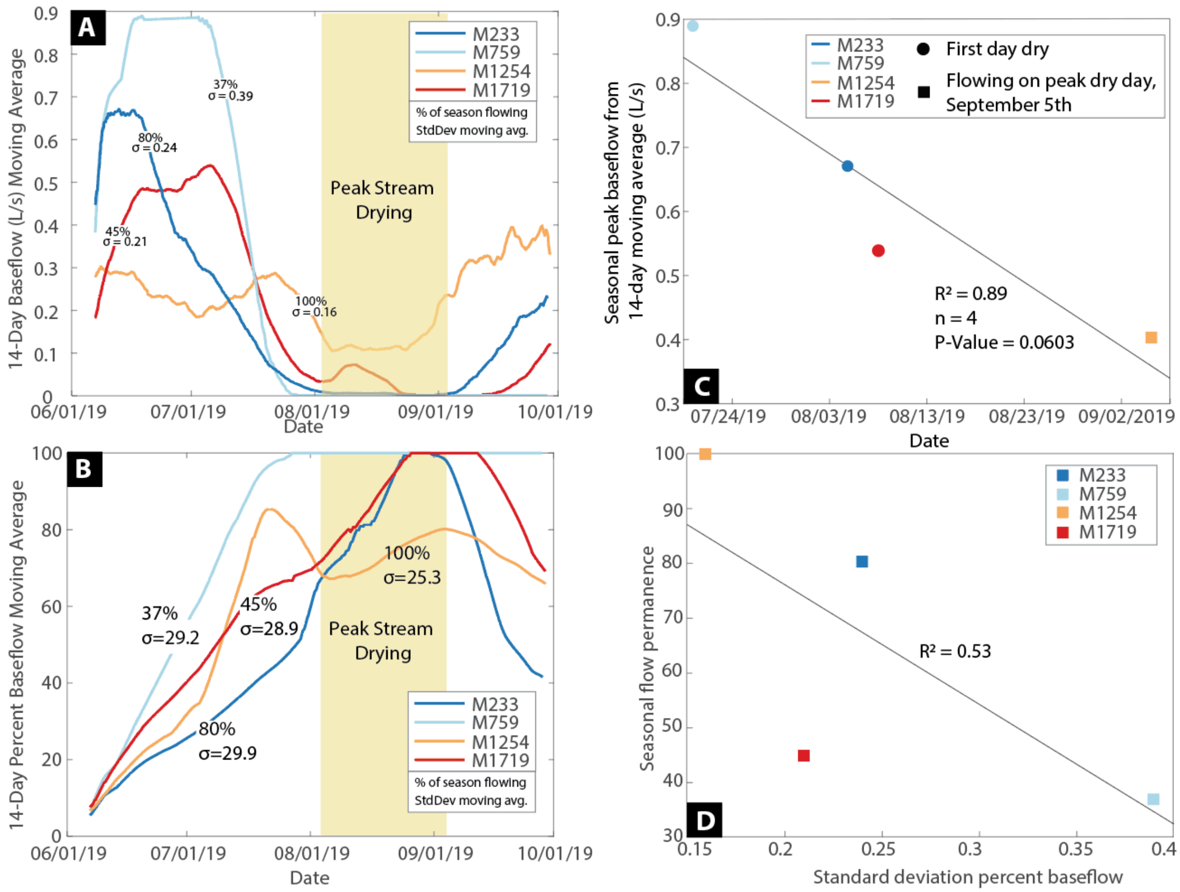

E

Baseflow Monitoring Location	Std.Dev. Baseflow (L/s)	Std. Dev. % Baseflow (%)	Seasonal flow permanence (%)	First day dry
M233	29.9	0.24	80%	Aug., 5
M759	29.2	0.39	37%	July, 20
M1254	25.3	0.16	100%	NA
M1719	28.9	0.21	45%	Aug., 8

Figure 3.5. 14-day moving average for baseflow **(A)** and 14-day moving average for percent baseflow **(B)** at the four baseflow monitoring locations in Murphy. The percent of season with flow for a given location is plotted above the standard deviation of the moving average for each baseflow monitoring location. The peak stream drying period (≥ 25% of sensors flowing) is shaded in yellow. When baseflow is more stable (i.e. lower standard deviation), surface flow is greater. **(C)** First day dry, or in the case that the sensor did not dry (M1254), the peak drying day September 5th, 2019, plotted against the peak magnitude of baseflow calculated over a 14-day moving average dataset. The larger the seasonal peak in baseflow, the earlier the location dried, and stayed dry. **(D)** Standard deviation of percent baseflow plotted against the seasonal flow permanence. When percent baseflow is more stable (i.e. lower standard deviation) flow persists throughout the season. **(E)** Table detailing metrics used in plots **A-D**. The seasonal flow permanence refers to the percent of the season that the baseflow monitoring locations detected surface flows.

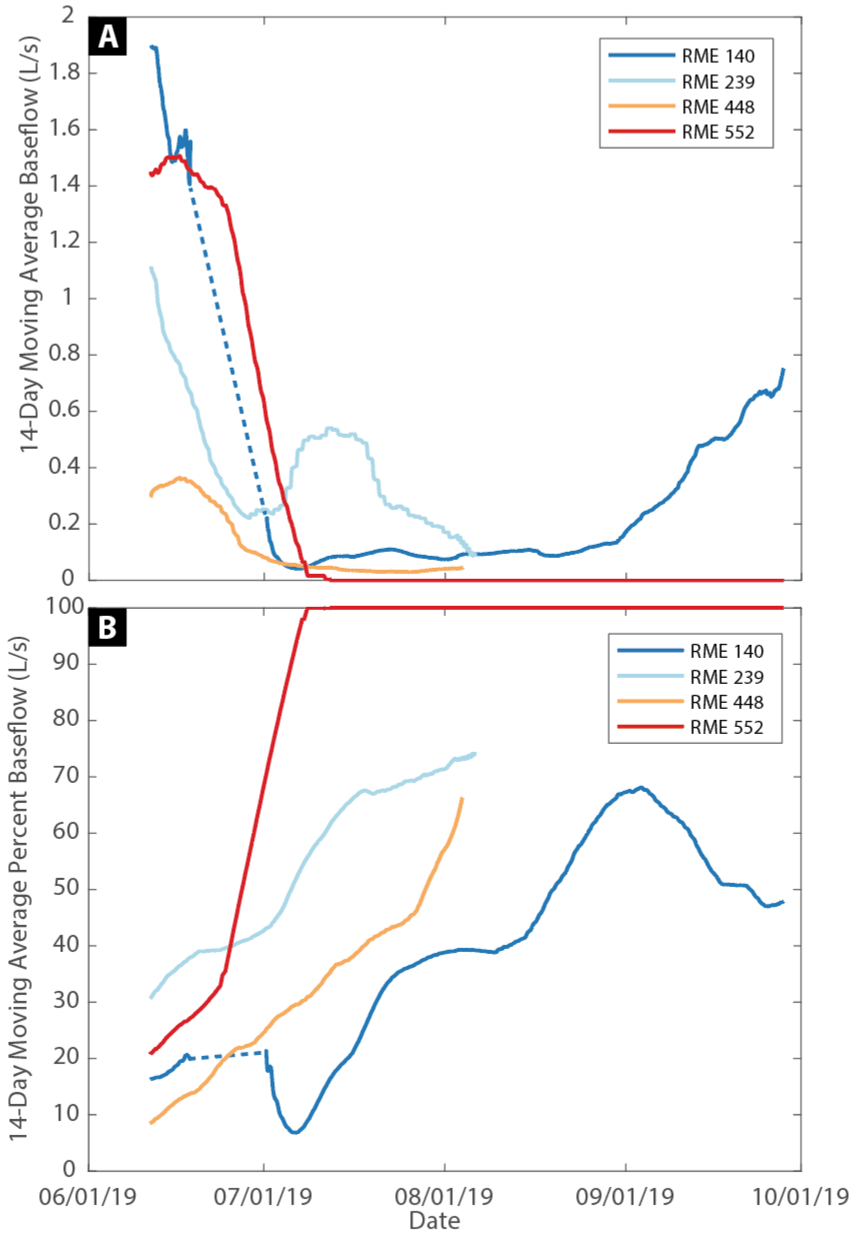

Figure 3.6. 14-day moving average for baseflow **(A)** and 14-day moving average for percent baseflow **(B)** at the four baseflow monitoring locations in RME. Lines are dashed when data is missing and show a linear interpolation between known data points. RME239 and RME448 were flowing through the entire experiment period, data is not displayed after early August due to animal interference.

3.5.5. Baseflow and stream drying

There is a strong correlation between the instantaneous flowing network extent and the average percent baseflow across the four monitoring stations in Murphy Creek at the same timestep (Figure 3.7). Here, and throughout the rest of the paper, we use "runoff" to describe near-surface flowpaths. At the start of the season, the stream was almost completely supported by runoff, and baseflow contributed to less than 10% of total discharge. During this time period, the entire channel below 1633 m exhibited spatially continuous flow. During the first week of June, the first drying occurred in Murphy Creek and the contribution of baseflow at each site increased. As additional sites exhibited drying, the average percent baseflow at all baseflow monitoring stations increased (Figure 3.7). Drying and percent baseflow continued to increase until September 6th when a large hailstorm caused nine of twenty-two dry sites to rewet rapidly and percent baseflow to decrease at all sites. The seasonal peak baseflow value (as calculated from the 14-day moving average) at each baseflow monitoring location had a negative correlation with the first day of drying (Figure 3.5C). The larger the peak in baseflow early in the season, the sooner the location dried and stayed dry throughout the summer. We did not assess the relationship between baseflow and stream drying at RME because only one baseflow monitoring location had continuous flow that we were able to measure throughout the season.

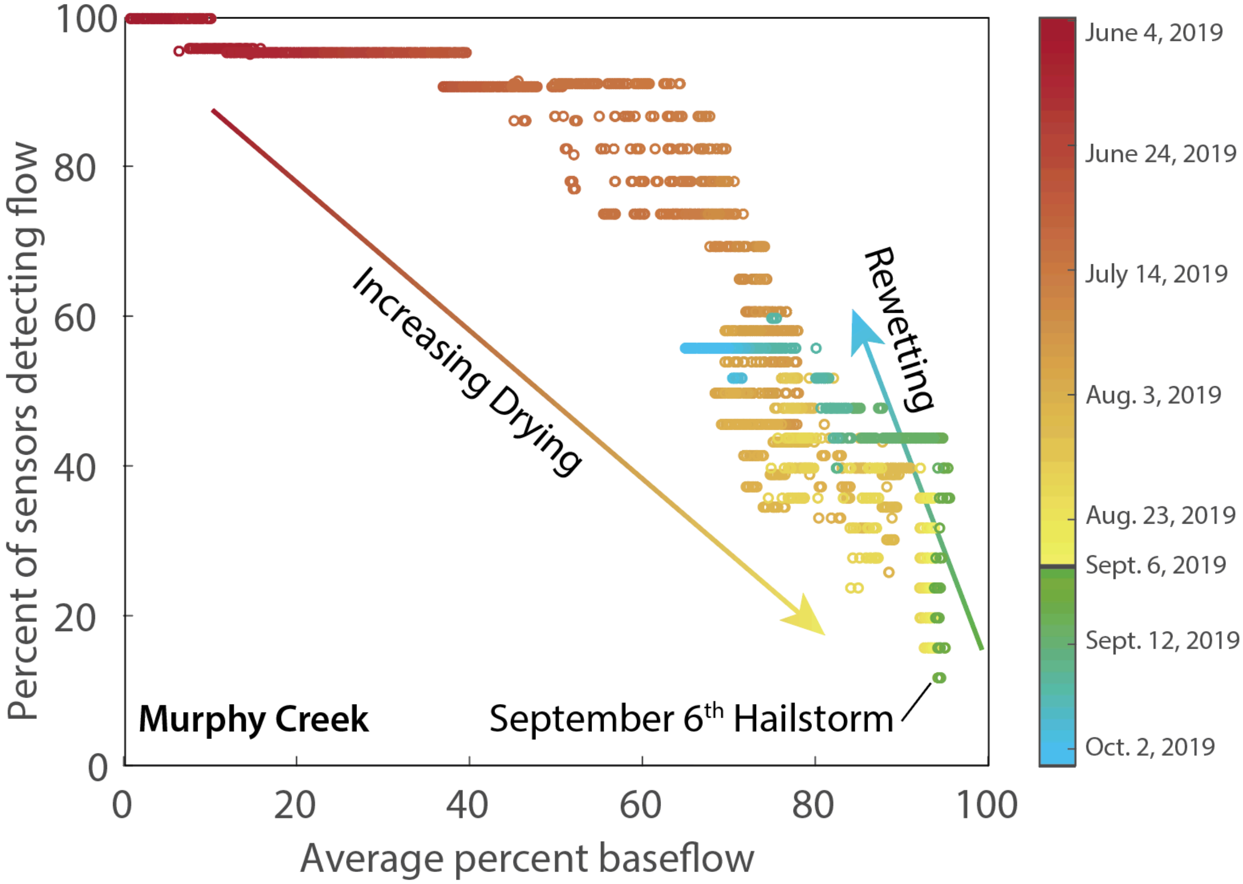

Figure 3.7. Average percent baseflow for the four baseflow monitoring locations at Murphy Creek plotted against the average percent of sensors (n = 25) that detected flow at the same timestep. Each point is colored by time where warm colors (red to orange to yellow gradient) display the seasonal flow recession until peak stream drying and cool colors (green to blue gradient) display a rewetting period at the end of the season. The rewetting period began after a heavy hailstorm on September 6th, 2019 that caused nine of twenty-two dry sensors to rapidly rewet. Trendlines showing increasing and decreasing baseflow patterns are displayed using the same color gradient. If the stream was dry at a baseflow monitoring location, percent baseflow is assumed to be 100%.

3.5.6. *Watershed topography and stream drying*

We assessed the relationships between geomorphic metrics such as elevation, upstream area, slope, curvature, and topographic wetness index (TWI) and seasonal flow permanence, measured as the percent of the season that a sensor was flowing at each location in the stream network for each of the 25 sensors in Murphy Creek. Elevation and slope were negatively correlated with seasonal flow permanence at each sensor location, whereas upstream watershed area and TWI were positively correlated (Figure 3.8). Consistent with the observations in Figure 3.8E, locations where the stream rarely flowed had a smaller TWI than locations where the flow persisted. Similarly, steeper locations typically ceased flowing earlier, stayed dry longer, and did not rewet during September and October storms (Figure 3.8D). Topographic metrics were not assessed at RME because of limited spatial variations in stream drying patterns; thus, the rest of the Results section only discusses data collected at Murphy Creek

Seasonal flow permanence is negatively correlated with the day when a sensor initially dried (Figure 3.8F). Unsurprisingly, sites that were dry for more of the season started drying earlier. However, the relationship between the initiation of drying and seasonal flow permanence was not a simple linear relationship. Instead we observed a step change associated with those sites that rewetted following the September hailstorm.

The down-valley subsurface storage capacity was a poor predictor of seasonal flow permanence at each sensor (Figure 3.9). Although the down-valley subsurface storage capacity varies along the length of the stream (0 to 81.4 m^2, average = 17.4 m^2); it also does not correlate well with other topographic attributes such as channel slope, upstream watershed area, or TWI (data not shown).

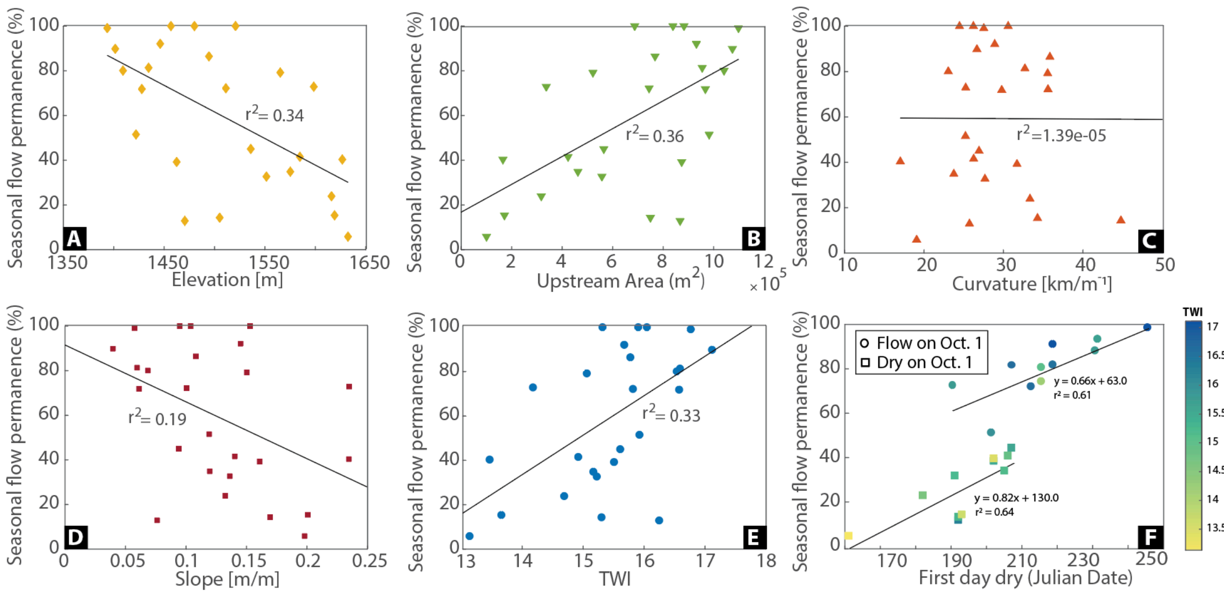

Figure 3.8. Regression between the seasonal flow permanence at each of the 25 sensors (4 baseflow, 21 Pendants) at Murphy Creek and topographic metrics, including elevation **(A)**, upstream watershed area **(B)**, curvature **(C)**, slope **(D)**, TWI **(E)**, and the first day of drying at each sensor **(F).** Upstream watershed area serves as the best individual predictor of flow. In Figure 3.8F, the first day of drying in Julian days for all sensors that dried in Murphy Creek (22 of 25) is plotted against seasonal flow permanence. Shape denotes whether flow was present at the end of the field season on October 1, 2019 (circle = flowing; square = dry). Sensors are colored by their TWI. Typically, when sensors dried earlier, they spent more of the season dry and had lower TWI values than sensors that dried later.

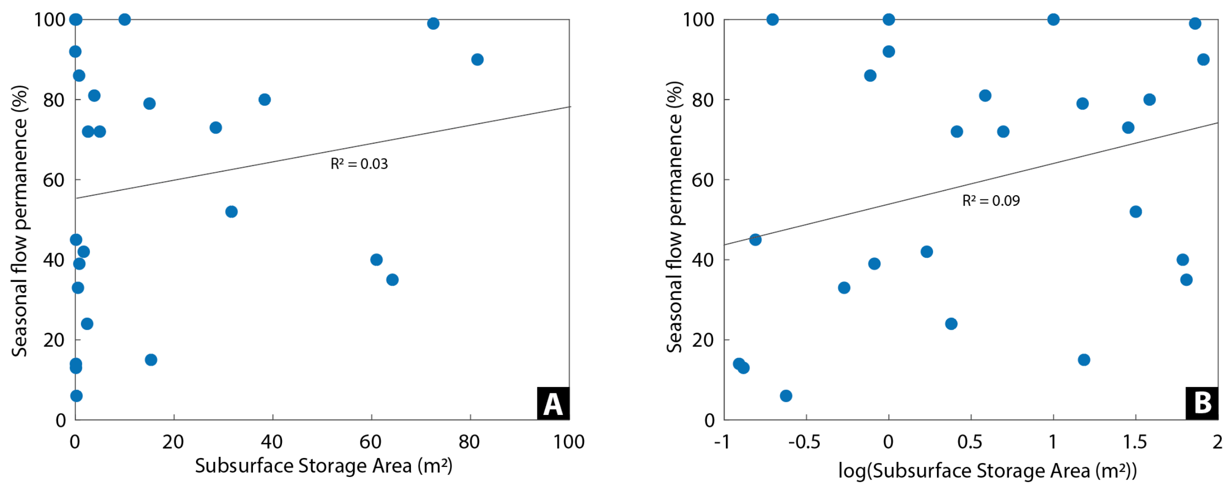

Figure 3.9. (A) Calculated down-valley subsurface storage capacity at each sensor location (n = 25) plotted against seasonal flow permanence, or the percent of the observation season that each sensor in Murphy Creek exhibited surface flow. Very low (<1 m^2) subsurface storage areas exist where the valley is deeply incised, and flow permanence varied widely at these sites. **(B)** Log transformation of the down-valley subsurface storage capacity plotted against the same seasonal flow permanence metric to account for the skewed distribution of subsurface storage areas. The relationship between flow permanence and the subsurface storage capacity is weak in both plots.

3.6. Discussion

3.6.1. Stream drying more likely when percent baseflow is high

Our study reveals a correlation between stream drying and the primary source of surface flows (i.e. runoff or baseflow) (Figure 3.7). This relationship is not surprising as groundwater has been long established to sustain streams during low-flow period periods between precipitation events (Freeze, 1974) and observed by many others (Godsey et al., 2013; Segura et al., 2019). However, direct observations of the correlation both during times of contraction and expansion are few (Queener, 2015).

We present evidence that suggests a low instantaneous flowing network extent is most probable when percent baseflow peaks and that a high instantaneous flowing network extent is probable when surface water is dominated by runoff and at least a small (<10 %) groundwater component to discharge is present. At the beginning of the season in Murphy Creek, the average percent baseflow in the stream was less than 10% (Figure 3.7) and the instantaneous flowing network extent was highest. The instantaneous flowing network extent is insensitive to average percent baseflow until a threshold of ~40% baseflow, above which there is a negative correlation between flowing extent and average percent baseflow. After the early September hailstorm, the trend reversed, suggesting that the source of surface flow is linked to flow permanence at a point throughout the season. The rapid rewetting event demonstrates that precipitation can quickly recharge the hyporheic zone as long as the following conditions are met. First, precipitation inputs must be greater than the subsurface discharge rate, and second, transmissivity and hydraulic conductivity must be small enough for subsurface flow to accumulate and contribute to surface flows. If the stream is primarily supported by surface runoff without a large groundwater component, as in the upper reaches of RME where streamflow is fed by melt from a seasonal snowdrift that disappeared in July, drying is probable when the source of flow (i.e. melting snow) ceases.

3.6.2. Stable baseflow flux yields persistent stream flow

By comparing baseflow variability with the seasonal flowing network extent, we find that when baseflow inputs are stable relative to total discharge, and despite seasonal decreases in discharge, a low seasonal flow permanence less probable. At Murphy Creek, we observe that when the standard deviation of percent baseflow is low, the seasonal flow permanence at the same location was higher (Figure 3.5D). We acknowledge that this conclusion is limited by a low number of observations (n = 4) and suggest that future studies further explore the relationship between baseflow and stream drying to corroborate our findings.

Stream drying occurs when combined runoff and groundwater inputs can no longer sustain surface water presence. We find that when a seasonally consistent and steady groundwater source is able to contribute to surface water as baseflow, surface water persists, even when precipitation is scarce. For example, in Murphy Creek, the only baseflow monitoring location (M1254) to flow continuously throughout the season had a relatively stable baseflow input (Figure 3.5A). We hypothesize that the local hydrologic characteristics at M1254 are more conducive to groundwater flow than at the other Murphy baseflow monitoring locations. To maintain surface flows sourced from baseflow, groundwater must discharge throughout the length of the stream to overcome losses from evapotranspiration (Winter, 2007). Our observations support this finding as areas without stable baseflow dried quickly (Figure 3.5A,C). A groundwater contribution to discharge is still present at the other three baseflow monitoring locations (M1719, M759, and M233), as evidenced by the return of flow later in the season as well as both upstream and downstream surface water presence, but this was still not sufficient to sustain surface flows.

In RME, we observe a slightly different pattern: the baseflow input (L/s) to the stream peaked in June, then declined and remained stable throughout the rest of the season when the snow drift was not supplying melt water to the stream. At RME448, the baseflow input remained relatively stable throughout the season, indicating a stable groundwater input (Figure 3.6A). We conclude that drying began after the runoff component to discharge declined, and that some stream segments dried despite groundwater presence in the subsurface because subsurface characteristics were not conducive to surface water presence. Subsurface characteristics have been identified as controls on baseflow in other studies (Mwakalila et al., 2002; Payn et al., 2012; Segura et al., 2019), and because we show that baseflow and stream drying are tightly coupled, we infer that the primary controls on baseflow are also important consider in stream drying studies.

3.6.3. Geomorphic qualities as a proxy for stream drying potential

Topographic controls are important factors affecting baseflow (Mueller et al., 2013; Mwakalila et al., 2002; Price, 2011; Segura et al., 2019) and flow permanence (Godsey and Kirchner, 2014; Zimmer and McGlynn, 2017a). This is because topography modulates flow partitioning between the subsurface and surface (Prancevic and Kirchner 2019), particularly when baseflow is dominant during low-flow periods (Segura et al. 2019). We show that seasonal flow permanence is correlated with percent baseflow (Figures 3.5D and 3.7), but it is currently unclear whether 1) topography directly impacts baseflow, and thus the probability of stream drying, or 2) if topography impacts subsurface properties such as hydraulic conductivity that dictate the ease with which water can pass through the subsurface, therefore controlling baseflow and subsequently stream drying.

We observed that topographic metrics such as upstream watershed area, TWI, elevation, slope, and curvature, moderately correlated with seasonal flow permeance, and suggest that such metrics can be used to predict the probability of stream drying at a given location (Figure 3.8). We built several multiple linear regression models based on combinations of all five parameters, but found no improvement in correlation quality. We evaluated the relationship between baseflow and topographic metrics in Murphy Creek (plots not shown), but were limited by the number of baseflow monitoring locations. Because we observe baseflow to correlate with seasonal flow permanence, we infer that the relationships between seasonal flow permanence and topographic metrics should also apply to baseflow.

Our findings validate the importance of topographic indicators as predictors of seasonal flow permanence (Prancevic and Kirchner, 2019), as we found moderate strong relationship between seasonal flow permanence and slope, upstream watershed area, elevation, and TWI (Figure 3.8). However, our findings contrast with the work of Whiting and Godsey (2016) and Prancevic and Kirchner (2019) in that we did not find a correlation between stream permanence and local curvature (Figure 3.8C). Instead we found that stream drying is probable where the upstream contributing area is low and slope is high: stream segments with low TWI also dried earlier and stayed dry longer (Figure 3.8).

In low TWI conditions, discharge inputs are lower thus leading to dry channels. Figure 3.8 displays the relationship between the initial timing of drying and seasonal flow permanence at the same location. Areas that rewetted had a higher TWI (circles in Figure 3.8F) and segments with a low TWI dried early. Low TWI segments are not as conducive to accumulating water, even when the average stream discharge was high early in the drying period. These areas also could not sustain surface flows after rainstorms provided supplementary water. In order for surface flow to exist when precipitation is scarce, substantial and stable water delivery from upstream/groundwater must be present. For example, in Murphy Creek when the upstream accumulating area was high and slopes were shallow (Figure 3.8), the probability of seasonal flow permanence increased because upstream water delivery was significant and slopes drained water relatively slowly.

Although flow permanence was correlated with topographic metrics, topography did not explain all variability in drying patterns, and the connection between topography and baseflow and how it impacts surface flow permanence is not clear. We estimated the down-valley subsurface capacity in attempt to further elucidate these connections. However, our preliminary estimates suggest that subsurface capacity varies significantly throughout the length of a single headwater stream (Figure 3.9) and is not significantly correlated with seasonal flow permanence.

Current stream drying prediction models have assumed constant hydraulic conductivity throughout the length of the stream (Ward et al., 2018) and assessed down-valley subsurface capacity by assuming that the slope of the valley bottom is a good approximation of the hydraulic gradient. Spatial variations in down-valley subsurface capacity are assumed to be due to changes in valley width, colluvium depth, slope, and heterogeneity in hydraulic conductivity. If subsurface flows are an important driver of drying, and hydraulic conductivity is assumed to be a constant, then down-valley capacity should vary with flow permanence. However, we estimated the down-valley subsurface capacity using DEM metrics and found it correlated poorly with flow permanence at any given location (Figure 3.9). This finding leads us to conclude that hydraulic conductivity should vary throughout the length of a headwater stream and should correlate well with stream permanence, consistent with low-flow modeling by Fleckenstein et al. (2006) and observations by Dohman et al. (in prep). Future stream drying studies and models will benefit from intensive hydraulic conductivity measurements despite the time and expenses involved.

3.7. Conclusion

Dense spatiotemporal baseflow and stream drying measurements were used to establish a relationship between stream drying and the primary source of surface flows. Over time, stream drying across the network was most probable when surface flows were dominated by baseflow. However, when baseflow inputs are seasonally stable at a single location, surface flow can persist, even as flows decrease. Furthermore, seasonal flow permanence was correlated with topographic metrics such as upstream watershed area, elevation, slope, and TWI. Despite the observed connections between stream drying and both baseflow and topographic metrics, we are still unable to fully explain spatiotemporal stream drying patterns. Subsurface characteristics such as hydraulic conductivity should be measured throughout the length of a headwater stream in order to fully capture drying heterogeneity.

3.8. References

Beven, K.J., Kirkby, M.J., 1979. A physically based, variable contributing area model of basin hydrology. Hydrol. Sci. Bull. 24, 43–69. https://doi.org/10.1080/02626667909491834

Blasch, K.W., Ferré, T.P.A., Christensen, A.H., Hoffmann, J.P., 2002. New Field Method to Determine Streamflow Timing Using Electrical Resistance Sensors. Vadose Zo. J. 1, 289. https://doi.org/10.2136/vzj2002.2890

Carey, S.K., Boucher, J.L., Duarte, C.M., 2013. Inferring groundwater contributions and pathways to streamflow during snowmelt over multiple years in a discontinuous permafrost subarctic environment (Yukon, Canada). Hydrogeol. J. 21, 67–77. https://doi.org/10.1007/s10040-012-0920-9

Costigan, K.H., Jaeger, K.L., Goss, C.W., Fritz, K.M., Goebel, P.C., 2016. Understanding controls on flow permanence in intermittent rivers to aid ecological research: integrating meteorology, geology and land cover. Ecohydrology 9, 1141–1153. https://doi.org/10.1002/eco.1712

Dohman, J., 2018. Three-dimensional subsurface controls on stream intermittency in a semi-arid landscape. Idaho State University.

Duvert, C., Butman, D.E., Ribolzi, O., Marx, A., Hutley, L.B., 2018. CO2 evasion along streams driven by groundwater inputs and geomorphic controls. Nat. Geosci. 11, 813–818. https://doi.org/10.1038/s41561-018-0245-y

Earman, S., Dettinger, M., 2011. Potential impacts of climate change on groundwater resources - A global review. J. Water Clim. Chang. 2, 213–229. https://doi.org/10.2166/wcc.2011.034

Fleckenstein, J.H., Niswonger, R.G., Fogg, G.E., 2006. River-aquifer interactions, geologic heterogeneity, and low-flow management. Ground Water 44, 837–852. https://doi.org/10.1111/j.1745-6584.2006.00190.x

Freeze, R.A., 1974. Streamflow generation. Rev. Geophys. https://doi.org/10.1029/RG012i004p00627

Frisbee, M.D., Phillips, F.M., Campbell, A.R., Liu, F., Sanchez, S.A., 2011. Streamflow generation in a large, alpine watershed in the southern Rocky Mountains of Colorado: Is streamflow generation simply the aggregation of hillslope runoff responses? Water Resour. Res. 47, 1–18. https://doi.org/10.1029/2010WR009391

Furey, P.R., Gupta, V.K., 2001. A physically based filter for separating base flow from streamflow time series. Water Resour. Res. 37, 2709–2722. https://doi.org/10.1029/2001WR000243

Ghosh, D.K., Wang, D., Zhu, T., 2016. On the transition of base flow recession from early stage to late stage. Adv. Water Resour. 88, 8–13. https://doi.org/10.1016/j.advwatres.2015.11.015

Godsey, S.E., Kirchner, J.W., 2014. Dynamic, discontinuous stream networks: Hydrologically driven variations in active drainage density, flowing channels and stream order. Hydrol. Process. 28, 5791–5803. https://doi.org/10.1002/hyp.10310

Godsey, S.E., Kirchner, J.W., Tague, C.L., 2013. Effects of changes in winter snowpacks on summer low flows: case studies in the Sierra Nevada, California, USA. https://doi.org/10.1002/hyp.9943

Goulsbra, C., Evans, M., Lindsay, J., 2014. Temporary streams in a peatland catchment: Pattern, timing, and controls on stream network expansion and contraction. Earth Surf. Process. Landforms 39, 790–803. https://doi.org/10.1002/esp.3533

Gutiérrez-Jurado, K.Y., Partington, D., Batelaan, O., Cook, P., Shanafield, M., 2019. What triggers streamflow for intermittent rivers and ephemeral streams in low-gradient catchments in mediterranean climates. Water Resour. Res. 55, 9926–9946. https://doi.org/10.1029/2019WR025041

Ilangakoon, N., Glenn, N.F., Spaete, L.P., Dashti, H., Li, A., 2016. 2014 lidar-derived 1m digital elevation model data set for Reynolds Creek Experimental Watershed, southwestern Idaho [WWW Document]. https://doi.org/http://doi.org/10.18122/B26C7X

Jaeger, K.L., Olden, J.D., 2012. Eletrical resistance sensor arrays as a means to quantify longitudinal connectivity of rivers. River Res. Appl. 28, 1843–1852. https://doi.org/10.1002/rra.1554

Jaeger, K.L., Olden, J.D., Pelland, N.A., 2014. Climate change poised to threaten hydrologic connectivity and endemic fishes in dryland streams. Proc. Natl. Acad. Sci. U. S. A. 111, 13894–13899. https://doi.org/10.1073/pnas.1320890111

Jensen, C.K., McGuire, K.J., McLaughlin, D.L., Scott, D.T., 2019. Quantifying spatiotemporal variation in headwater stream length using flow intermittency sensors. Environ. Monit. Assess. 191. https://doi.org/10.1007/s10661-019-7373-8

Kirchner, J.W., 2009. Catchments as simple dynamical systems: Catchment characterization, rainfall-runoff modeling, and doing hydrology backward. Water Resour. Res. 45, 1–34. https://doi.org/10.1029/2008WR006912

Klos, Z.P., Link, T.E., Abatzoglou, J.T., 2014. Extent of the rain-snow transition zone in the western U.S. under historic and projected climate. Geophys. Prospect. 6413–6419. https://doi.org/10.1002/2014GL061184.Received

Kormos, P.R., Marks, D., Seyfried, M., Havens, S., Hendrick, A., Lohse, K.A., Masarik, M., Flores, A.N., 2016. 31 years of spatially distributed air temperature, humidity, precipitation amount and precipitation phase from a mountain catchment in the rain-snow transition zone. https://doi.org/10.18122/B2B59V

Kormos, P.R., McNamara, J.P., Seyfried, M.S., Marshall, H.P., Marks, D., Flores, A.N., 2015. Bedrock infiltration estimates from a catchment water storage-based modeling approach in the rain snow transition zone. J. Hydrol. 525, 231–248. https://doi.org/10.1016/j.jhydrol.2015.03.032

Levick, L.R., Goodrich, D.C., Hernandez, M., Fonseca, J., Semmens, D.J., Stromberg, J., Tluczek, M., Leidy, R.A., Scianni, M., Guertin, D.P., 2008. The ecological and hydrological significance of ephemeral and intermittent Streams in the arid and semi-arid American Southwest.

Liu, F., Hunsaker, C., Bales, R.C., 2013. Controls of streamflow generation in small catchments across the snow-rain transition in the Southern Sierra Nevada, California. Hydrol. Process. 27, 1959–1972. https://doi.org/10.1002/hyp.9304

Lundquist, J.D., Dettinger, M.D., Stewart, I.T., Cayan, D.R., 2009. Variability and Trends in Spring Runoff in the Western United States. Clim. Warm. West. North Am. Evid. Environ. Eff. 1–35.

McDonnell, J.J., Sivapalan, M., Vaché, K., Dunn, S., Grant, G., Haggerty, R., Hinz, C., Hooper, R., Kirchner, J., Roderick, M.L., Selker, J., Weiler, M., 2007. Moving beyond heterogeneity and process complexity: A new vision for watershed hydrology. Water Resour. Res. https://doi.org/10.1029/2006WR005467

Miller, M.P., Susong, D.D., Shope, C.L., Heilweil, V.M., Stolp, B.J., 2014. Continuous estimation of baseflow in snowmelt-dominated streams and rivers in the Upper Colorado River Basin: A chemical hydrograph separation approach. Water Resour. Res. 50, 6986–6999. https://doi.org/10.1002/2013WR014939

Moore, R.D.D., 2003. Introduction to salt dilution gauging for streamflow measurement: Part 1. Streamline, Watershed Manag. Mulletin 7, 20–23.

Mote, P.W., Li, S., Lettenmaier, D.P., Xiao, M., Engel, R., 2018. Dramatic declines in snowpack in the western US. npj Clim. Atmos. Sci. 1. https://doi.org/10.1038/s41612-018-0012-1

Mueller, M.H., Weingartner, R., Alewell, C., 2013. Importance of vegetation, topography and flow paths for water transit times of base flow in alpine headwater catchments. Hydrol. Earth Syst. Sci. 17, 1661–1679. https://doi.org/10.5194/hess-17-1661-2013

Mwakalila, S., Feyen, J., Wyseure, G., 2002. The influence of physical catchment properties on baseflow in semi-arid environments. J. Arid Environ. 52, 245–258. https://doi.org/10.1006/jare.2001.0947

Nolin, A.W., Daly, C., 2006. Mapping “at risk” snow in the Pacific Northwest. J. Hydrometeorol. 7, 1164–1171. https://doi.org/10.1175/JHM543.1

Partington, D., Brunner, P., Simmons, C.T., Werner, A.D., Therrien, R., Maier, H.R., Dandy, G.C., 2012. Evaluation of outputs from automated baseflow separation methods against simulated baseflow from a physically based, surface water-groundwater flow model. J. Hydrol. 458–459, 28–39. https://doi.org/10.1016/j.jhydrol.2012.06.029

Payn, R.A., Gooseff, M.N., McGlynn, B.L., Bencala, K.E., Wondzell, S.M., 2012. Exploring changes in the spatial distribution of stream baseflow generation during a seasonal recession. Water Resour. Res. 48, 1–15. https://doi.org/10.1029/2011WR011552

Peirce, S.E., Lindsay, J.B., 2015. Characterizing ephemeral streams in a southern Ontario watershed using electrical resistance sensors. Hydrol. Process. 29, 103–111. https://doi.org/10.1002/hyp.10136

Pierson, F.B., Slaughter, C.W., Cram, Z.K., 2000. Monitoring discharge and suspended sediment, Reynolds Creek Experimental Watershed, Idaho, USA. ARS Tech. Bull. NWRC.

Prancevic, J.P., Kirchner, J.W., 2019. Topographic Controls on the Extension and Retraction of Flowing Streams. Geophys. Res. Lett. 46, 2084–2092. https://doi.org/10.1029/2018GL081799

Price, K., 2011. Effects of watershed topography, soils, land use, and climate on baseflow hydrology in humid regions: A review. Prog. Phys. Geogr. 35, 465–492. https://doi.org/10.1177/0309133311402714

Queener, N., 2015. Spatial and temporal variability in baseflow and stream drying in the Mattole River Headwaters. Humboldt State University. https://doi.org/10.1007/springerreference_226434

Schwanghart, W., Scherler, D., 2014. Short Communication: TopoToolbox 2 - MATLAB-based software for topographic analysis and modeling in Earth surface sciences. Earth Surf. Dyn. 2, 1–7. https://doi.org/10.5194/esurf-2-1-2014

Segura, C., Noone, D., Warren, D., Jones, J.A., Tenny, J., Ganio, L.M., 2019. Climate, Landforms, and Geology Affect Baseflow Sources in a Mountain Catchment. Water Resour. Res. 55, 5238–5254. https://doi.org/10.1029/2018WR023551

Seyfried, M., Lohse, K., Marks, D., Flerchinger, G., Pierson, F., Holbrook, W.S., 2018. Reynolds Creek Experimental Watershed and Critical Zone Observatory. Vadose Zo. J. 17, 1–20. https://doi.org/10.2136/vzj2018.07.0129

Sørensen, R., Zinko, U., Seibert, J., 2006. On the calculation of the topographic wetness index: Evaluation of different methods based on field observations. Hydrol. Earth Syst. Sci. 10, 101–112. https://doi.org/10.5194/hess-10-101-2006

USGS, 2019. Specific Conductance: U.S. Geological Survey Techniques and Methods, in: Book 9, Handbooks for Water-Resources Investigations. pp. 684–684. https://doi.org/https://doi.org/10.3133/tm9A6.3

Ward, A.S., Schmadel, N.M., Wondzell, S.M., 2018. Simulation of dynamic expansion, contraction, and connectivity in a mountain stream network. Adv. Water Resour. 114, 64–82. https://doi.org/10.1016/j.advwatres.2018.01.018

Whiting, J.A., Godsey, S.E., 2016. Discontinuous headwater stream networks with stable flowheads, Salmon River basin, Idaho. Hydrol. Process. 30, 2305–2316. https://doi.org/10.1002/hyp.10790

Winter, T.C., 2007. The role of ground water in generating streamflow in headwater areas and in maintaining base flow. J. Am. Water Resour. Assoc. 43, 15–25. https://doi.org/10.1111/j.1752-1688.2007.00003.x

Wittenberg, H., Sivapalan, M., 1999. Watershed groundwater balance estimation using streamflow recession analysis and baseflow separation. J. Hydrol. 219, 20–33. https://doi.org/10.1016/S0022-1694(99)00040-2

Yu (于松延), S., Bond, N.R., Bunn, S.E., Xu, Z., Kennard, M.J., 2018. Quantifying spatial and temporal patterns of flow intermittency using spatially contiguous runoff data. J. Hydrol. 559, 861–872. https://doi.org/10.1016/j.jhydrol.2018.03.009

Zimmer, M.A., McGlynn, B.L., 2017a. Ephemeral and intermittent runoff generation processes in a low relief, highly weathered catchment. Water Resour. Res. 53, 7055–7077. https://doi.org/10.1002/2016WR019742

Zimmer, M.A., McGlynn, B.L., 2017b. Bidirectional stream–groundwater flow in response to ephemeral and intermittent streamflow and groundwater seasonality. Hydrol. Process. 31, 3871–3880. https://doi.org/10.1002/hyp.11301

3.9. <u>Appendix A:</u> Data modification and data tables

Specific Conductivity Quality Control and Corrections

Specific conductivity measurements had two common errors: sporadic erroneously high values and drifting readings between deployments. Erroneously high values may be due to short-term, in-stream disturbance such as animals stirring sediment or urinating in the stream. Most sensors showed a gradual increase in SC following deployment, likely due to sediment build up in the PVC logger housing. We corrected these electrical conductivity sensor errors using linear interpolation as described below.

To correct the sporadic errors, we first removed erroneous values, and then applied the following gap-filling approach. If the erroneous readings occurred continuously for four or fewer 15-minute timesteps, we linearly interpolated between the previous and subsequent hours' values. For gaps between one hour and one day, we filled with the average of the previous and next day's values at the same time. For gaps longer than one day, we again applied a linear interpolation between the remaining values. If there was an error at the same time step for two or more subsequent days, linear interpolation of values before and after the erroneous readings were used to correct the water level readings.

For the drifting data, we took a different approach. Every time the electrical conductivity loggers were relaunched, the PVC housing and loggers were cleaned of any accumulated sediment or organic matter. Sometimes SC values were much lower after cleaning and relaunching. If this step change occurred, electrical conductivity had always gradually increased to unrealistically high values prior to cleaning and relaunching. We assumed that the gradually increasing readings were due to sediment build up in the sensor. This hypothesis is validated by the fact that gradual unrealistic increases in EC were only observed during low flows in August and September, and were not present when flows were high enough to prevent sediment from accumulating. To correct for the drifting values, the slope of the increasing electrical conductivity values was determined. Next, the estimated slope for the time period showing error was determined by subtracting the EC value before the sediment accumulated from the EC value reported after relaunching. The difference between the slopes was subtracted from the increasing slope line so that the reported EC values were realistic and diel variation was maintained.

Water Level Quality Control and Correction

Each water level logger was downloaded and relaunched a minimum of five times throughout the experiment period. Often, the reported water level before and after relaunch differed due to not replacing the logger in the exact same position in the stream, despite efforts to do so. To correct for variation in logger position, water level was corrected after each relaunch, starting at the end of the record and working backward. The difference at each relaunch was determined and subtracted from all preceding measurements so that the water level immediately before and after relaunching were identical.

During each field visit, we also measured discharge to generate a stage-discharge relationship at each water level logger in both streams. When discharge was measured, in-stream water level was also observed using a ruler at the location of the water level logger. The water level reading for that timestep was corrected using a simple offset to match the observed water level. All water level readings since the previous discharge measurement were corrected using the same offset. In addition, if the electrical conductivity logger read zero, indicating no flow, but the water level logger read non-zero flow, the water level reading was forced to zero. The water level immediately before drying and after drying were forced to the height of the electrical conductivity logger sensor plus the thickness of the PVC housing (1.6 cm).

The water level record was corrected using a combination of in-person water level observations and EC logger records. If there was a discrepancy between the observed water level and the measured water level, the reported water level and all preceding measurements were adjusted to reflect the difference. The water level record was always corrected from the end (t_2) of the record backwards in time so that any applied offset also applied to all prior data until the previous in-person observation or EC interpreted drying (t_1). In some cases, the offset determined at t_2 that was applied to preceding measurements did not match the offset determined at earlier measurement t_1. This resulted in a corrected water level at t_1 that was either higher or lower than the observed water level at that point. This likely happened if there were changes in the bed geometry, and we adjusted for this offset by assuming it was a linear drift between t_1 and t_2. To correct for this drift, the difference between the offsets at t_2 and t_1 were subtracted from one another and divided between the number of observations between the two timesteps. The incremental change per timestep was added to the measured water level so that the final water level at every timestep reflected by the validation at both timesteps while still reflecting diel variation in water level.

Similar to the EC loggers, the water level reading occasionally spiked or fell unrealistically. As with the EC loggers, we linearly interpolated across the gaps created by those erroneous readings. We applied the same 1-hour and 1-day thresholds described above.

Data Exclusion

There are several moments in both the RME and Murphy discharge and or specific conductivity records where no data is reported. Observations were removed due to measurement errors that could not be corrected. Baseflow data at RME239 and RME448 had to be truncated from mid-August onward because sensors were buried in >=10 cm of sediment after cows seasonal grazing commenced in the watershed. Other isolated instances of data removal are detailed in the supplementary data file.

4. Chapter 4: Conclusion

4.1. Summary

In this study we used a dense spatiotemporal stream drying dataset along with spatiotemporally distributed baseflow observations. To our knowledge, we are the first to observe and report wet-dry cycling that precedes long-term stream drying throughout the length of a headwater stream. We also identify the importance of evapotranspiration on stream drying controls and suggest that spatiotemporally distributed evaporation and transpiration measurements be collected both in the riparian zone and on hillslopes. We establish a relationship between baseflow and stream drying and identify that stream drying is most probable when the influence of baseflow peaks. Finally, we show that persistent stream flow is more probable in areas with a stable baseflow input.

Two of the most challenging problems in hydrology right now are understanding spatial distributions of ET and subsurface characteristics, such as hydraulic conductivity. Stream drying presents a possible opportunity towards better characterization of both problems with sufficient complementary information: the location of drying within a stream network may allow us to understand subsurface patterns in hydraulic conductivity whereas the timing of diel cycling may allow us to probe the spatial patterns of riparian ET. We recommend that future stream drying studies incorporate dense spatiotemporal flow observations with spatially distributed hydraulic conductivity measurements and geophysical measurements. We also recommend considering both evaporation and transpiration and measuring temporally continuous transpiration both in riparian channels and on hillslopes.

4.2. Implications for stream management and the updated Clean Water Rule

Intermittent streams are both dynamic and extensive, making them difficult to accurately characterize (Jensen et al., 2017). For example, as part of the United States Geological Survey (USGS) National Map: National Boundaries Dataset, Murphy Creek was mapped as a 2.15 km intermittent stream. The 2.15 km flowing length matches April 2016 flow observations from MacNeille et al. (in prep), overestimates the flowing length by ~800 m based on our June 2019 observations, and severely overestimates our early September 2019 observations (we did not map the stream during the peak drying period, but during that time only 14% of our 25 sensors exhibited flow). The flowing length of an intermittent stream is difficult to summarize with a single length estimate because intermittent streams are spatiotemporally dynamic. Instead understanding the mechanisms controlling their expansion and contraction behavior is essential to managing our water resources.

In 2015, the United States Environmental Protection Agency (EPA) established that under the Clean Water Act tributary streams including perennial, ephemeral, and intermittent streams were protected under the Clean Water Rule because they are connected chemically, physically, and biological to downstream waters. In 2019, the EPA updated the Clean Water Rule to simplify the definition of waters protected by the Clean Water Act. However, in this redefinition, ephemeral features are no longer characterized as tributaries (Department of Defense, 2019). Under this rule, the upper reaches of Murphy Creek are no longer regulated, even though they flow into Reynolds Creek, which is connected to the Salmon River that supplies water resources to Idaho, Oregon, and Washington. Furthermore, the differences between the NHD and our observations makes it difficult to know which stream segments are accurately characterized. This discrepancy highlights how important it is to continue to develop our understanding of these headwater systems in order to protect and manage United States water resources.

4.3. Proposed hierarchy of stream drying controls

In this thesis we explored a number of established stream drying controls as identified by previous work (see Table 2.2). Due to the complex nature of these controls and their variability among field locations in different landscapes and climates, the relative importance of stream drying controls has not yet been established. In Table 4.1, we present a list of controls ranked from most important to least important. However, the hierarchy in the table is only informed from findings discussed in this thesis and may not stand at different spatiotemporal scales or different locations.

We identify climate and weather patterns to be the most important control on surface flow as precipitation is the initial source of all surface and subsurface flows. Surface flow cannot exist if there is nothing sourcing it. The second most important control is subsurface storage volume because if bedrock is exposed at the surface, water in the shallow subsurface cannot accumulate and source surface flows. The third most important control are subsurface properties that enable groundwater to pass through the subsurface, and thus reach surface flow channels. Similarly, we identify baseflow inputs as the 4th control: we showed that surface water ceases when precipitation is scarce if baseflow is the primary flow control. Topography is ranked 5th; we observe it to be a good predictor of flow permanence, but it does not accurately predict all flow permanence, suggesting that some other physical property is a more important control. The final two controls in our list are evapotranspiration losses and land cover. As explained in Chapter 2, we suggest that evapotranspiration losses (that may vary systematically with land cover) control the timing of stream drying once other climatic, geologic, and geomorphic controls are met.

Table 4.1. Proposed hierarchy of stream drying controls as inferred from findings discussed in this thesis.

Importance (1 = high)	Control
1	Climate & weather patterns
2	Subsurface storage volume
3	Subsurface properties (i.e. hydraulic conductivity, permeability, porosity, soil type, grain size etc.)
4	Baseflow inputs
5	Topography (i.e. upstream watershed area, slope, topographic wetness index)
6	Evapotranspiration losses
7	Land cover

4.4. Implications for future stream drying studies

We observe stream drying to be spatiotemporally complex and identify many potential controls on stream drying patterns such as hydraulic conductivity, baseflow, watershed topography, and evapotranspiration demands. Intermittent streams do not behave the same everywhere because local controls are so influential. Results from this thesis suggest that it is important to collect dense spatiotemporal measurements of multiple stream drying controls in order to create a comprehensive stream drying model. In the following paragraphs, we suggest multiple stream drying controls as foci for future stream drying studies.

The relationship between transpiration and diel cycling is complicated due to the numerous feedbacks in the riparian corridor (Barnard et al., 2010). Previous studies have identified that transpiration on hillslopes is important to in-stream diel cycling (Barnard et al., 2010; Wondzell et al., 2010), but no truly comprehensive model integrates the impact of hillslope, riparian, and in-stream processes on diel cycling in headwater streams during low-flow, baseflow-dominated periods. Furthermore, findings from this thesis suggest that shade from riparian vegetation may impact local evapotranspiration, thus potentially causing drying to occur sooner in a location without shade versus a location with shade where all other controls are the same. We did not directly investigate the role of transpiration on stream drying, but expect that demands are not uniform throughout the length of a stream due variable stream drying patterns and riparian vegetation characteristics. We propose that future studies should collect spatiotemporal measurements of evaporation, hillslope and riparian transpiration, in-stream water level, and the presence of flow in order to create a more comprehensive diel cycling model.

We also noted that the ability of water to pass easily through the subsurface is a major control on stream drying, and that these subsurface properties vary throughout the length of a headwater stream. We propose incorporating both spatially distributed hydraulic conductivity and geophysical information into stream drying models. Results from this study suggest that subsurface controls are likely a primary stream drying control.

Twenty-five spatially distributed sensors did not capture all of the stream drying that occurred in Murphy Creek. However, we learned significant new information about stream drying patterns, particularly that wet-dry pulses during diel cycling due to evapotranspiration are common in drying streams. We suggest that future stream drying studies attempt to characterize stream drying patterns using spatially distributed sensors because they are inexpensive and easy to deploy. Stream drying patterns are not the same everywhere, and we expect that expanded monitoring will increase our understanding of intermittent streams.

4.5. References

Barnard, H. R. et al. Mechanistic assessment of hillslope transpiration controls of diel subsurface flow: a steady-state irrigation approach. Ecohydrology 3, 133–142 (2010).

Department of Defense. Definition of '"Waters of the United States"'—Recodification of Pre-Existing Rules. 84, (2019).

Jensen, C. K., McGuire, K. J. & Prince, P. S. Headwater stream length dynamics across four physiographic provinces of the Appalachian Highlands. Hydrol. Process. 31, 3350–3363 (2017).

Macneille, R. et al., in prep

Wondzell, S. M., Gooseff, M. N. & McGlynn, B. L. An analysis of alternative conceptual models relating hyporheic exchange flow to diel fluctuations in discharge during baseflow recession. Hydrol. Process. 24, 686–694 (2010).

5. Appendix A: Data modification and data tables

5.1. Data Modification

Specific Conductivity Quality Control and Corrections

Specific conductivity (SC) measurements had two common errors: sporadic erroneously high values and drifting readings between deployments. Erroneously high values may be due to short-term, in-stream disturbance such as animals stirring sediment or urinating in the stream. Most sensors showed a gradual increase in SC following deployment, likely due to sediment build up in the PVC logger housing. We corrected these electrical conductivity sensor errors using linear interpolation as described below.

To correct the sporadic errors, we first removed erroneous values, and then applied the following gap-filling approach. If the erroneous readings occurred continuously for four or fewer 15-minute timesteps, we linearly interpolated between the previous and subsequent hours' values. For gaps between one hour and one day, we filled with the average of the previous and next day's values at the same time. For gaps longer than one day, we again applied a linear interpolation between the remaining values. If there was an error at the same time step for two or more subsequent days, linear interpolation of values before and after the erroneous readings were used to correct the water level readings.

For the drifting data, we took a different approach. Every time the electrical conductivity loggers were relaunched, the PVC housing and loggers were cleaned of any accumulated sediment or organic matter. Sometimes SC values were much lower after cleaning and relaunching. If this step change occurred, electrical conductivity had always gradually increased to unrealistically high values prior to cleaning and relaunching. We assumed that the gradually increasing readings were due to sediment building up in the sensor. This hypothesis is validated by the fact that gradual unrealistic increases in EC were only observed during low flows in August and September, and were not present when flows were high enough to prevent sediment from accumulating. To correct for the drifting values, the slope of the increasing electrical conductivity values was determined. Next, the estimated slope for the time period showing error was determined by subtracting the EC value before the sediment accumulated from the EC value reported after relaunching. The difference between the slopes was subtracted from the increasing slope line so that the reported EC values were realistic and diel variation was maintained.

Water Level Quality Control and Correction

Each water level logger was downloaded and relaunched a minimum of five times throughout the experiment period. Often, the reported water level before and after relaunch differed due to not replacing the logger in the exact same position in the stream, despite efforts to do so. To correct for variation in logger position, water level was corrected after each relaunch, starting at the end of the record and working backward. The difference at each relaunch was determined and subtracted from all preceding measurements so that the water level immediately before and after relaunching were identical.

During each field visit, we also measured discharge to generate a stage-discharge relationship at each water level logger in both streams. When discharge was measured, in-stream water level was also observed using a ruler at the location of the water level logger. The water level reading for that timestep was corrected using a simple offset to match the observed water level. All water level readings since the previous discharge measurement were corrected using the same offset. In addition, if the electrical conductivity logger read zero, indicating no flow, but the water level logger read non-zero flow, the water level reading was forced to zero. The water level immediately before drying and after drying were forced to the height of the electrical conductivity logger sensor plus the thickness of the PVC housing (1.6 cm).

The water level record was corrected using a combination of in-person water level observations and EC logger records. If there was a discrepancy between the observed water level and the measured water level, the reported water level and all preceding measurements were adjusted to reflect the difference. The water level record was always corrected from the end (t_2) of the record backwards in time so that any applied offset also applied to all prior data until the previous in-person observation or EC interpreted drying (t_1). In some cases, the offset determined at t_2 that was applied to preceding measurements did not match the offset determined at earlier measurement t_1. This resulted in a corrected water level at t_1 that was either higher or lower than the observed water level at that point. This likely happened if there were changes in the bed geometry, and we adjusted for this offset by assuming there was linear drift between t_1 and t_2. To correct for this drift, the difference between the offsets at t_2 and t_1 were subtracted from one another and divided between the number of observations between the two timesteps. The incremental change per timestep was added to the measured water level so that the final water level at every timestep reflected the validation at both timesteps while still retaining diel variation in water level.

Similar to the EC loggers, the water level reading occasionally spiked or fell unrealistically. As with the EC loggers, we linearly interpolated across the gaps created by those erroneous readings. We applied the same 1-hour and 1-day thresholds described above.

Data Exclusion

There are several moments in both the RME and Murphy discharge and/or specific conductivity records where no data is reported. Observations were removed when we encountered measurement errors that could not be corrected. Baseflow data at RME239 and RME448 had to be truncated from mid-August onward because sensors were buried in >=10 cm of sediment after seasonal grazing commenced in the watershed. Other isolated instances of data removal are detailed in the supplementary data file.

5.2. Tables

Table A1. List of sensors and their locations at Murphy Creek.

Sensor ID	Field Sensor Name	Type	UTM 11S		Elevation (m)
			Easting	Northing	
M91	MPA1	PA	514599.10	4789190.60	1394
M153	MPA2	PA	514526.90	4789143.60	1401
M233	ECWL1	EC/WL	514464.10	4789098.10	1409
M380	MPA3	PA	514345.30	4789034.80	1422
M454	MPA15	PA	514278.00	4789016.60	1428
M523	MPA4	PA	514214.50	4789030.50	1435
M624	MPA5	PA	514120.38	4789028.12	1446
M716	MPA16	PA	514033.24	4789020.35	1457
M759	ECWL2	EC/WL	514009.23	4788989.97	1462
M823	MPA17	PA	513955.74	4788964.10	1471
M918	MPA6	PA	513864.30	4788963.33	1480
M1036	MPA7	PA	513749.08	4788971.46	1494
M1121	MPA18	PA	513668.62	4788982.83	1505
M1166	MPA8	PA	513626.10	4788968.40	1511
M1254	ECWL3	EC/WL	513546.80	4788975.30	1521
M1377	MPA19	PA	513449.15	4789016.89	1536
M1452	MPA9	PA	513375.32	4789001.97	1551
M1572	MPA10	PA	513271.00	4789045.00	1565
M1653	MPA20	PA	513205.10	4789086.70	1575
M1719	MPA11	PA	513144.00	4789104.80	1585
M1799	ECWL4	EC/WL	513071.60	4789132.80	1598
M1909	MPA12	PA	512974.40	4789170.00	1616
M1951	MPA21	PA	512960.40	4789169.00	1619
M1984	MPA13	PA	512910.00	4789197.30	1632
M1993	MPA14	PA	512932.50	4789165.50	1627

Table A2. List of sensors and their locations at RME. Easting and northing are in UTM zone 11S.

Sensor ID	Field Sensor Name	Type	Easting	Northing	Elevation (m)
RME76	PA1	PA	519859.7	4768621.2	2029
RME140	ECWL1	EC/WL	519853.7	4768553.8	2034
RME194	PA2	PA	519831.2	4768506.6	2037
RME239	ECWL2	EC/WL	519846.2	4768466.9	2040
RME343	PA4	PA	519798.9	4768370.5	2047
RME344	PA3	PA	519872.9	4768372.7	2047
RME413	PA5	PA	519804.1	4768302.0	2055
RME448	ECWL3	EC/WL	519903.1	4768301.8	2053
RME470	PA6	PA	519943.0	4768299.0	2059
RME552	ECWL4	EC/WL	520015.7	4768266	2063
RME676	PA7	PA	520104.6	4768206.2	2073
RME838	PA8	PA	520184.4	4768070.5	2094

Table A3. Discharge and method in Murphy Creek. * = flow was too low for salt dilution

Date	Time	Field Sensor Name	Sensor ID	Method	Discharge [L/s]
6/6/19	8:12	M1	M233	Salt Dilution	11.42
6/6/19	9:07	M2	M759	Salt Dilution	9.85
6/6/19	9:42	M3	M1254	Salt Dilution	8.59
6/6/19	10:25	M4	M1799	Salt Dilution	5.86
6/12/19	9:34	M1	M233	Salt Dilution	6.67
6/12/19	14:21	M2	M759	Salt Dilution	4.75
6/12/19	13:03	M3	M1254	Salt Dilution	4.03
6/12/19	15:00	M4	M1799	Salt Dilution	3.16
7/8/19	15:14	M1	M233	Salt Dilution	0.76
7/10/19	8:14	M1	M233	Salt Dilution	1.43
7/10/19	9:17	M2	M759	Salt Dilution	0.78
7/10/19	10:30	M3	M1254	Salt Dilution	0.83
7/10/19	12:21	M4	M1799	Salt Dilution	0.64
8/8/19	-	M1	M233	-	DRY
8/8/19	-	M2	M759	-	DRY
8/8/19	8:59	M3	M1254	Salt Dilution	0.15
8/8/19	11:31	M4	M1799	Salt Dilution	0.05
9/11/19	-	M1	M233	-	*
9/9/19	-	M2	M759	-	DRY
9/9/19	13:25	M3	M1254	Salt Dilution	0.11
9/9/19	-	M4	M1799	-	DRY
9/30/19	10:32	M1	M233	Salt Dilution	0.42
9/30/19	-	M2	M759	-	DRY
9/30/19	13:50	M3	M1254	Salt Dilution	0.22
10/2/19	9:48	M4	M1799	Salt Dilution	0.14

Table A4. Discharge and method in RME. * = flow was too low for salt dilution

Date	Time	Field Sensor Name	Sensor ID	Method	Discharge
6/5/19	9:20	RME 1	RME140	Flow Tracker	15.40
6/5/19	9:40	RME 2	RME239	Flow Tracker	8.00
6/5/19	10:15	RME 3	RME448	Salt Dilution	11.17
6/5/19	10:50	RME 4	RME552	Salt Dilution	6.69
6/11/2019	10:00	RME 1	RME140	Flow Tracker	6.70
6/11/2019	11:20	RME 2	RME239	Flow Tracker	4.80
6/11/2019	13:10	RME 3	RME448	Salt Dilution	7.08
6/11/2019	14:25	RME 4	RME552	Salt Dilution	3.13
7/8/19	9:42	RME 1	RME140	Salt Dilution	2.40
7/8/19	15:17	RME 2	RME239	Salt Dilution	0.62
7/9/19	16:13	RME 3	RME448	Salt Dilution	0.30
7/9/19	-	RME 4	RME552	-	DRY
8/7/19	13:05	RME 1	RME140	Salt Dilution	0.14
8/7/19	14:27	RME 2	RME239	Salt Dilution	0.09
8/7/19	16:33	RME 3	RME448	Salt Dilution	0.01
8/7/19	-	RME 4	RME552	-	DRY
9/10/19	10:23	RME 1	RME140	Salt Dilution	0.58
9/10/19	10:43	RME 2	RME239	Salt Dilution	0.42
9/10/19	-	RME 3	RME448	-	*
9/10/19	-	RME 4	RME552	-	DRY
10/1/19	10:10	RME 1	RME140	Salt Dilution	0.61
10/1/19	10:43	RME 2	RME239	Salt Dilution	0.28
10/1/19	-	RME 3	RME448	-	*
10/1/19	-	RME 4	RME552	-	DRY

Table A5. Topographic and stream drying metrics at each sensor in Murphy. See section 3.4 and Appendix B for definitions and methods for each metric calculation.

Sensor ID	Percent flowing [%]	Slope [m/m]	Upstream Watershed Area [m^2]	Curvature [km^{-1}]	TWI [unitless]	Subsurface Storage Capacity [m^2]
M91	99.1	0.057	1098226	27.53	16.8	72.5
M153	89.8	0.040	1074195	26.66	17.1	81.4
M233	80.1	0.069	1040963	23.06	16.5	38.3
M380	51.5	0.119	981921	25.22	15.9	31.6
M454	71.9	0.061	967011	29.79	16.6	5
M523	81.4	0.060	954569	32.70	16.6	3.8
M624	92.1	0.145	931648	28.90	15.7	0
M716	100.0	0.095	882397	26.22	16.0	0.2
M759	39.2	0.161	873238	31.70	15.5	0.8
M823	12.9	0.076	867099	25.73	16.2	0.1
M918	100.0	0.104	838750	24.47	15.9	10
M1036	86.4	0.108	767713	35.85	15.8	0.8
M1121	14.3	0.170	749423	44.79	15.3	0.1
M1166	72.2	0.101	744206	35.61	15.8	2.6
M1254	100.0	0.153	687277	30.59	15.3	0
M1377	45.0	0.094	564836	26.93	15.6	0.2
M1452	32.7	0.136	557268	27.67	15.2	0.5
M1572	79.2	0.150	521753	35.57	15.1	15
M1653	34.9	0.120	462334	23.76	15.2	64.2
M1719	41.5	0.140	423416	26.25	14.9	1.7
M1799	72.9	0.235	336988	25.25	14.2	28.4
M1909	23.9	0.132	317280	33.34	14.7	2.4
M1951	15.4	0.201	171383	34.29	13.7	15.3
M1984	40.3	0.235	165348	17.02	13.5	61
M1993	5.8	0.198	100375	19.08	13.1	0.2

6. Appendix B: Down-valley subsurface capacity calculation

We extracted the topographic profiles (Z(x)) perpendicular to stream flow at each of the sensor locations and found the minimum elevation in the profile min(Z(x)) at the thalweg in the stream, T. See Figure 2.2 for a schematic of this approach including the locations described here. We then found the location of the maximum value of the second derivative of the topographic profile from A to the topographic minimum ($x_{\frac{d^2z}{dx^2}\max from\ A\ to\ T}$) and the topographic minimum to D ($x_{\frac{d^2z}{dx^2}\max from\ T\ to\ D}$): the locations of these maximum changes in slope are points B and C. The slopes and y-intercepts between points A and B ($S_{North}, Y_{int_{North}}$) and between C and D ($S_{South}, Y_{int_{South}}$) were found and projected into the subsurface until the lines met. The north and south subscripts refer to the projection on the north and south facing slopes, respectively. The down-valley subsurface capacity (SSC_{DV}) is the area (m^2) between the actual topographic profile and the projected slopes $\left(SSC_{DV\_N}\ and\ SSC_{DV\_S}\right)$.

$$A = w - T\ , D = T + w \qquad \text{Equation (1)}$$

$$B = x_{\frac{d^2z}{dx^2}\max from\ A\ to\ T}\ , C = x_{\frac{d^2z}{dx^2}\max from\ Tto\ D} \qquad \text{Equation (2)}$$

$$S_N = \frac{(Z_A - Z_B)}{(X_A - X_B)}\ ,\ S_S = \frac{(Z_C - Z_D)}{(X_C - X_D)} \qquad \text{Equation (3)}$$

$$SSC_{DV\_N} = \int_{B(x)}^{:T(x)} z(x) - \left(S_N(x) + Y_{int_{North}}\right) \qquad \text{Equation (4)}$$

$$SSC_{DV\_S} = \int_{T(x)}^{C(x)} z(x) - \left(S_S(x) + Y_{int_{South}}\right) \qquad \text{Equation (5)}$$

$$SSC = SSC_{DV\_North} + SSC_{DV\_South} \qquad \text{Equation (6)}$$

7. Appendix C: Advice for future graduate students studying stream drying controls

C.1 Determining scale

One of the first steps in planning a stream drying study is determining the spatial and temporal scales for your instrumentation. I recommend choosing the same temporal scale as any existing instrumentation in your watershed unless you have a scientific reason to choose a different scale (i.e. if other instruments are running at 1-hour intervals, set your loggers to the same interval for easy analysis). Spatial scales are more complicated. I observed drying to vary within 10-meter segments. The more closely spaced your sensors the better, but make sure you are within the limits of your time and financial budgets.

C.2 Order equipment with time to test

A Master's project timeline is inherently crammed. Ensure that you order your equipment as early as possible so that you can test it before going in the field. HOBO Pendant sensor batteries do not drop linearly, but rather seem to randomly drop and rise at regular exponential intervals that are not necessarily representative of their actual battery life. Sensors that showed a 32% battery life in the field later showed 100% battery life after a week of sitting in the lab. Early testing might have revealed this and saved stress in the field.

C.3 HOBO water level loggers and in-stream water level

If you have the time, resources, and permits to build wells to measure water level, I would recommend doing so. If building wells is not realistic, HOBO water level loggers are a secondary option. I would recommend installing a *very high-quality* barometer to ensure that you have quality air pressure to calculate water level. I found that the resolution of the HOBO barometers was not high enough to reliably calculate in-stream water level. Also, if you use wells or in-stream water level loggers, manually measure the water level after every launch so that you can truth any unrealistic values. I would also recommend collecting as many subsurface property measurements as possible at any location with wells or in-stream water level loggers, particularly hydraulic conductivity.

C.4 Tips for managing a dense spatiotemporal dataset

I collected ~450,000 datapoints during my field season and found that Excel is not equipped to handle a dataset of this size. It is important to download field data at regular intervals so that you can identify problems before it is too late. However, frequent downloading means lots of data files so it is important to organize and name data files in a manner that makes sense to you.

I recommend saving your data in Excel or a text-based format then importing into the coding program of your choice for analysis (e.g., MATLAB, R, Python, etc.). I learned to code using MATLAB which made cleaner plots than Excel, and also generated them faster and easier after processing the data. I was able to remake the plots for my project countless times, such as after finding a mistake in the analysis or when I chose to color things differently. I would recommend learning a coding program so that modifying figures is easy after you make corrections to your raw data or change the way you are analyzing. As of spring 2020, MATLAB and all associated toolboxes are free to ISU students.

C.5 Prepare field gear ahead of time

I recommend packing for the field a week before you are scheduled to leave. This allows you time to purchase whatever consumable you may be running out of and to order replacement batteries for equipment if they are running low. It also gives you time to double check your packing list to ensure that you have everything you need. If you are able, I recommend placing all gear in an action packer or two. After every field campaign, reorganize and clean the gear, but keep it stored in the travel container, so that you are less likely to forget something the next time around. Be mindful of a balance here and acknowledge others using the lab likely want a clean and organized space.

C.6 Take more field photos than you think you should

Take photos of your equipment every time you visit. Take photos of people. Take photos of the landscape throughout the season. And finally, take more pictures than feels necessary in the moment. Many of my pictures turned out blurry or the intended object was unrecognizable, and I wish I had taken more.

C. 7 Remote sensing and working in the DML

I recommend acquiring an external hard drive at the start of your project and saving all mapping and satellite images to it. These data are often large and will quickly take up precious space on a personal computer. Working on an external hard drive also allows you to work off multiple computers in the DML and classroom and avoids losing work on any public server. With that said, be sure to back up your external hard drive.